SINGLE AND MULTI-ANTENNA MC-DS-CDMA WITH JOINT DETECTION FOR BROADBAND BLOCK-FADING CHANNELS

D.J. BASILIO

2009

UNIVERSITEIT VAN PRETORIA
UNIVERSITY OF PRETORIA
YUNIBESITHI YA PRETORIA

SINGLE AND MULTI-ANTENNA MC-DS-CDMA WITH JOINT DETECTION FOR BROADBAND BLOCK-FADING CHANNELS

By

Daniel Jorge Basilio

Study leaders: Dr. B.T. Maharaj and Prof. L.P. Linde

Submitted in partial fulfilment of the requirements for the degree

Master of Engineering (Electronic)

in the

Department of Electrical, Electronic & Computer Engineering

of the

Faculty of Engineering, Built Environment & Information Technology

UNIVERSITY OF PRETORIA

May 2009

SUMMARY

SINGLE AND MULTI-ANTENNA MC-DS-CDMA WITH JOINT DETECTION FOR BROADBAND BLOCK-FADING CHANNELS

by

Daniel Jorge Basilio

Study leaders: Dr. B.T. Maharaj and Prof. L.P. Linde

Department of Electrical, Electronic & Computer Engineering

Master of Engineering (Electronic)

In the context of broadband wireless communications using code division multiple access (CDMA), the main multiple access (MA) options include single-carrier direct sequence CDMA (SC-DS-CDMA) using time-domain direct sequence spreading [1, p. 728], multicarrier CDMA (MC-CDMA) using frequency-domain spreading [2, 3] and multicarrier DS-CDMA (MC-DS-CDMA) using time-domain direct sequence spreading of the individual sub-carrier signals [4, 5]. It was shown in [6] that MC-DS-CDMA has the highest degrees of freedom in the family of CDMA schemes that can be beneficially exploited during the system design and reconfiguration procedures. An amalgam of MC-CDMA and MC-DS-CDMA known as time and frequency domain spreading (TF-domain spreading) MC-DS-CDMA was proposed in [6]. TF-domain spreading MC-DS-CDMA has several benefits over conventional MC-DS-CDMA with regard to both capacity and performance [7]. However, in contrast to conventional MC-DS-CDMA, TF-domain spreading MC-DS-CDMA introduces MUI, which necessitates the use of joint detection at the receiver. Recently, multiple input multiple output (MIMO) or multi-antenna TF-domain spreading MC-DS-CDMA schemes have been proposed in the literature that efficiently exploit both the spatial and frequency diversity available in MIMO frequency-selective channels [8, 9]. Although an extensive amount of research has been done on single and multi-antenna TF-domain spreading MC-DS-CDMA schemes that achieve both spatial and frequency diversity in frequency-selective slow fading channels [6–9], very little research considers the time-selectivity of the wireless channels encountered. Thus, the

above-mentioned schemes may not be sufficiently efficient, when communicating over wireless channels exhibiting both frequency-selective and time-selective fading. There are very few MC-DS-CDMA schemes in the literature that consider the time-selectivity of the wireless channels encountered.

This study considers the design of single and multi-antenna TF-domain spreading MC-DS-CDMA, for frequency-selective block-fading channels, which are capable of exploiting the full diversity available in the channel (i.e. spatial, frequency and temporal diversity), using various methods of joint detection at the receiver. It has been shown that the diversity gain in block-fading channels can be improved by coding across multiple fading blocks [10–12]. Single-antenna TF-domain spreading MC-DS-CDMA is considered for the quasi-synchronous uplink channel, and multi-antenna TF-domain spreading MC-DS-CDMA is considered for the synchronous downlink channel. Numerous simulated bit error rate (BER) performance curves, obtained using a triply selective MIMO channel platform, are presented in this study using optimal and sub-optimal joint detection algorithms at the receiver. In addition, this study investigates the impact of spatial correlation on the BER performance of the MC-DS-CDMA schemes considered. From these simulated results, one is able to conclude that TF-domain spreading MC-DS-CDMA designed for frequency-selective block-fading channels performs better than previously proposed schemes designed for frequency-selective slow fading channels, owing to the additional temporal diversity exploited under the block-fading assumption.

Keywords:

Block-fading, joint detection, MC-CDMA, MC-DS-CDMA, MIMO, SC-DS-CDMA, spatial correlation, TF-domain spreading, triply selective.

OPSOMMING

SINGLE AND MULTI-ANTENNA MC-DS-CDMA WITH JOINT DETECTION FOR BROADBAND BLOCK-FADING CHANNELS

deur

Daniel Jorge Basilio

Studie leiers: Dr. B.T. Maharaj and Prof. L.P. Linde

Departement Elektriese, Elektroniese & Rekenaar Ingenieurswese

Meester in Ingenieurswese (Elektronies)

In die konteks van breëband- draadlose kommunikasie deur die gebruik van kodeverdeling-veelvuldige toegang (KVVT) behels die belangrikste veelvuldigetoegang- (VT) opsies enkel-draer direkte-sekwensie KVVT (ED-DS-KVVT), deur die gebruik van tyd-domein direkte sekwensie-verspreiding [1, p. 728], veelvuldigedraer-KVVT (VD-KVVT) deur die gebruik van frekwensiedomein-verspreiding [2, 3] en VD-DS- KVVT deur die gebruik van tyd-domein direkte sekwensie-verspreiding van die individuele sub-draerseine [4, 5]. Daar is in [6] aangetoon dat VD-DS-KVVT die hoogste vlakke van vryheid in die familie KVVT-skemas het wat voordelig benut kan word gedurende sisteemontwerp en rekonfigurasieprosedures. 'n Amalgaam van VD-KVVT en VD-DS-KVVT bekend as tyd-en-frekwensiedomeinverspreiding (TF-domeinverspreiding) VD-DS-KVVT is voorgestel in [6]. TF-domeinverspreiding VD-DS-KVVT het verskeie voordele bo konvensionele VD-DS-KVVT wat sowel kapasiteit as werkverrigting betref [7]. In teenstelling met konvensionele VD-DS-KVVT benut TF-domeinverspreiding VD-DS-KVVT multi-gebruiker-interferensie, wat die gebruik van gesamentlike opsporing by die ontvanger noodsaak. In die onlangse verlede is in die literatuur veelvuldige-inset-veelvuldige-uitset-(VIVU) of veelvuldige-antenna TF-domeinverspreiding VD-DS-KVVT-skemas voorgestel wat sowel die ruimtelike as frekwensiediversiteit wat in VIVU frekwensie-selektiewe kanale beskikbaar is, effektief gebruik [8, 9]. Hoewel uitgebreide navorsing onderneem is oor enkel- en multi-antenna TF-domeinverspreiding VD-DS-KVVT-skemas wat sowel ruimtelike

as frekwensie diversiteit in frekwensie-selektiewe stadig deinende kanale bereik [6–9], oorweeg baie min navorsing die tyd-selektiwiteit van die draadlose kanale wat betrokke is. Bogenoemde skemas mag dus nie effektief genoeg wees nie wanneer kommunikasie plaasvind oor draadlose kanale wat sowel frekwensie-selektiewe as tyd-selektiewe wegsterwing toon. Baie min VD-DS-KVVT-skemas in die literatuur skenk aandag aan die tyd-selektiwiteit van die betrokke draadlose kanale. Die studie ondersoek die ontwerp van enkel- en multi-antenna TF-domeinverspreiding VD-DS-KVVT vir frekwensie-selektiewe blokwegsterwingkanale, wat in staat is om die volle diversiteit wat in die kanaal beskikbaar is, te benut (i.e. ruimtelike, frekwensie- en tyddiversiteit), deur die gebruik van verskeie metodes van gesamentlike opsporing by die ontvanger. Daar is aangetoon dat die diversiteitwins in blokwegsterwingkanale verbeter kan word deur kodering oor veelvuldige deinende blokke [10–12]. Enkel-antenna TF-domeinverspreiding VD-DS-KVVT word oorweeg vir die kwasi-sinchroniese opverbinding-kanaal, en multi-antenna TF-domeinverspreiding VD-DS-KVVT vir die sinchroniese afverbinding-kanaal. Talryke gesimuleerde bisfouttempo (BFT) werkverrigtingkurwes wat verkry is deur die gebruik van ’n drie-voudige selektiewe VIVU-kanaalplatform, word in hierdie studie aangebied, deur die gebruik van optimale en sub-optimale gesamentlike opsporingsalgoritmes by die ontvanger. Daarbenewens ondersoek hierdie studie die impak van ruimtelike korrelasie op die BFT-werkverrigring van die VD-DS-KVVT-skemas wat oorweeg word. Uit hierdie gesimuleerde resultate is dit moontlik om tot die gevolgtrekking te kom dat TF-domeinverspreiding VD-DS-KVVT wat ontwerp is vir frekwensie-selektiese blokwegsterwingkanale beter werkverrigting toon as vroeër voorgestelde skemas wat ontwerp is vir frekwensie-selektiewe stadig deinende kanale, te danke aan die ekstra tyddiversiteit wat deur die blokwegsterwing-aanname benut word .

Sleutelwoorde:

Blokwegsterwing, gesamentlike opsporing, VD-KVVT, VD-DS-KVVT, VIVU, ED-DS-KVVT, ruimtelike korrelasie, TF-domeinverspreding, drie-voudige selektiewe Kanaal.

I dedicate this work to my loving family and friends, for their continuous support and encouragement during this study.

UNIVERSITEIT VAN PRETORIA
UNIVERSITY OF PRETORIA
YUNIBESITHI YA PRETORIA

ACKNOWLEDGEMENTS

I would like to thank the following people and institutions.

- First and foremost, my appreciation and thanks go to my parents for their enduring love, support and encouragement.
- I am especially grateful to my supervisors, Dr. B.T. Maharaj and Prof. L.P. Linde, for their support and guidance during this study.
- I would also like to thank my engineering friends K.P. Maré, Danie Louw and Philip Botha for our insightful and intellectual discussions during this study.
- Credit goes to the University of Pretoria (UP) and the Sentech Chair in Broadband Wireless Communication (BWMC) for the financial sponsorship of my Masters degree.

CONTENTS

List of Figures

List of Tables

List of Abbreviations

AWGN	Additive White Gaussian Noise
BER	Bit Error Rate
BPSK	Binary Phase Shift Keying
CDMA	Code Divison Multiple Access
CIR	Channel Impulse Response
CSI	Channel State Information
DS-CDMA	Direct Sequence Code Divison Multiple Access
FFT	Fast Fourier Transform
FIR	Finite Impulse Response
ICI	Inter-channel Interference
IIR	Infinite Impulse Response
ISI	Inter-symbol Interference
LCP	Linear Constellation Precoding
MA	Multiple Access
MC	Multicarrier
MF	Matched Filter
MIMO	Multiple Input Multiple Output
ML	Maximum Likelihood
MMSE	Minimum Mean Square Error
MRC	Maximum Ratio Combining
MUI	Multi-user Interference
OFDM	Orthogonal Frequency Division Multiplexing
OFDMA	Orthogonal Frequency Division Multiple Access
PDF	Probability Distribution Function
PDP	Power Delay Profile
PG	Processing Gain
PN	Pseudo-Noise

PSD	Power Spectral Density
QAM	Quadrature Amplitude Modulation
QPSK	Quadrature Phase Shift Keying
SC	Single Carrier
SF	Spreading Factor
SFB	Space Frequency Block
SISO	Single Input Single Output
SNR	Signal-to-noise Ratio
STFB	Space Time Frequency Block
STS	Space Time Spreading
TF	Time and Frequency
UP	University of Pretoria
ZCZ	Zero Correlation Zone
ZF	Zero Forcing

NOTATION

$\mathbf{A}$	The matrix $\mathbf{A}$
$\mathbf{a}$	The column vector $\mathbf{a}$
$E[.]$	The expected value
$(.)^{\mathcal{T}}$	The transpose operation
$(.)^{\mathcal{H}}$	The hermitian transpose operation
$(.)^*$	The complex conjugate
j	The imaginary unit ($j = \sqrt{-1}$)
$\mathbf{I}_N$	The $N \times N$ identity matrix
$\mathbf{0}_{P\times N}$	The $P \times N$ all zero matrix
$\otimes$	The Kronecker product
tr(.)	The trace of a matrix
$\|.\|$	The determinant of a matrix, or cardinality of a set, or the magnitude of an element
$\mathbb{N}$	The positive integer set
$\mathbb{Z}$	The integer ring
$\mathbb{Q}$	The rational number field
$\mathbb{R}$	The real number field
$\mathbb{C}$	The complex number field
$diag(d_1, \ldots, d_P)$	A diagonal matrix with diagonal entries $d_1, \ldots, d_P$
$\mathbb{Z}(j)$	The ring of Gaussian integers, whose elements are in the form of $p + jq$, where $p, q \in \mathbb{Z}$
$\mathbb{Q}(j)$	The smallest sub-field of $\mathbb{C}$ including both $\mathbb{Q}$ and j
$\mathbb{Q}(j)(\alpha)$	The smallest sub-field of $\mathbb{C}$ including both $\mathbb{Q}(j)$ and α, where α is algebraic over $\mathbb{Q}(j)$
$\mathbf{F}_N$	The $N \times N$ FFT matrix, with its $(p,q)_{th}$ element equal to $(1/\sqrt{N})\exp(-j2\pi(p-1)(q-1)/N)$
$\lceil x \rceil$	The smallest integer larger than x

$\lfloor x \rfloor$	The largest integer smaller than x
$real(x)$	The real part of x
$imag(x)$	The imaginary part of x
$(x)mod(y)$	The remainder of division of x by y
$gcd(x, y)$	The largest positive integer that divides both x and y without remainder
$a \not\equiv b \ (mod\ n)$	$(a - b)$ is not divisible by n (a and b are not congruent modulo n)
$\mathbf{X}^{1/2}$	The square root of the matrix $\mathbf{X}$

COMMONLY USED SYMBOLS

$\mathcal{A}$	The signal constellation, such as PSK or QAM
$\mathbf{M}_T$	The number of transmit antennas
$\mathbf{M}_R$	The number of receive antennas
$L+1$	The number of Rayleigh fading paths
M_B	The number of fading blocks
T_c	The time domain spreading sequence chip interval on each sub-carrier
T_{sym}	The symbol duration before serial to parallel conversion
T_s	The sampling interval
σ_n^2	The noise variance
σ_s^2	The transmitted symbol variance
L_{seq}	CDMA spreading sequence length
M_{seq}	CDMA spreading sequence family size
Z_0	Zero correlation zone length in chips
Δf_c	The coherence bandwidth of the channel
$(\Delta t)_c$	The coherence time of the channel

CHAPTER ONE
INTRODUCTION

1.1 BACKGROUND AND MOTIVATION

1.1.1 Background

1.1.1.1 OFDM

Orthogonal frequency division multiplexing (OFDM) dates back approximately 40 years, where a patent was applied for in the mid-1960s [14, 15]. However, it was only in the early 1990s that advances in hardware for digital signal processing made OFDM a realistic option for wireless systems. OFDM is a parallel data transmission scheme in which high data rates can be achieved by transmitting data on orthogonal sub-carriers, where each sub-carrier's bandwidth is less than or equal to the coherence bandwidth of the channel. The inter-symbol interference (ISI) and inter-channel interference (ICI) in OFDM systems are reduced by the insertion of guard intervals and code synchronization is made easier by the extended symbol period engendered by the associated serial to parallel conversion preceding the parallel transmission of low-rate sub-channels. With the aid of a cyclic prefix insertion at the transmitter and removal at the receiver, it converts a frequency-selective fading channel into parallel flat fading sub-channels [16], thereby simplifying channel equalization and symbol decoding. OFDM leads to a promising multi-user interference (MUI)-free multiple-access technique that is termed orthogonal frequency-division multiple access (OFDMA) [17], where every user's symbols are transmitted on one or more sub-carriers. Since sub-carriers retain their orthogonality even after propagation through frequency-selective channels, MUI is eliminated by design. However, uncoded OFDMA does not exploit the channel frequency diversity

without employing error-control coding [18], which introduces redundancy. Thus, an inherent problem in OFDMA systems is the problem of obtaining frequency diversity, without sacrificing bandwidth efficiency.

1.1.1.2 SC-DS-CDMA

In single carrier direct sequence code division multiple access (SC-DS-CDMA), each user's symbols are spread by a user-specific spreading sequence, which expands the bandwidth compared with the data rate of each user [1, p. 728]. Typically, a pseudo-noise (PN) sequence is used to spread the information signal to the allocated frequency bandwidth. SC-DS-CDMA systems, in general, allow multiple users to transmit independent information within the same bandwidth simultaneously, using carefully designed spreading sequences. Each user is assigned a PN sequence that is either orthogonal to the sequences of all the other users or the sequence possesses appropriate cross-correlation properties that minimize the MUI. This sequence is superimposed on the information signal, making the signal appear noise-like to all other users. Only the intended receiver has a replica of the same sequence and uses it to extract the information signal. The sequence is also known as a spreading sequence, since it spreads the bandwidth of the original data signal into a much higher bandwidth before transmission. An SC-DS-CDMA system is also able to achieve narrow-band interference suppression [1, p. 729], owing to the time spreading operation at the transmitter and the time de-spreading operation at the receiver. In addition, the wide-band nature of SC-DS-CDMA transmissions allows the receiver to resolve signals propagating through different paths with a RAKE receiver [1, p. 843], and thus multipath diversity is achieved to combat the fading effects in frequency-selective channels. However, direct-sequence CDMA schemes with multiple users suffer from MUI and ISI, resulting in a significant degradation in performance [1, p. 840]. The MUI and ISI are directly related to the autocorrelation and cross-correlation properties of the spreading sequences employed.

1.1.1.3 Multicarrier CDMA

In recent years, CDMA systems based on the combination of CDMA schemes and OFDM signalling, which are referred to as multicarrier CDMA schemes, have attracted much attention in the field of wireless communications [2–5, 19, 20]. Multicarrier CDMA schemes can be categorized into two main types. In the first scheme, a data symbol is first spread by a

spreading code of length Q and then converted into Q parallel chip sequences, with each chip modulating a different sub-carrier. Q is usually chosen to be equal to the number of sub-carriers employed. The spreading operation that occurs in this scheme is in the frequency domain, and is thus referred to as frequency-domain spreading. This type of scheme is commonly referred to in the literature as multicarrier CDMA (MC-CDMA) [2, 3, 19, 20]. The benefit of MC-CDMA is that it achieves frequency diversity because each symbol is transmitted over several independently faded sub-carriers, which experience independent fades. If some sub-carriers experience destructive fades, diversity combining can be used at the receiver to recover the data (i.e. maximum ratio combining [MRC]). In addition, it was shown in [21] that single-user synchronization in an MC-CDMA system does not depend on the autocorrelation or other properties of the spreading sequences, which is an advantage compared with conventional SC-DS-CDMA systems. However, the mutual interference between synchronous or asynchronous users in an MC-CDMA system does depend on the cross-correlation properties of the spreading sequences employed [21]. The drawback of MC-CDMA is that it may experience high levels of MUI when the channel is heavily loaded (many users). MUI occurs because each chip of each user's spreading sequence experiences independent fading. This tends to destroy the orthogonality between the different users spreading sequences, even when the users sequences are orthogonal and perfectly aligned in time. Thus, an MC-CDMA system introduces MUI and degrades the bit error rate (BER) performance. As a result, MC-CDMA systems perform best under low user loads.

In the second scheme, the original data stream is first serial to parallel converted into N sub-streams. Each sub-stream is then spread in the time-domain using a user-specific time-domain spreading code. Thus, each sub-carrier's signal is similar to that of a conventional normal SC-DS-CDMA scheme. This type of scheme is commonly referred to in the literature as MC direct sequence CDMA (MC-DS-CDMA) [4, 5]. The benefit of MC-DS-CDMA is that, by careful design, it can provide MA without the excessive MUI that can occur in MC-CDMA systems. This is possible because all the spreading sequence chips are transmitted on the same sub-carrier, which experiences correlated fading provided that the channel varies slowly. It also provides narrow-band interference suppression on each sub-carrier. MC-DS-CDMA systems have several advantages over MC-CDMA and SC-DS-CDMA systems, including higher design flexibility [4, 6]. However, MC-DS-CDMA systems (like OFDMA systems) are unable to exploit the channel frequency diversity without employing error control coding [22], which

introduces some redundancy and thus reduces bandwidth efficiency.

1.1.1.4 TF-domain spreading MC-DS-CDMA

Recently, time and frequency domain (TF-domain) spreading MC-DS-CDMA schemes have been proposed in the literature [13, 23, 24], to achieve frequency diversity without losing the bandwidth efficiency of the transmitted signal in frequency-selective slow fading channel conditions. TF-domain spreading MC-DS-CDMA can be seen as a combination of MC-DS-CDMA and MC-CDMA, which relies on joint detection at the receiver, and generally has higher receiver decoding complexity compared to conventional MC-DS-CDMA.

1.1.1.5 MIMO assisted MC-DS-CDMA

The employment of multiple antennas at both the transmitter and the receiver, which is widely referred to as the multiple input multiple output (MIMO) technique, constitutes a cost-effective approach to high-throughput wireless communications. A MIMO or multi-antenna system has the following advantages over a single input single output (SISO) or single-antenna system:

- A significant increase in both the system's capacity and spectral efficiency. The capacity of a wireless link increases linearly with the minimum of the number of transmitter or receiver antennas [25].
- Dramatic reduction of the effects of fading due to increased diversity [26, 27]. This is particularly beneficial when the different channels fade independently.

In recent years, space-time block coding has received much attention as an effective MIMO diversity technique used for combating fading in wireless communications [26, 27]. Inspired by space-time block codes, in [28], an attractive transmit diversity scheme based on space-time spreading (STS) has been proposed for employment in CDMA systems. An STS scheme designed for supporting two transmit antennas and one receive antenna has also been included in the CDMA 2000 standard [28]. However in [28], only the performance of SC-DS-CDMA systems using STS was investigated. The performance of TF-domain spreading MC-DS-CDMA incorporating STS has recently been investigated in [8]. Other multi-antenna or MIMO MC-DS-CDMA schemes have also been proposed that achieve spatial and frequency diversity without employing STS [9]. The sub-channels of a MIMO system are usually space-selective (caused by angle spread at the transmitter and receiver), time-selective (caused

by Doppler spread), and frequency-selective (caused by delay spread), which are referred to as triply selective MIMO channels. These selectivities may substantially affect the MIMO system's performance [25, 29]. None of the above-mentioned MIMO MC-DS-CDMA schemes considers the effects of antenna correlation on system performance.

1.1.2 Motivation

Most of the single and multi-antenna MC-DS-CDMA schemes proposed thus far in the literature only consider frequency-selective slow fading conditions, and do not consider block-fading conditions [10, 12], where temporal diversity can be exploited. In addition, none of the MIMO MC-DS-CDMA schemes proposed in the literature consider the effects of antenna correlation on system performance. The motivation for this study is split into two sections. The first section considers single-antenna MC-DS-CDMA systems designed for the quasi-synchronous uplink channel. Only single-antenna MC-DS-CDMA is considered for the uplink in view of the fact that the small size of the mobile units limits both the spatial resolution of the antenna array and the diversity gain [28]. Multi-antenna transmit diversity techniques are thus more feasible for the downlink. The second section considers multi-antenna MC-DS-CDMA for the downlink.

1.1.2.1 Single-antenna TF-domain spreading MC-DS-CDMA for the quasi-synchronous uplink

In DS-CDMA systems, the spreading sequences characterize the associated ISI as well as the MUI properties. Traditional orthogonal codes, such as Walsh-Hadamard codes [30, p. 381] and orthogonal Gold codes [31], retain their orthogonality only in case of perfect synchronization, but they exhibit non-zero off-peak autocorrelations and cross-correlations in asynchronous or quasi-synchronous scenarios. Consequently, these correlation properties limit the achievable performance in the quasi-synchronous uplink channel when multiple users are supported. Owing to these limitations, considerable research efforts have been invested in designing spreading sequences, which exhibit zero correlation values, when the relative delay-induced code offset is in the so-called Zero Correlation Zone (ZCZ) or interference-free window of the spreading sequence [32–37]. Recently, TF-domain spreading MC-DS-CDMA has been proposed for the quasi-synchronous uplink channel using ZCZ sequences [13, 24]. However, these schemes only consider frequency-selective slow fading conditions and only exploit frequency diversity. None of the above schemes consider more general block-fading channel

conditions, where the fading coefficients are constant over one fading block, but are independent from one block to another one. It has been shown that the diversity gain in block-fading channels can be improved by coding across multiple fading blocks [10–12, 38]. Thus, one of the motivations in this study is the design of a TF-domain spreading MC-DS-CDMA system using ZCZ codes capable of achieving frequency and temporal diversity in frequency-selective block-fading channel conditions.

1.1.2.2 Multi-antenna TF-domain spreading MC-DS-CDMA for the synchronous downlink

The performance of TF-domain spreading MC-DS-CDMA incorporating STS has recently been investigated in [8, 39]. The system achieves spatial and frequency diversity in the downlink. Other multi-antenna or MIMO MC-DS-CDMA schemes have also been proposed for the downlink that achieve spatial and frequency diversity without employing STS [9]. However, the systems in [8, 9, 39] only consider frequency-selective slow fading channel conditions where only frequency and spatial diversity are exploited. To the best knowledge of the author, no multi-antenna MC-DS-CDMA schemes have been proposed in the literature that achieve spatial, frequency and temporal diversity in frequency-selective block-fading [10–12, 38] channel conditions. Thus, a second motivation in this study is the design of a multi-antenna TF-domain spreading MC-DS-CDMA system that achieves spatial, frequency and temporal diversity in frequency-selective block-fading channel conditions. In addition, the schemes in [8, 9, 39] assume that the MIMO sub-channels are statistically independent where there is no spatial or antenna correlation. This is generally not a true assumption in practice [29, 40]. Thus, a final motivation for this study is to analyze the effects of antenna or spatial correlation on the performance of multi-antenna MC-DS-CDMA systems.

1.2 AUTHOR'S CONTRIBUTIONS AND OUTPUTS

The primary goal of this study was the investigation and performance of single and multi-antenna TF-domain spreading MC-DS-CDMA for frequency selective, spatially selective and block-fading channels.

1.2.1 Contributions related to system design and BER simulations

1.2.1.1 Single-antenna TF-domain spreading MC-DS-CDMA for the quasi-synchronous uplink

The contributions are given in the list that follows.

- In Chapter 5, a single-antenna TF-domain spreading MC-DS-CDMA system using ZCZ sequences, designed specifically for quasi-synchronous uplink transmissions, is proposed to exploit frequency and temporal diversity in frequency-selective and block-fading [10, 11, 38] channels. This is in contrast to previously proposed schemes designed only to exploit frequency diversity in frequency-selective slow fading channels [13, 24].

- In Chapter 7, the performance of the system is investigated at the receiver using maximum likelihood (ML) optimal decoding as well as ML sphere decoding [41–44]. In addition, the performance is also investigated using linear joint detection schemes such as the matched filter (MF), zero forcing (ZF) and minimum mean square error (MMSE) block linear detectors at the receiver [45, p. 99-104].

1.2.1.2 Multi-antenna TF-domain spreading MC-DS-CDMA for the synchronous downlink

The contributions are given in the list that follows.

- In Chapter 6, two multi-antenna TF-domain spreading MC-DS-CDMA systems, designed specifically for synchronous downlink transmissions, are proposed to exploit spatial, frequency and temporal diversity (full diversity) in spatially selective, frequency-selective and block-fading [10, 11, 38] channels. This is in contrast to previously proposed schemes designed only to exploit spatial and frequency diversity in frequency-selective slow fading channels [8, 9]. The first scheme employs STS [8, 28] to achieve spatial diversity, where joint decoding is done over time and frequency at the receiver. The second scheme considered achieves full diversity without using STS, but instead uses space time frequency block (STFB) codes, which have recently been proposed for MIMO-OFDM systems [46].

- In Chapter 7, the performance of both the above-mentioned schemes are evaluated, using BER as a figure of merit. The performance of each system is investigated using ML

optimal decoding as well as ML sphere decoding [41–44] at the receiver. In addition, the performance is also investigated using linear joint detection schemes such as the MF, ZF and MMSE block linear detectors at the receiver [45, p. 99-104].

- In Chapter 7, the performance of both the above-mentioned schemes are evaluated when antenna spatial correlation is introduced using the triply selective MIMO channel model proposed in [40]. This is in contrast to previous schemes that assume the channel fading coefficients of the different MIMO sub-channels are statistically independent and uncorrelated [8, 9].

1.2.2 Publications

The published and submitted conference and journal articles resulting from this study are listed below.

1.2.2.1 Published

- D.J. Basilio, K.P. Maré and B.T. Maharaj, "Performance of Space-Time-Frequency Block-Coded MC-DS-CDMA in Correlated Conditions ", *in Proceedings of IEEE WCNC 2009*, Budapest, Hungary, 4-8 April 2009, CDROM.

- D.J. Basilio, B.T. Maharaj and L.P. Linde, "Uplink MC-DS-CDMA using ZCZ sequences for frequency-selective block-fading channels ", *in Proceedings of IEEE AFRICON 2009*, Kenya, 23 September 2009, CDROM.

1.2.2.2 Submitted

Journal papers have been submitted for publication.

1.3 OUTLINE OF DISSERTATION

This dissertation consists of eight chapters. Chapter 2 first summarizes some of the important performances measures used in the analysis of CDMA spreading sequences, followed by the construction of Walsh-Hadamard and orthogonal Gold sequences for CDMA systems. Finally, ZCZ sequences are discussed and the construction of almost optimal quadriphase ZCZ sequences is detailed. In chapter 3, the discrete time triply selective MIMO channel

model proposed in [40] is discussed in detail. This channel is used as a platform for BER simulations in Chapter 7. Chapter 4 introduces algebraic linear constellation precoding, followed by the analysis of several joint detection schemes for CDMA systems. Uplink TF-domain spreading MC-DS-CDMA using ZCZ sequences for frequency-selective block-fading channels is discussed in Chapter 5, using several joint detection schemes at the receiver. Chapter 6 investigates downlink TF-domain spreading MC-DS-CDMA schemes designed for frequency-selective block-fading channels. Chapter 7 presents the simulation results obtained during this study. In Chapter 8 conclusions are drawn from the results obtained, and future research areas are also discussed.

CHAPTER TWO

CDMA SPREADING CODES

A CDMA system comprises a set of spreading codes, each assigned to a different user. Ideally, each user's spreading code should have an impulsive-like periodic autocorrelation function, with an out-of-phase autocorrelation of zero. In addition, any two user codes in the set should ideally be completely uncorrelated (zero periodic cross-correlation for all shifts). Furthermore, the number of codes in the CDMA set (family size) determines the number of users the CDMA system can accommodate, in a given frequency band. Thus, ideally this should be as large as possible. Generally speaking, the CDMA code length L_{seq}, family size M_{seq}, autocorrelation side lobe and maximum cross-correlation value are bound by certain mathematical theoretical limits, such as the Welch bound [47]. The Welch bound states that there are absolutely no such ideal codes that exist in the binary field, finite field or even complex field. The autocorrelation and cross-correlation properties contradict each other, so that smaller side-lobes of autocorrelation lead to larger side-lobes of cross-correlation and vice versa [47]. Because of these limitations, an asynchronous CDMA system will introduce MUI in additive white Gaussian noise (AWGN) and multipath channels. Traditionally, CDMA systems are interference limited [1, p. 901], since capacity and performance are determined by the interference affecting the system. The non-zero autocorrelation side-lobes of codes in the set lead to ISI, and the non-zero cross-correlation between the codes in the set lead to MUI. The side-lobes of the autocorrelation and the cross-correlation functions should be as small as possible to reduce the near-far effect, and suppress ISI and MUI [45]. The next sub-section summarizes some of the important performance measures used in the analysis of CDMA spreading sequences.

2.1 PERFORMANCE MEASURES

The length of the spreading sequence L_{seq} is given by the number of chips in the sequence. It is a cardinal factor in the determination of a spread spectrum system's processing gain (PG). It also influences the correlation characteristics of the spreading codes. The family size M_{seq} refers to the number of codes in the code set, which in general grows with the sequence length L_{seq}. The periodic autocorrelation of a continuous length-L_{seq} spreading sequence, $s(t)$, having chips of duration T_c, is defined as follows [48, p. 203]:

$$R_{s(t),s(t)}(\tau) = \int_0^{L_{seq}.T_c} s(t)s^*((t+\tau)mod(L_{seq}.T_c))dt \tag{2.1}$$

The periodic autocorrelation function gives an indication of the signal amplitude to be expected at the output of a coherent, perfectly synchronous correlator receiver. The periodic cross-correlation measures the periodic similarity between two different spreading sequences having a relative phase shift of τ seconds. It is defined as follows for the continuous length-L_{seq} spreading sequences $s_1(t)$ and $s_2(t)$, both consisting of L_{seq} chips of duration T_c [48, p. 204]:

$$R_{s_1(t),s_2(t)}(\tau) = \int_0^{L_{seq}.T_c} s_1(t)s_2^*((t+\tau)mod(L_{seq}.T_c))dt \tag{2.2}$$

The periodic cross-correlation characteristics of the sequences in a spreading sequence family dictate the degradation in performance in a multi-user spread spectrum system due to MUI. Lower periodic cross-correlation values deliver less MUI, resulting in better BER performances. A very popular lower bound on the periodic cross-correlation for the length L_{seq} sequences $s_1(t)$ and $s_2(t)$ from a family of size-M_{seq}, is the Welch bound [47], given by:

$$\max\{R_{s_1(t),s_2(t)}(\tau)\} \geq L_{seq}\sqrt{\frac{M_{seq}-1}{M_{seq}.L_{seq}-1}} \tag{2.3}$$

If $L_{seq} \to \infty$, the Welch bound simplifies to $\max\{R_{s_1(t),s_2(t)}(\tau)\} \approx \sqrt{L_{seq}}$. If the chip-rate is denoted by f_c, and the symbol rate is denoted by f_s, then the spreading factor (SF) is defined as

$$SF = \frac{f_c}{f_s} \tag{2.4}$$

The PG of a spread spectrum system, which is directly related to its SF, is calculated as follows [48, p. 204]:

$$PG = 10\log_{10}(SF) = 10\log_{10}(\frac{f_c}{f_s}) \tag{2.5}$$

which is given in dB. The spread spectrum system's ability to suppress narrowband interference depends on the PG.

2.2 ORTHOGONAL SEQUENCES

2.2.1 Walsh-Hadamard sequences

If perfectly synchronized with respect to each other, Walsh-Hadamard codes [30, p. 381] are perfectly orthogonal. That is, Walsh-Hadamard codes are optimal codes to avoid interference among users in the link from base station to mobile terminals (downlink) [30, p. 381]. The simplest matrix of two orthogonal Walsh-Hadamard sequences is

$$\mathbf{C}_1 = \begin{pmatrix} 1 & 1 \\ 1 & -1 \end{pmatrix} \tag{2.6}$$

The code of user one is the first column (i.e. (1, 1)), the code of user two is the second column, (i.e. (1, -1)). Clearly (1, 1) is orthogonal to (1, -1). This matrix can be extended using a recursive technique. For $n + 1$ users, the matrix is found from the code matrix for n users, according to

$$\mathbf{C}_{n+1} = \begin{pmatrix} \mathbf{C}_n & \mathbf{C}_n \\ \mathbf{C}_n & \bar{\mathbf{C}}_n \end{pmatrix} \tag{2.7}$$

where $\bar{\mathbf{C}}$ is the modulo-2 complement of $\mathbf{C}$. Each column of $\mathbf{C}_{n+1}$ is a different Walsh-Hadamard spreading code. Thus, the Walsh-Hadamard code family size is $M_{seq} = L_{seq}$. Fig. 2.1 depicts the modulus of the normalized periodic autocorrelation function of a randomly selected length $L_{seq} = 16$ Walsh-Hadamard sequence. The modulus of the normalized periodic cross-correlation between two randomly selected Walsh-Hadamard sequences of length $L_{seq} = 16$ in a Walsh-Hadamard sequence set is shown in Fig. 2.2. It should be noted that, in general, not all sequences in a Walsh-Hadamard sequence set have zero periodic cross-correlation for all shifts as in Fig. 2.2.

2.2.2 Orthogonal Gold sequences

Gold sequences [1, p. 769] are constructed from a preferred pair of maximal length sequences [1, p. 766], by the element-by-element multiplication of one sequence with every time shift of the second sequence. Orthogonal Gold sequences can then be constructed from this family of Gold sequences by appending an additional '1'to the end of each sequence [31]. Two m-sequences of lengths (L_{seq} - 1) are represented by $\mathbf{s}$ and $\mathbf{g}$, where

$$\mathbf{s} = [s[0]\ s[1]\ \cdots\ s[L_{seq} - 2]]^{\mathcal{T}} \tag{2.8}$$

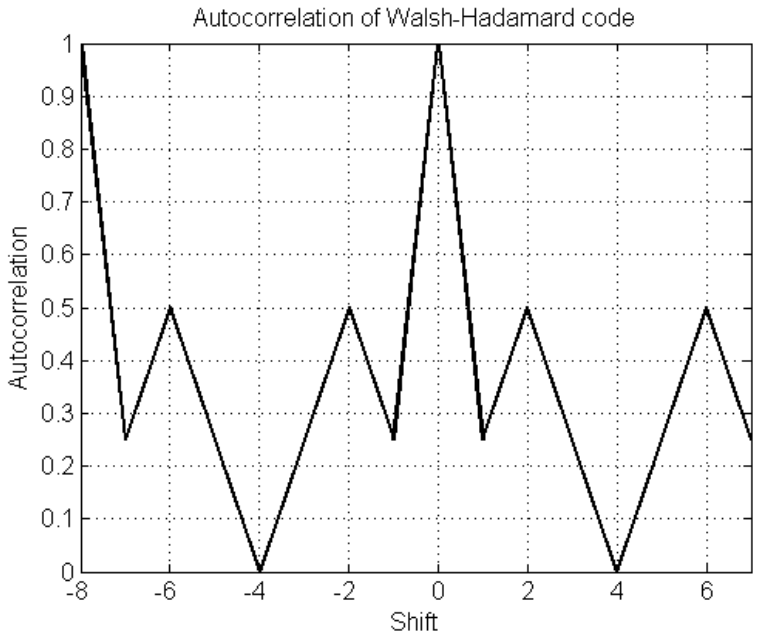

FIGURE 2.1: Modulus of the normalized periodic autocorrelation of a Walsh-Hadamard sequence of length $L_{seq} = 16$.

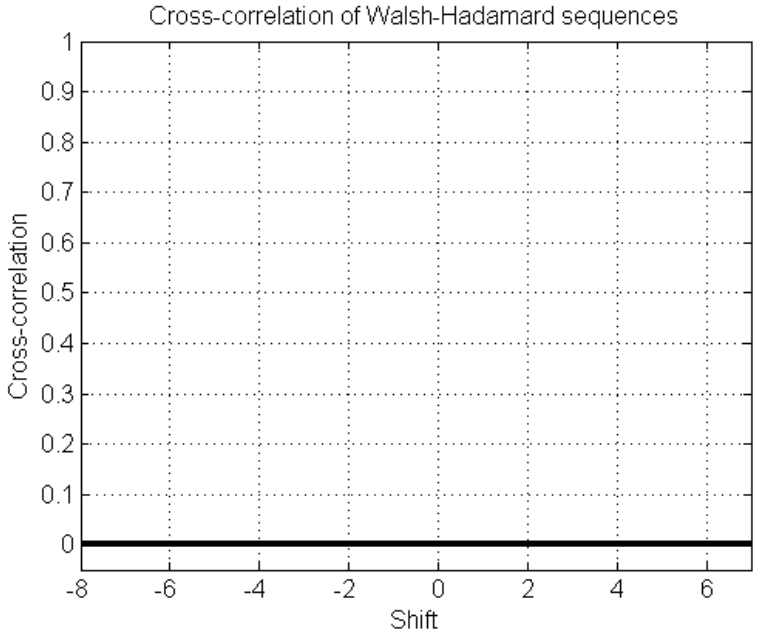

FIGURE 2.2: Modulus of the normalized periodic cross-correlation between two Walsh-Hadamard sequences of length $L_{seq} = 16$.

$$\mathbf{g} = [g[0]\ g[1]\ \cdots\ g[L_{seq} - 2]]^{\mathcal{T}} \tag{2.9}$$

The Gold construction method on these two sequences forms the set of sequences given by

$$\mathbf{c}_k = \begin{cases} \mathbf{s} \times T^k(\mathbf{g}), & for\ 0 \leq k < L_{seq} - 1 \\ \mathbf{s}, & for\ k = L_{seq} - 1 \\ 0, & otherwise \end{cases} \tag{2.10}$$

where $T^k(\mathbf{g})$ represents a cyclic shift of $\mathbf{g}$ by k shifts and '×' is the element-by-element multiplication. As shown in (2.10), the final member of the set is one of the original m-sequences, $\mathbf{s}$. The resulting sequence set is known as the Gold sequence set. If one performs

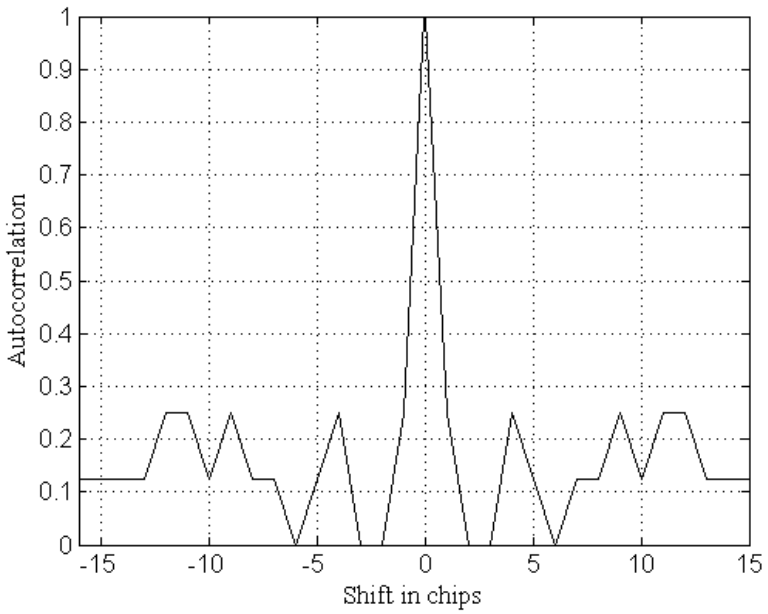

FIGURE 2.3: Modulus of the normalized periodic autocorrelation function of an orthogonal Gold sequence of length $L_{seq} = 32$.

the following three-step procedure on each of the constructed Gold sequences, orthogonal sequences are produced [31]:

1. Make the first chip of each sequence a '1'.
2. If the first chip of the sequence was already '1'and has not, therefore, been altered by step 1, then append a '-1'to the end of the sequence.
3. If the first chip of the sequence was a '-1'to begin with and has, therefore, been altered by step 1, then append a '1'to the end of the sequence.

Fig. 2.3 depicts the modulus of the normalized periodic autocorrelation function of an orthogonal Gold sequence, of length $L_{seq} = 32$. The modulus of the normalized periodic

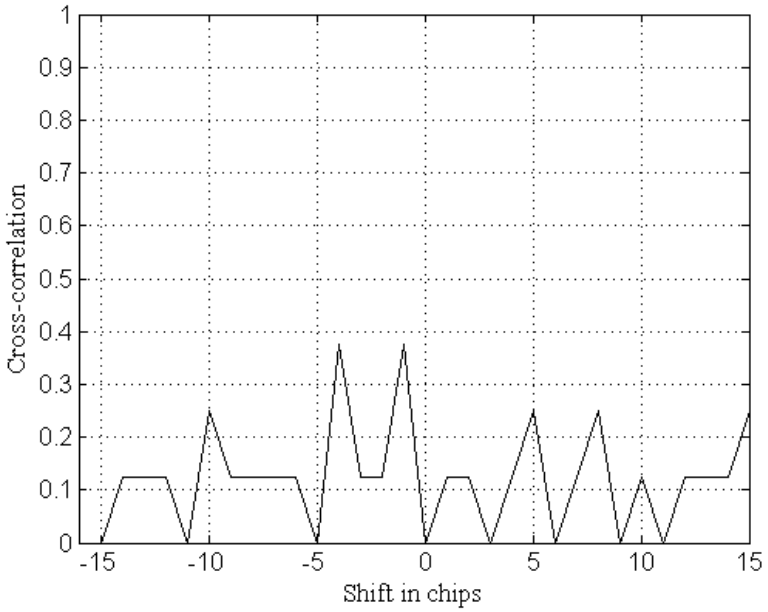

FIGURE 2.4: Modulus of the normalized periodic cross-correlation function between two orthogonal Gold sequences of length $L_{seq} = 32$.

cross-correlation function between two randomly selected Gold sequences of length $L_{seq} = 32$, in the same set, is shown in Fig. 2.4.

2.3 ZCZ SEQUENCES

Traditional orthogonal spreading codes [31], such as orthogonal Gold codes and Walsh-Hadamard codes, exhibit non-zero off-peak autocorrelations and cross-correlations, which limits the achievable performance, in asynchronous or quasi-synchronous scenarios. Consequently, to suppress both multipath interference and MUI, the sidelobes of the correlations should be as small as possible. ZCZ codes have the following two advantages over other orthogonal codes [49].

1. There is no interference between users separated by propagation delay differences that are within a zero correlation zone (interference-free window) of Z_0, and thus ZCZ codes reduce MUI in a quasi-synchronous uplink communication system.

2. Interference due to delayed replicas of each user's signal in a multipath channel will be eliminated, on condition that each user's delay spread is no bigger than the ZCZ length of Z_0.

The set of ZCZ codes is denoted as (L_{seq}, M_{seq}, Z_0)-ZCZ. For a sequence set $\{\mathbf{s}_q\}_{q=0}^{M_{seq}}$ with family size M_{seq}, and sequence length L_{seq}, the periodic correlation characteristics of ZCZ codes are defined as follows:

$$\Psi_{s,r}(\tau) = \sum_{l=0}^{L_{seq}-1} s_q[l]s_r^*[(l+\tau)mod(L_{seq})] = \begin{cases} \eta L_{seq}, & \tau = 0, \ r = s \\ 0, & \tau = 0, \ r \neq s \\ 0, & 0 \leq |\tau| \leq Z_0 \end{cases} \tag{2.11}$$

$$\eta = \frac{1}{L_{seq}} \sum_{l=0}^{L_{seq}-1} |s_r[l]| \leq 1 \tag{2.12}$$

where each sequence element $s_q[l]$ is a complex number and Z_0 is the ZCZ length in chips. The parameter $\eta \leq 1$, is only equal to one when every sequence element $s_q[l]$ has unit amplitude, otherwise $\eta < 1$. In [50], theoretical limits were derived for the ZCZ code length L_{seq}, family size M_{seq}, and zero correlation zone Z_0, as an extension of the Welch bound. For a given ZCZ length, the theoretical upper bound is given by

$$Z_0 \leq \frac{L_{seq}}{M_{seq}} - 1 \tag{2.13}$$

Equation (2.13) suggests that to obtain a large ZCZ length, the code length L_{seq} needs to be considerably larger than the family size M_{seq}. Thus, the desirable properties of these sequences come at the cost of supporting only a small number of users, compared to other orthogonal codes, such as Walsh-Hadamard codes. Various constructions for ZCZ sequences including binary, ternary and polyphase sequences have been proposed in the literature [32–37]. Binary ZCZ code constructions are given in [32–34]. These binary sequences achieve a ZCZ length of $Z_0 = L_{seq}/(2.M_{seq})$, which is lower than the upper bound in (2.13). Up to this point, no binary constructions have achieved a ZCZ length of larger than $Z_0 = L_{seq}/(2.M_{seq})$. Ternary sequence sets that reach the upper bound in (2.13) have been constructed in [51]. However, ternary sequence sets are undesirable because zeros are transmitted, resulting in non-constant modulus transmissions. Furthermore, the autocorrelation function of a ZCZ ternary sequence at zero-shift decreases in proportion to the number of zeros in the sequence (i.e. $\eta < 1$). This results in a lower BER performance when these sequences are applied to real synchronous CDMA communication systems. Quadriphase ZCZ sequence sets with $\eta = 1$ have been constructed in [37], using a recursive method and a perfect sequence. These sequence sets are said to be almost optimal and they achieve a ZCZ length of

$$Z_0 = \frac{7.L_{seq}}{8.M_{seq}} \tag{2.14}$$

In the next section, the almost optimal quadriphase sequence construction in [37] is detailed without proof.

2.3.1 Construction of quadriphase ZCZ sequences based on a perfect sequence

Let $\mathbf{a}_0 = [a[0] \ \cdots \ a[l-1]]^{\mathcal{T}}$ be a perfect sequence with an ideal autocorrelation function.

$$R_{\mathbf{a}_0} = \sum_{k=0}^{l-1} a[k]a^*[(k+\tau)mod(l)] = \begin{cases} E_{\mathbf{a}_0}, \ \tau = 0 \\ 0, \ otherwise \end{cases} \tag{2.15}$$

$$E_{\mathbf{a}_0} = \sum_{k=0}^{l-1} a[k]a^*[k] = \sum_{k=0}^{l-1} |a[k]|^2 \tag{2.16}$$

The perfect sequences $\mathbf{a}_i$ $(1 \leq i \leq l_1 - 1)$, of length $l = l_0 l_1$ are defined as follows.

$$\mathbf{a}_i = [a[il_0] \ a[il_0+1] \ \cdots \ a[l-1] \ a[0] \ \cdots \ a[il_0-1]]^{\mathcal{T}} \tag{2.17}$$

The $l_1 \times l_1$ unitary matrix is defined as

$$\mathbf{B}_n = \frac{1}{\sqrt{l_1}} \begin{pmatrix} b^n_{0,0} & b^n_{0,1} & \cdots & b^n_{0,l_1-1} \\ b^n_{1,0} & b^n_{1,1} & \cdots & b^n_{1,l_1-1} \\ \vdots & \vdots & \ddots & \vdots \\ b^n_{l_1-1,0} & b^n_{l_1-1,1} & \cdots & b^n_{l_1-1,l_1-1} \end{pmatrix} \tag{2.18}$$

A sequence set $\mathbf{S}_0$ with l_1 perfect sequences of length l is defined as follows

$$\mathbf{S}_0 = \{\mathbf{s}^0_0, \ldots, \mathbf{s}^0_{l_1-1}\} = \{\mathbf{a}_0, \ldots, \mathbf{a}_{l_1-1}\} \tag{2.19}$$

$$\mathbf{s}^0_i = [s[0]^{0,i} \ \cdots \ s[l-1]^{0,i}]^{\mathcal{T}}$$

$$= [a[il_0] \ a[il_0+1] \ \cdots \ a[l-1] \ a[0] \ \cdots \ a[il_0-1]]^{\mathcal{T}} \tag{2.20}$$

Using $\mathbf{B}_n$ and $\mathbf{S}_0$, a sequence set $\mathbf{S}_n$ is defined as

$$\mathbf{S}_n = \{\mathbf{s}^n_0, \ldots, \mathbf{s}^n_{l_1-1}\} \tag{2.21}$$

$$\mathbf{s}^n_0 = [s[0]^{n,i} \ \cdots \ s[ll^n_1 - 1]^{n,i}]^{\mathcal{T}} \tag{2.22}$$

where $s[j]^{n,i}$ is defined by the recursive process

$$s[j]^{n,i} = b^n_{i,(j)mod(l_1)} s[\lceil j/l_1 \rceil]^{n-1,(j)mod(l_1)} \tag{2.23}$$

By the above process one can obtain quadriphase ZCZ sequences $(ll^n_1, l_1, (l-2)l^{n-1}_1)$-ZCZ that are almost optimal.

2.3.1.1 Example

If one uses a perfect sequence of length $l = 16$, $l_0 = l_1 = 4$, given by

$$\mathbf{a}_0 = [1\ 1\ 1\ 1\ j\ -1\ -j\ 1\ -1\ 1\ -1\ 1\ -j\ -1\ j]^{\mathcal{T}} \tag{2.24}$$

then using the procedure described in the previous section, one obtains

$$\mathbf{a}_0 = [1\ 1\ 1\ 1\ j\ -1\ -j\ 1\ -1\ 1\ -1\ 1\ -j\ -1\ j]^{\mathcal{T}} \tag{2.25}$$

$$\mathbf{a}_1 = [1\ j\ -1\ -j\ 1\ -1\ 1\ -1\ 1\ -j\ -1\ j\ 1\ 1\ 1\ 1]^{\mathcal{T}} \tag{2.26}$$

$$\mathbf{a}_2 = [1\ -1\ 1\ -1\ 1\ -j\ -1\ j\ 1\ 1\ 1\ 1\ 1\ j\ -1\ -j]^{\mathcal{T}} \tag{2.27}$$

$$\mathbf{a}_3 = [1\ -j\ -1\ j\ 1\ 1\ 1\ 1\ 1\ j\ -1\ -j\ 1\ -1\ 1\ -1]^{\mathcal{T}} \tag{2.28}$$

Let the unitary matrix $\mathbf{B}_1$ (n=1) be defined as

$$\mathbf{B}_1 = \frac{1}{2}\begin{pmatrix} 1 & 1 & 1 & 1 \\ 1 & j & -1 & -j \\ 1 & -1 & 1 & -1 \\ 1 & -j & -1 & j \end{pmatrix} \tag{2.29}$$

Using the recursive procedure described in the previous section a (64,4,14)-ZCZ quadriphase

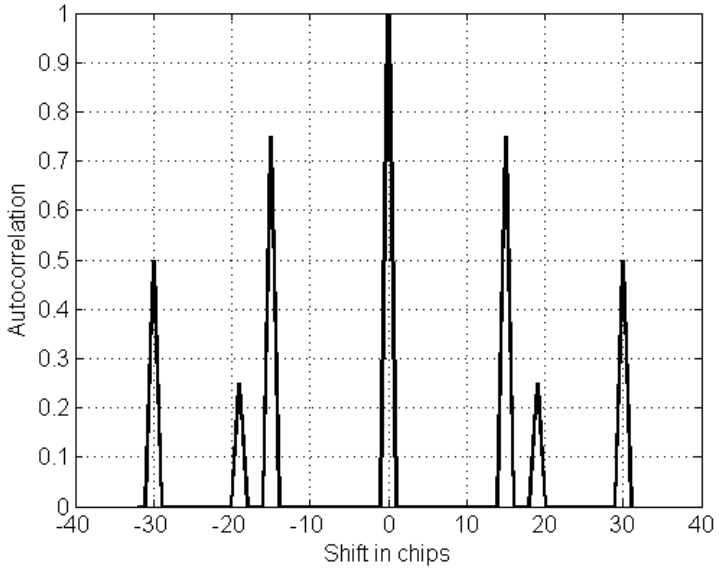

FIGURE 2.5: Modulus of the normalized periodic autocorrelation of a sequence in a (64,4,14)-ZCC quadriphase sequence set.

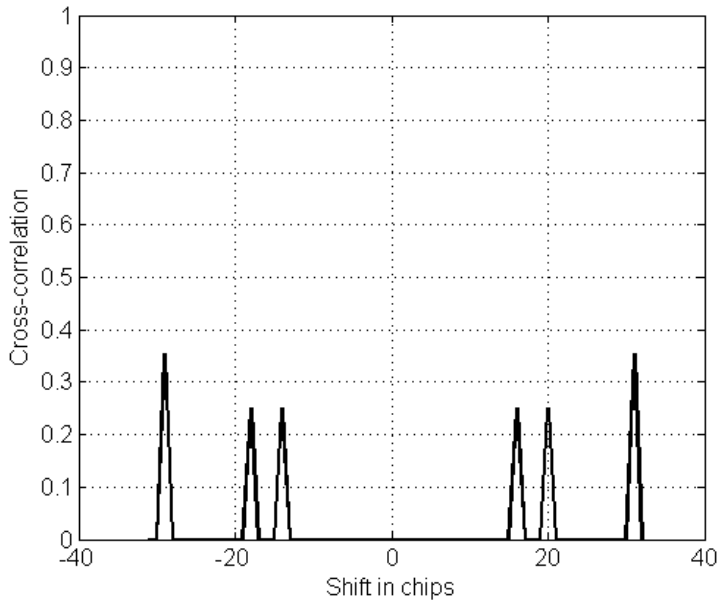

FIGURE 2.6: Modulus of the normalized periodic cross-correlation between two sequences in a (64,4,14)-ZCC quadriphase sequence set.

sequence set is constructed. The modulus of the normalized periodic autocorrelation of a (64,4,14)-ZCZ quadriphase sequence in the set is shown in Fig.2.5. The modulus of the normalized periodic cross-correlation between two quadriphase ZCZ sequences in the set is shown in Fig.2.6. From Fig. 2.5 and 2.6, one observes that the periodic auto and cross-correlation functions are ideal in an interference-free window of Z_0=14 chip shifts on either side of the zero shift.

CHAPTER THREE

ALGEBRAIC LINEAR CONSTELLATION PRECODING AND JOINT DETECTION

3.1 LINEAR NON-REDUNDANT CONSTELLATION PRECODING

Non-redundant linear constellation precoding (constellation rotation), is a way of achieving signal space diversity without sacrificing data rates [52–56]. It was originally developed for single-antenna transceivers with an interleaver [52] and later on also used for multi-antenna systems [56]. First, the basic idea behind constellation rotation is discussed in the next section,

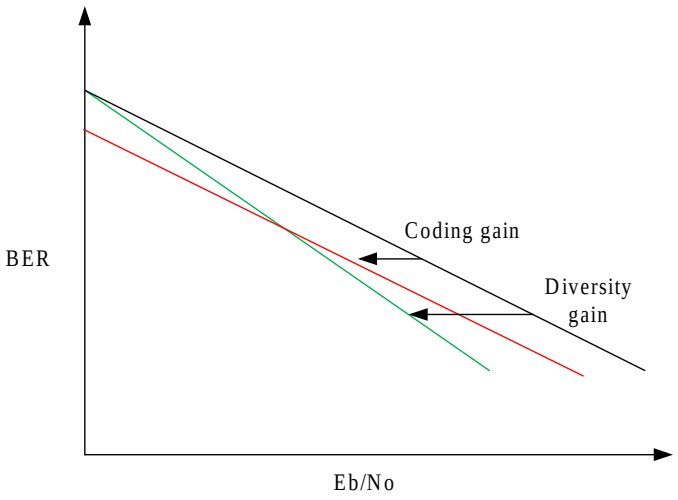

FIGURE 3.1: The effect of coding gain and diversity on the error-rate performance.

followed by some preliminaries from algebraic number theory. Finally, algebraic precoder constructions that maximize coding and diversity gains are explained. If the BER is plotted versus the signal-to-noise ratio (SNR) per bit on a log-log scale, the diversity order can be interpreted as the slope of the curve, whereas the coding advantage corresponds to the horizontal

shift of the curve. Fig. 3.1 highlights the differences between diversity gain and coding gain. From Fig. 3.1, the diversity order dominates the performance on the error-rate curve at medium to large SNR values.

3.1.1 Introduction to constellation rotations

The idea behind diversity achieving constellation rotations will be explained by means of an example. Consider the basic transmission system shown in Fig3.2. Assume a flat fading channel

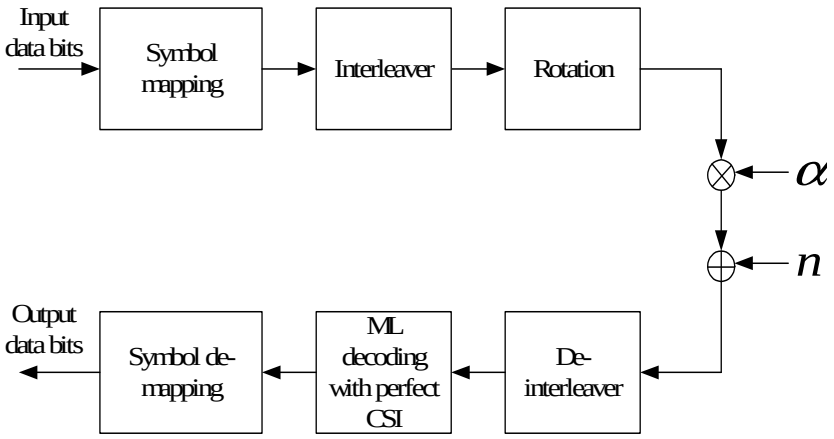

FIGURE 3.2: Basic transceiver with interleaving.

where α is the complex zero mean Gaussian fading coefficient. The fading coefficients are also

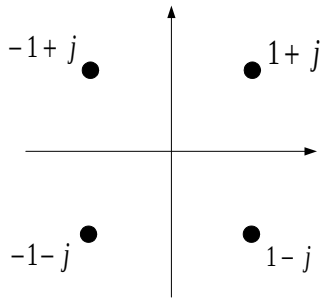

FIGURE 3.3: The figure shows a simple 4-QAM constellation.

assumed to be independent from one symbol to the next. It is further assumed that perfect channel state information (CSI) is available at the receiver, and thus the phase of the fading coefficients can be removed at the receiver. Thus each transmitted data symbol is scaled by a real, Rayleigh distributed fading coefficient. The data bits are mapped to 4-QAM symbols from the constellation depicted in Fig.3.3. The interleaver switches quadrature components of consecutive symbols, in order to ensure that the real and imaginary part of each symbol

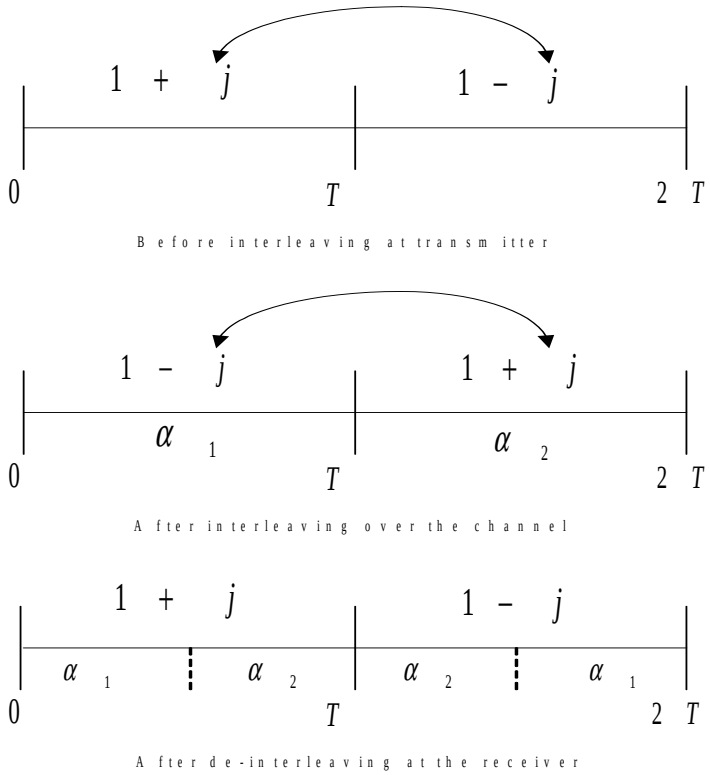

FIGURE 3.4: The figure shows the interleaving operation performed on the 4-QAM symbols over two symbol intervals.

experiences independent fading. The interleaving operation is illustrated over two symbol intervals for two arbitrarily selected 4-QAM symbols ($1 + j$ and $1 - j$) in Fig.3.4. Thus, the idea is to get each dimension of each symbol to experience independent fading. Suppose now that a fading of 0.5 affects the imaginary component and a fading of 1 affects the real component. The white dots represent the faded 4-QAM lattice constellation at the receiver in Fig.3.5. From

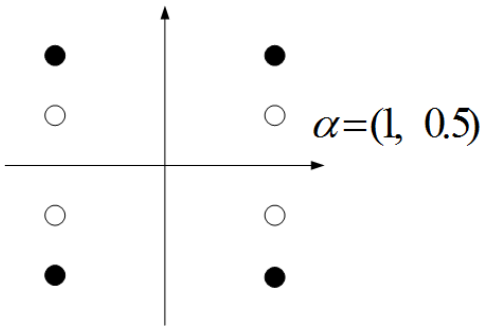

FIGURE 3.5: 4-QAM constellation with interleaving at the receiver.

Fig. 3.5, the deeper the fade gets in any one dimension, the more the symbols will tend to collapse on one another. Thus, the 4-QAM constellation with interleaving is said to have only

first-order signal space diversity [57, p. 10]. Consider now the rotated 4-QAM constellation with interleaving in Fig.3.6. It is again assumed that a fading of 0.5 affects the imaginary

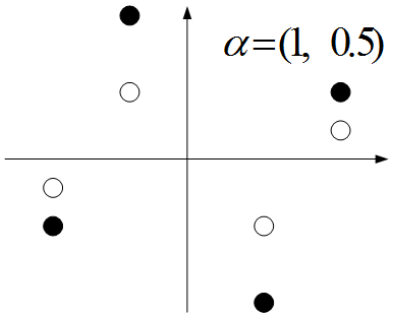

FIGURE 3.6: Rotated 4-QAM constellation with interleaving at the receiver.

component and a fading of 1 affects the real component. In the rotated version, where all coordinates are distinct, the fading in any one dimension will not cause the symbols to collapse on one another. Each symbol needs to fade in two dimensions in order to collapse on any other symbol. Thus, the constellation in Fig. 3.6 is said to have second order signal space diversity [57, p. 10] and is more resistant to noise, even in the presence of a deep fade. It is clear that any small rotation would be enough to obtain maximum signal space diversity, but in order to optimize the choice, one must select the one that will give the lowest probability of error. This depends on the minimum product distance or coding gain of the constellation. It was shown in [52, 53], that by increasing the diversity order of multi-dimensional constellations, it is possible to achieve the performance over a Gaussian channel. The rotation operation (precoding) for a block of symbols $\mathbf{s}$, can in general be written as a matrix multiplication

$$\mathbf{x} = \mathbf{M}_R\mathbf{s} \tag{3.1}$$

where $\mathbf{M}_R$ is the precoder (rotation matrix). Originally, the construction of these precoders was based on the parameterization of real, orthogonal matrices [56, 58]. These constructions are based on exhaustive search, and become infeasible for large size constellations. Constructions based on algebraic number theory, which lead to fading-resilient constellations, have also been proposed in the literature [52, 53, 55, 57]. These are available in closed form and achieve large coding gains. Only algebraic precoders are analyzed in this section in view of the optimal coding gain that they provide.

3.1.2 Algebraic number theory preliminaries

Some important definitions, facts and lemmas are necessary before detailing the construction of algebraic precoders, which are given in the list that follows. The definitions, facts and lemmas as well as their proofs' can be found in [53, 54, 59]. The definitions are given as follows:

1. *Cyclotomic polynomial*: If $P \in \mathbb{N}$, the P_{th} cyclotomic polynomial is defined as $\Phi_P(x) = \prod_{k\in\mathcal{K}}(x - e^{\frac{j2\pi k}{P}})$, where $\mathcal{K} = \{k : gcd(k, P) = 1 \text{ and } k \in [1, P)\}$ and $\phi(P)$ is its degree.

2. *Extension of an embedding*: If η is an embedding of $\mathbb{Q}(j)(\alpha)$ in $\mathbb{C}$ that fixes $\mathbb{Q}(j)$ in such a way that $\eta(z) = z$, $\forall\ z \in \mathbb{Q}(j)$, then η is called a $\mathbb{Q}(j)$-isomorphism of $\mathbb{Q}(j)(\alpha)$.

3. *Relative norm of a field*: Let $\alpha = \alpha_1, \ldots, \alpha_K$ denote the complex roots of the minimal polynomial of α over $\mathbb{Q}(j)$ and let η_m, $m = 1, \ldots, K$, be K distinct $\mathbb{Q}(j)$-isomorphisms of $\mathbb{Q}(j)(\alpha)$ such that $\eta_m(\alpha) = \alpha_m$. Consider $\beta \in \mathbb{Q}(j)(\alpha)$ and define the relative norm of β from the field $\mathbb{Q}(j)(\alpha)$ as $\mathcal{N}(\beta) = \mathcal{N}_{\frac{\mathbb{Q}(j)(\alpha)}{\mathbb{Q}(j)}}(\beta) = \prod_{m=1}^{K} \eta_m(\beta)$.

4. *Integral over* $\mathbb{Z}(j)$: An element β is said to be integral over $\mathbb{Z}(j)$, if β is a root of a monic polynomial with coefficients in $\mathbb{Z}(j)$. Clearly, every element in $\mathbb{Z}(j)$ is integral over $\mathbb{Z}(j)$.

The facts are given in the list that follows.

1. The polynomial $\Phi_P(x)$ is the minimal polynomial $m_{\alpha,\mathbb{Q}}(x)$ of $\alpha = \exp(\frac{j2\pi}{P})$ and $\Phi_P(\alpha^i) = 0$ for any $i \in \mathbb{Z}$ such that $gcd(i, P) = 1$.

2. If $K = 2^q$ where $q \in \mathbb{N}$, then the $m_{\alpha,\mathbb{Q}(j)}(x)$ of $\alpha = \exp(j2\pi/2^{q+2})$ is $x^K - j = 0$ with all distinct roots $\alpha_m = \alpha e^{\frac{j2\pi(m-1)}{K}}$ for $m = 1, \ldots, K$.

3. If $\mathbb{Q}(j)(\alpha)$ is a finite extension of the field $\mathbb{Q}(j)$ with degree denoted by $[\mathbb{Q}(j)(\alpha) : \mathbb{Q}(j)] = K$, then $\{1, \alpha, \ldots, \alpha^{K-1}\}$ forms a basis of $\mathbb{Q}(j)(\alpha)$ over $\mathbb{Q}(j)$.

4. The set of elements of $\mathbb{Q}(j)(\alpha)$, which are integral over $\mathbb{Z}(j)$, is a sub-ring of $\mathbb{Q}(j)(\alpha)$ containing $\mathbb{Z}(j)$.

5. If $\beta \in \mathbb{Q}(j)(\alpha)$ is integral over $\mathbb{Z}(j)$, then the relative norm of β from $\mathbb{Q}(j)(\alpha) \in \mathbb{Z}(j)$.

6. If P is an odd integer and $\alpha = e^{\frac{j2\pi}{P}}$ then $\mathbb{Q}(\alpha) \cap \mathbb{Q}(j) = \mathbb{Q}$.

7. If $gcd(p, q) = 1$ and $p, q \in \mathbb{N}$ then $\phi(pq) = \phi(p)\phi(q)$.

The following lemma's (proven in [54]) are also necessary and are given as follows.

- If $\phi(P) = 4q + 2$ for $q \in \mathbb{N}$, then $P \not\equiv 0 \ (mod\ 4)$.
- If $P \not\equiv 0 \ (mod\ 4)$, then the $m_{\alpha,\mathbb{Q}(j)}(x)$ of $\alpha = \exp(j2\pi/P)$ is $\Phi_P(x)$ and its degree is $\phi(P)$.
- All roots of $m_{\alpha,\mathbb{Q}(j)}(x)$ of $\alpha = \exp(j2\pi/P)$ with $P \in \mathbb{N}$ have unit modulus.

3.1.3 Precoder design

The optimal precoder design is now detailed for any $K \times 1$ symbol block $\mathbf{s}$, with symbols taken from some constellation $\mathcal{A}$ (i.e. PSK or QAM). The $K \times K$ precoder can be expressed as $\mathbf{\Theta}$. The design criteria for $\mathbf{\Theta}$ can be summarized as follows:

- *Maximum Diversity Gain Criterion.* Design a $K \times K$ matrix $\mathbf{\Theta}$ with $\text{tr}(\mathbf{\Theta}\mathbf{\Theta}^{\mathcal{H}}) = K$ such that $\forall \in [1, K]$

$$|\theta_k^{\mathcal{T}}(\mathbf{s} - \mathbf{s}')| \neq 0, \ \forall \mathbf{s} \neq \mathbf{s}' \in \mathcal{A}^K \tag{3.2}$$

  where $\theta_k^{\mathcal{T}}$ denotes the k_{th} row of $\mathbf{\Theta}$; and $\mathbf{s}$ and $\mathbf{s}'$ are two $K \times 1$ vectors with elements drawn for $\mathcal{A}$.

- *Maximum Coding Gain Criterion.* Design a $K \times K$ matrix $\mathbf{\Theta}$ with $\text{tr}(\mathbf{\Theta}\mathbf{\Theta}^{\mathcal{H}}) = K$ to maximize

$$\xi_{lcp} = \min_{\forall \mathbf{s} \neq \mathbf{s}'} \prod_{k=1}^{K} |\theta_k^{\mathcal{T}}(\mathbf{s} - \mathbf{s}')|^2 \tag{3.3}$$

If the coding gain criterion is satisfied, the diversity gain criterion will automatically be satisfied. The precoder design applies to any K, and quadrature amplitude modulation (QAM), binary phase shift keying (BPSK) and quaternary phase shift keying (QPSK) constellations. The matrix $\mathbf{\Theta}$ can in general be written as a Vandermonde matrix

$$\mathbf{\Theta} = \frac{1}{\beta} \begin{pmatrix} 1 & \alpha_1 & \cdots & \alpha_1^{K-1} \\ 1 & \alpha_2 & \cdots & \alpha_2^{K-1} \\ \vdots & \vdots & & \vdots \\ 1 & \alpha_K & \cdots & \alpha_K^{K-1} \end{pmatrix} \tag{3.4}$$

where β is a normalization factor chosen to impose the power constraint $tr(\Theta\Theta^{\mathcal{H}}) = K$. The selection of parameters $\{\alpha_k\}_{k=1}^K$ depends on K as follows.

- If $K \in \mathcal{K}_1 = \{\phi(P) : P \neq 0 \ (mod\ 4)\}$ with $\phi(P)$ denoting the number of positive integers that are less than and relatively prime to P, then $\{\alpha_k\}_{k=1}^K$ are roots of the equation $\psi_P(x) =$

0, where $\psi_P(x)$ is defined as $\psi_P(x) = \prod_{p\in\mathcal{P}}(x - e^{\frac{j2\pi p}{P}})$, with $\mathcal{P} = \{p : gcd(p, P) = 1 \text{ and } p \in [1, P)\}$.

- If $K \in \mathcal{K}_2 = \{2^p : p \in \mathbb{N}\}$ with $\mathbb{N}$ denoting the set of positive integers, $\{\alpha_k\}_{k=1}^{K}$ are chosen to be roots of $x^K - j = 0$. In this case, $\mathbf{\Theta}$ is a unitary matrix and can be compactly expressed as

$$\mathbf{\Theta} = \mathbf{F}_K diag(1, \alpha_1, \ldots, \alpha_1^{K-1}) \tag{3.5}$$

It is important to note that if K is not a power of 2, then $\mathbf{\Theta}$ is not unitary. Unitary constellation precoding offers a distinct advantage over non-unitary $\mathbf{\Theta}$ options: a unitary $\mathbf{\Theta}$ corresponds to a rotation and preserves distances among the K-dimensional constellation points. A non-unitary $\mathbf{\Theta}$ draws some pairs of constellation points closer (and some farther). This distance-preserving property of unitary precoders also guarantees that if such rotated constellations are to be used over an AWGN channel, the performance will remain invariant. It was proven in [54] that if $K \in \mathcal{K}_1 \cup \mathcal{K}_2$, the maximum possible diversity and coding gain is achieved. If K is not a power of 2 then there is a possible 30% loss in coding gain [55]. Unitary design examples are given for $K = 2, 4$ and 8 in Table 3.1.

TABLE 3.1: Design examples of a unitary Θ when $K = 2, 4$ and 8.

K	α_1	α_2	α_3	α_4	α_5	α_6	α_7	α_8
2	$e^{\frac{-j\pi}{4}}$	$e^{\frac{-j5\pi}{4}}$						
4	$e^{\frac{-j\pi}{8}}$	$e^{\frac{-j5\pi}{8}}$	$e^{\frac{-j9\pi}{8}}$	$e^{\frac{-j13\pi}{8}}$				
8	$e^{\frac{-j\pi}{16}}$	$e^{\frac{-j5\pi}{16}}$	$e^{\frac{-j9\pi}{16}}$	$e^{\frac{-j13\pi}{16}}$	$e^{\frac{-j17\pi}{16}}$	$e^{\frac{-j21\pi}{16}}$	$e^{\frac{-j25\pi}{16}}$	$e^{\frac{-j29\pi}{16}}$

3.2 JOINT DETECTION RECEIVERS FOR CDMA SIGNALS

Generally, precoding necessitates the use of joint detection at the receiver to exploit diversity and coding gains. Joint detection receivers are derivatives of the well known single-user equalizers, used to equalize signals distorted by ISI in multipath channels [45, p. 81]. The joint detection algorithms considered in this section can be used as single-user equalizers or as multi-user detectors [60], depending on the application. First, the basic MF detector (or single-user detector) is considered [1, p. 911], [45, p. 99] followed by other linear joint detectors, namely the ZF block linear detector [45, p. 102] and the MMSE block linear detector

[45, p. 104]. Finally, optimal ML detection is considered [1, p. 906], followed by almost optimal ML sphere decoding [57, p. 25], [42–44]. Some advantages of joint detection are given as follows [45, p. 123]:

- Joint detection combats ISI and MUI in frequency selective channels. Thus, the receiver is near-far resistant and the output signal of the receiver does not require further equalization.
- All the users' signals are detected simultaneously, which makes joint detection especially useful for base station receivers.

The disadvantages are listed as follows

- For asynchronous transmissions the complexity of the joint detection algorithms increase.
- Channel estimation is required at the receiver to do joint detection, which requires the use of training sequences or a mid-amble for channel estimation. This results in a reduction in data rate and capacity.

In the analysis of the joint detectors considered in this section, two assumptions are made:

1. Only synchronous transmissions are considered.
2. Perfect CSI is available at the receiver but not at the transmitter.

3.2.1 Linear joint detectors

3.2.1.1 MF detector

The MF detector is a filter that maximizes the SNR at the required sampling instant at its output for a given received waveform. Consider the block diagram of a simple transmission scheme given in Fig. 3.7. The received signal at the input to the joint receiver can be expressed as

$$y_i = (b_i * d_i) + n_i \tag{3.6}$$

where y_i is the result of convolution between the data samples, d_i, and the channel impulse response (CIR), b_i, plus the corruption due to the AWGN, n_i. The symbol $*$ denotes the convolution operation. Following the approach in [45, p. 99], the z-transforms of d_i, b_i, y_i and n_i can be expressed as

$$Y(z) = B(z)D(z) + N(z) \tag{3.7}$$

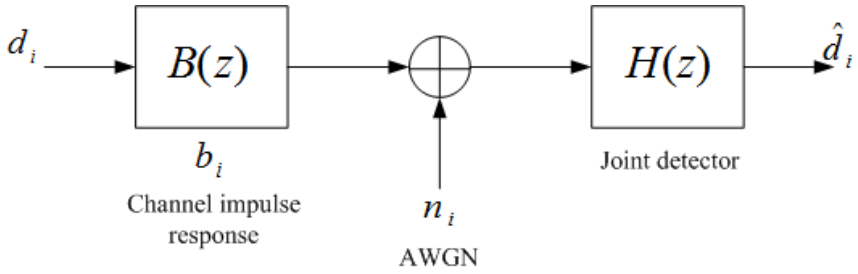

FIGURE 3.7: Block diagram of a simple transmission scheme.

and the z-transform of the data estimates $\hat{d}_i$ can be expressed as

$$\hat{D}(z) = H(z)B(z)D(z) + H(z)N(z) \tag{3.8}$$

where $H(z)$ is the z-transform of the MF detector. Assuming that the data elements d_i are uncorrelated with a variance of σ_s^2, the power spectral density of the signal can be expressed as

$$\Upsilon = |D(z)|^2|H(z)B^*(z)|^2 = \sigma_s^2|H(z)B^*(z)|^2 \tag{3.9}$$

The PSD of the noise component of $\hat{D}(z)$ (i.e. $H(z)N(z)$) can be expressed as $\frac{N_0}{2}|H(z)|^2$ where $\frac{N_0}{2}$ is the double-sided PSD of white Gaussian noise. The SNR is thus given by

$$SNR = \frac{\sigma_s^2|H(z)B^*(z)|^2}{\frac{N_0}{2}|H(z)|^2} \tag{3.10}$$

The Schwartz inequality [45] states

$$|H(z)B^*(z)|^2 \leq |H(z)|^2|B(z)|^2 \tag{3.11}$$

Thus, in order to maximize the SNR at the filter output (i.e. $|H(z)B^*(z)|^2 \leq |H(z)|^2|B(z)|^2$) the following must hold:

$$H(z) = cB^*(z) \tag{3.12}$$

where $c \neq 0$ is a scalar constant. In matrix form $H(z) = B^*(z)$ is represented by the $K \times K$ matrix $\mathbf{H} = \mathbf{B}^{*\mathcal{T}} = \mathbf{B}^{\mathcal{H}}$ and the $K \times 1$ vector of signal estimates d_i can be expressed as

$$\hat{\mathbf{d}} = \mathbf{B}^{\mathcal{H}}\mathbf{B}\mathbf{d} + \mathbf{B}^{\mathcal{H}}\mathbf{n} \tag{3.13}$$

where $\mathbf{B}$ is the CIR matrix, $\mathbf{n}$ is a column vector of the AWGN samples and $\mathbf{d}$ is a column vector of the transmitted data samples. The resultant vector $\hat{\mathbf{d}}$ is sent to a hard decision block in order to detect the corrupted symbols.

3.2.1.2 ZF block linear detector

The received signal column vector of length K, at the input to the joint detector, can be expressed as

$$\mathbf{y} = \mathbf{A}\mathbf{d} + \mathbf{n} \tag{3.14}$$

where $\mathbf{d}$ is a $K \times 1$ vector of symbols taken from some constellation $\mathcal{A}$, $\mathbf{A}$ is the $K \times K$ combined channel response (precoder and CIR) and $\mathbf{n}$ is the $K \times 1$ Gaussian noise vector. The covariance of the Gaussian noise vector is given by $\frac{N_0}{2}\mathbf{R}_s$. The joint probability density function of $\mathbf{y}$ conditioned on $\mathbf{d}$ is given as [45, p. 103]

$$p(\mathbf{y}|\mathbf{d}) = \frac{1}{\sqrt{(N_0\pi)^K det(\mathbf{R}_s)}} \exp(-\frac{1}{N_0}(\mathbf{y} - \mathbf{A}\mathbf{d})^{\mathcal{H}}\mathbf{R}_s^{-1}(\mathbf{y} - \mathbf{A}\mathbf{d})) \tag{3.15}$$

The best estimate of $\mathbf{d}$ is the one that minimizes the likelihood function

$$\Lambda(\mathbf{d}) = (\mathbf{y} - \mathbf{A}\mathbf{d})^{\mathcal{H}}\mathbf{R}_s^{-1}(\mathbf{y} - \mathbf{A}\mathbf{d}) \tag{3.16}$$

The result of this minimization yields $\hat{\mathbf{d}} = \mathbf{A}^{-1}\mathbf{y}$. If $\mathbf{n}$ is a vector of zero mean independent Gaussian noise samples, $\hat{\mathbf{d}}$ can also be expressed as

$$\hat{\mathbf{d}} = (\mathbf{A}^{\mathcal{H}}\mathbf{A})^{-1}\mathbf{A}^{\mathcal{H}}\mathbf{y} \tag{3.17}$$

The resultant vector $\hat{\mathbf{d}}$ is sent to a hard decision block in order to detect the corrupted symbols. This detector is known as the ZF detector or the de-correlating detector (when used as a multi-user detector). The ZF detector forces the ISI and MUI to zero. However, the removal of ISI and MUI is performed at the expense of noise enhancement. The noise at the output of the estimator is increased compared to the noise at the input to the estimator, hence resulting in SNR degradation [45, p. 104].

3.2.1.3 MMSE block linear detector

The $K \times 1$ received data vector is expressed as

$$\mathbf{y} = \mathbf{A}\mathbf{d} + \mathbf{n} \tag{3.18}$$

The MMSE block detector minimizes the simple quadratic form [45, p. 105]:

$$\begin{aligned} Q(\hat{\mathbf{d}}) &= E[(\mathbf{d} - \hat{\mathbf{d}})^{\mathcal{H}}(\mathbf{d} - \hat{\mathbf{d}})] \\ &= E[(\mathbf{d} - \mathbf{M}\mathbf{y})^{\mathcal{H}}(\mathbf{d} - \mathbf{M}\mathbf{y})] \end{aligned} \tag{3.19}$$

where $\hat{\mathbf{d}} = \mathbf{My}$. It is assumed that $K \times K$ matrix $\mathbf{M}$ is the MMSE estimator. In order to minimize the mean squared error, the error vector $\mathbf{e} = \mathbf{d} - \hat{\mathbf{d}}$ has to be set orthogonal (by the MMSE detector) to the detector's $K \times 1$ input vector $\mathbf{y}$. This implies that

$$E[(\mathbf{d} - \hat{\mathbf{d}})\mathbf{y}^{\mathcal{H}}] = \mathbf{0}_{K\times K} \tag{3.20}$$

$$E[(\mathbf{dy}^{\mathcal{H}} - \mathbf{Myy}^{\mathcal{H}})] = \mathbf{0}_{K\times K} \tag{3.21}$$

$$E[(\mathbf{dy}^{\mathcal{H}})] - \mathbf{M}E[\mathbf{yy}^{\mathcal{H}}] = \mathbf{0}_{K\times K} \tag{3.22}$$

$$\mathbf{R}_{dy} - \mathbf{MR}_{y} = \mathbf{0}_{K\times K} \tag{3.23}$$

$$\therefore \ \mathbf{M} = \mathbf{R}_{dy}\mathbf{R}_{y}^{-1} \tag{3.24}$$

where $\mathbf{R}_{dy} = E[\mathbf{dy}^{\mathcal{H}}]$ and $\mathbf{R}_{y} = E[\mathbf{yy}^{\mathcal{H}}]$. $\mathbf{R}_{dy}$ can be expressed as

$$\begin{aligned}\mathbf{R}_{dy} &= E[\mathbf{d}(\mathbf{Ad} + \mathbf{n})^{\mathcal{H}}] \\ &= E[\mathbf{dd}^{\mathcal{H}}\mathbf{A}^{\mathcal{H}} + \mathbf{dn}^{\mathcal{H}}]\end{aligned} \tag{3.25}$$

If the transmitted data vector, $\mathbf{d}$, and the noise vector, $\mathbf{n}$, are uncorrelated with each other (i.e. $E[\mathbf{dn}^{\mathcal{H}}] = 0$), one arrives at:

$$\mathbf{R}_{dy} = \mathbf{R}_{d}\mathbf{A}^{\mathcal{H}} \tag{3.26}$$

where $\mathbf{R}_{d} = E[\mathbf{dd}^{\mathcal{H}}]$. The matrix $\mathbf{R}_{y}$ is expressed as

$$\mathbf{R}_{y} = \mathbf{AR}_{d}\mathbf{A}^{\mathcal{H}} + \mathbf{R}_{s} \tag{3.27}$$

where $\mathbf{R}_{s}$ is the covariance matrix of the noise. Substituting equations (3.26) and (3.27) into equation (3.24), one obtains

$$\mathbf{M} = (\mathbf{A}^{\mathcal{H}}\mathbf{R}_{s}^{-1}\mathbf{A} + \mathbf{R}_{d}^{-1})^{-1}\mathbf{A}^{\mathcal{H}}\mathbf{R}_{s}^{-1} \tag{3.28}$$

If the noise samples are uncorrelated with each other and have a variance of σ_n^2 and the transmitted data symbols are also uncorrelated with each other and have a variance of σ_s^2 then $\mathbf{M}$ is expressed as [45, p. 108]

$$\mathbf{M} = (\mathbf{A}^{\mathcal{H}}\mathbf{A} + \frac{\sigma_n^2}{\sigma_s^2}\mathbf{I}_K)\mathbf{A}^{\mathcal{H}} \tag{3.29}$$

ISI and MUI are still present at the MMSE detector output because this technique does not seek to eliminate the ISI and MUI at the cost of noise amplification. Instead, it attempts to achieve a balance between the different types of data corruption in order to minimize the mean squared estimation error [45, p. 108]. The MMSE block linear detector and the ZF block linear detector were shown to have similar complexities in terms of additions and multiplications in [45, p. 113].

3.2.2 ML detection

Consider ML detection for the received signal vector

$$\mathbf{y} = \mathbf{A}\mathbf{d} + \mathbf{n} \tag{3.30}$$

3.2.2.1 Optimal ML detection

The optimal detector is the maximum-likelihood receiver that yields the optimal estimate of the $K \times 1$ transmitted data vector, $\mathbf{d}$ from

$$\hat{\mathbf{d}}_{opt} = \arg\{\min_{\mathbf{d}}\{\| \mathbf{y} - \mathbf{A}\mathbf{d} \|^2\}\} \tag{3.31}$$

which can also be expressed as

$$\hat{\mathbf{d}}_{opt} = \arg\{\min_{\mathbf{d}}\{ \mathbf{d}^{\mathcal{H}}\mathbf{A}^{\mathcal{H}}\mathbf{A}\mathbf{d} - 2real(\mathbf{d}^{\mathcal{H}}\mathbf{A}^{\mathcal{H}}\mathbf{y}) \}\} \tag{3.32}$$

Only the second term on the right-hand side of (3.32) depends on the received signal vector $\mathbf{y}$. However, it is pre-multiplied by $\mathbf{A}^{\mathcal{H}}$, where the product is nothing but the output of the MF. Hence, MF outputs represent sufficient statistics to perform maximum likelihood detection. Exhaustive search ML detection has a complexity on the order of $\mathcal{O}(|\mathcal{A}|^K)$ [1, p. 908], where $|\mathcal{A}|$ is the cardinality of the constellation alphabet.

3.2.2.2 Near optimal ML sphere decoding

The received signal column vector of length K, at the input to the joint detector, can be expressed as

$$\mathbf{y} = \mathbf{A}\mathbf{d} + \mathbf{n} \tag{3.33}$$

The principle of the sphere decoding algorithm is to search for the closest lattice point to the received signal $\mathbf{y}$, within a sphere of radius C_r, centred at the received signal [57, p. 25], [42]. The key idea that makes the sphere decoder efficient is that the number of lattice (constellation) points which can be found inside a sphere is a lot smaller than the number of points within a hypercube containing the hypersphere as the dimension of the space grows. Fig. 3.8 illustrates the idea behind sphere decoding. The white circle represents the multi-dimensional received signal point. The black circles represent all the possible multi-dimensional transmitted signal points. The choice of C_r is absolutely crucial to the speed of the algorithm. In practice, C_r can be adjusted according to the noise (and eventually the fading) variance [57, p. 33]. When

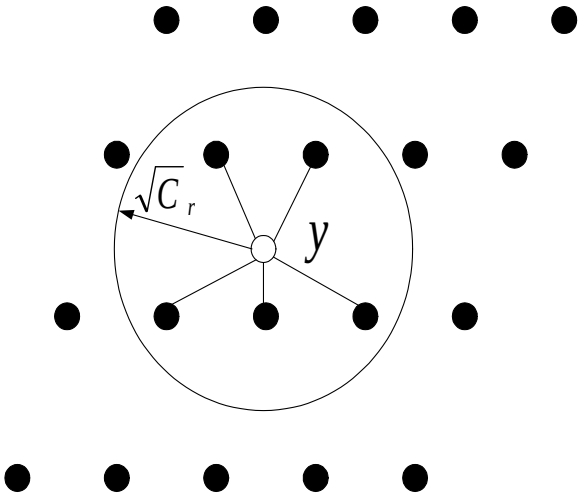

FIGURE 3.8: The figure illustrates the idea behind sphere decoding.

a failure is detected, one can either declare an erasure on the detected symbol, or increase C_r. One can write the received signal vector as

$$\begin{aligned}\acute{\mathbf{y}} &= [real(\mathbf{y}^{\mathcal{T}})\ imag(\mathbf{y}^{\mathcal{T}})] \\ &= \acute{\mathbf{d}}\begin{pmatrix} real(\mathbf{A}^{\mathcal{T}}) & imag(\mathbf{A}^{\mathcal{T}}) \\ -imag(\mathbf{A}^{\mathcal{T}}) & real(\mathbf{A}^{\mathcal{T}}) \end{pmatrix} + \acute{\mathbf{n}} \\ &= \acute{\mathbf{d}}\mathbf{M}_H + \acute{\mathbf{n}} \end{aligned} \tag{3.34}$$

where $\acute{\mathbf{d}} = [real(\mathbf{d}^{\mathcal{T}})\ imag(\mathbf{d}^{\mathcal{T}})] \in \mathbb{Z}^{2K}$ and $\acute{\mathbf{n}} = [real(\mathbf{n}^{\mathcal{T}})\ \ imag(\mathbf{n}^{\mathcal{T}})] \in \mathbb{R}^{2K}$. Thus, one can represent $\mathbf{y}$ as a lattice sphere packing [42], and use the sphere decoder for almost optimal detection. The problem is to solve the following:

$$\min_{\acute{\mathbf{x}}\in\Lambda} \|\acute{\mathbf{y}} - \acute{\mathbf{x}}\|^2 = \min_{\mathbf{w}\in\acute{\mathbf{y}}-\Lambda} \|\mathbf{w}\|^2 \tag{3.35}$$

where $\acute{\mathbf{x}} = \acute{\mathbf{d}}\mathbf{M}_H$ and $\Lambda = \{\acute{\mathbf{d}}\mathbf{M}_H \mid \acute{\mathbf{d}} \in \mathbb{Z}^{2K}\}$. One searches for the shortest vector $\mathbf{w}$ in the translated lattice $\acute{\mathbf{y}} - \Lambda$ in the $2K$-dimensional Euclidean space $\mathbb{R}^{2K}$. The vector $\acute{\mathbf{y}}$ can be expressed as $\acute{\mathbf{y}} = \mathbf{u}\mathbf{M}_H$ with $\mathbf{u} = [u[0] \cdots u[2K-1]] \in \mathbb{R}^{2K}$ and $\mathbf{w} = \mathbf{e}\mathbf{M}_H$, where $\mathbf{e} = \mathbf{u} - \acute{\mathbf{d}} = [e[0] \cdots e[2K-1]] \in \mathbb{R}^{2K}$. The solution to $\|\mathbf{w}\|^2$ can be expressed as

$$\|\mathbf{w}\|^2 = \mathbf{e}\mathbf{M}_H\mathbf{M}_H^{\mathcal{T}}\mathbf{e}^{\mathcal{T}} = \mathbf{e}\mathbf{G}_H\mathbf{e}^{\mathcal{T}} \leq C_r \tag{3.36}$$

The Cholesky factorization of the matrix $\mathbf{G}_H$ yields $\mathbf{G}_H = \mathbf{R}_H^{\mathcal{T}}\mathbf{R}_H$, where $\mathbf{R}_H$ is an upper triangular matrix. Then

$$\|\mathbf{w}\|^2 = \mathbf{e}\mathbf{R}_H^{\mathcal{T}}\mathbf{R}_H\mathbf{e}^{\mathcal{T}} = \sum_{i=0}^{2K-1}\left(r_{i,i}e[i] + \sum_{j=i+1}^{2K-1} r_{i,j}e[j]\right)^2 \leq C_r \tag{3.37}$$

where $r_{i,j}$ is the element in the $(i+1)_{th}$ row and $(j+1)_{th}$ column of $\mathbf{R}_H$. Substituting $q_{i,i} = r_{i,i}^2$ for $i = 0, \ldots, 2K-1$ and $q_{i,j} = \frac{r_{i,j}}{r_{i,i}}$ for $i = 0, \ldots, 2K-1$ and $j = i+1, \ldots, 2K-1$, one can write

$$\|\mathbf{w}\|^2 = \sum_{i=0}^{2K-1} q_{i,i} b[i]^2 \leq C_r \tag{3.38}$$

where

$$b[i] = e[i] + \sum_{j=i+1}^{2K-1} q_{i,j} e[j] \quad i = 0, \ldots, 2K-1 \tag{3.39}$$

The sphere decoding process can be summarized using the flow chart in Fig. 3.9. Sphere

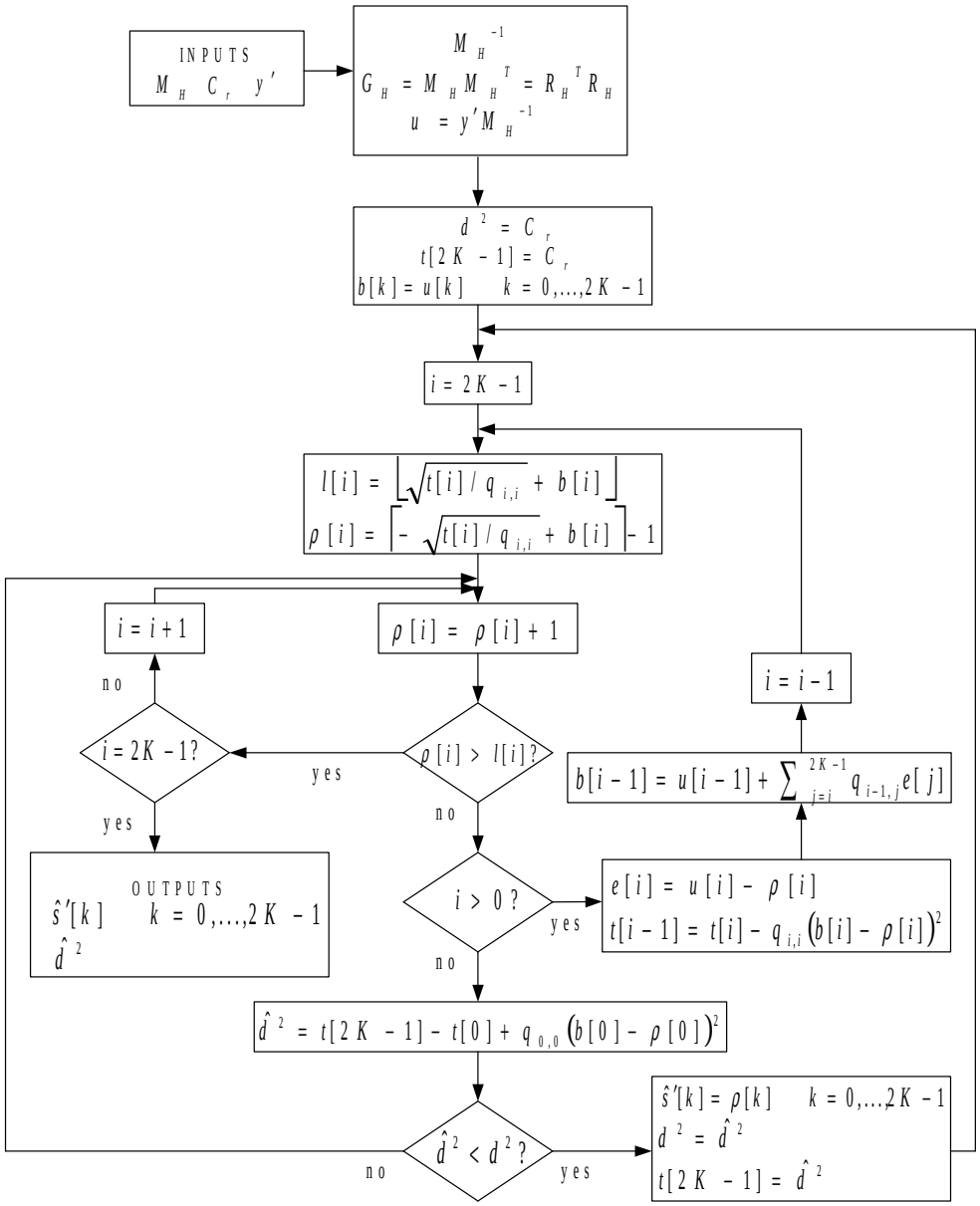

FIGURE 3.9: The sphere decoding process.

decoding complexity is independent of the underlying constellation size, which is very useful for high data rate transmission. The overall complexity of sphere decoding is in the order of $O(K^{\alpha})$, where $3 \leq \alpha \leq 4$ [43, 44].

CHAPTER FOUR

MIMO CHANNEL MODEL

In this section, the triply selective discrete time MIMO channel model proposed in [40] is briefly discussed. The model is used for BER simulations in Chapter 7.

4.1 MIMO CHANNEL DESCRIPTION

Consider the wideband MIMO wireless channel shown in Fig. 4.1, which contains M_T transmit antennas and M_R receive antennas. The time-invariant impulse responses of the transmit and receive filter for each transmit and receive antenna are denoted by $p_T[t]$ and $p_R[t]$, respectively, and both are normalized with energy of unity. Let $g_{m,n}[t,\tau]$ be the time-varying impulse response of the $(m,n)_{th}$ sub-channel connecting the n_{th} transmit antenna and the m_{th} receive antenna, where $g_{m,n}[t,\tau]$ is defined as the response at time t to an impulse applied to the sub-channel at time $t-\tau$ [40]. The symbol $v_m[t]$ is the zero-mean complex-valued white Gaussian noise with a two-sided power spectral density N_0. The symbol $s_n[k]$ is transmitted from the n_{th} transmit antenna at a symbol period of T_{sym} at time instant k. The received signal $y_m[t]$ at the m_{th} receive antenna is sampled at a sampling period of T_s, where $T_s = \frac{T_{sym}}{\gamma}$. If $\gamma = 1$, then the sampling rate at the receiver is equal to the symbol rate at the transmitter. The combined impulse response of the $(m,n)_{th}$ sub-channel is expressed as

$$h_{m,n}[t,\tau] = p_R[\tau] * g_{m,n}[t,\tau] * p_T[\tau] \tag{4.1}$$

The received signal at receive antenna m can be expressed as

$$y_m[t] = \sum_{n=1}^{M_T} \sum_{k=-\infty}^{\infty} s_n[k] h_{m,n}[t, t-kT_{sym}] + z_m[t] \tag{4.2}$$

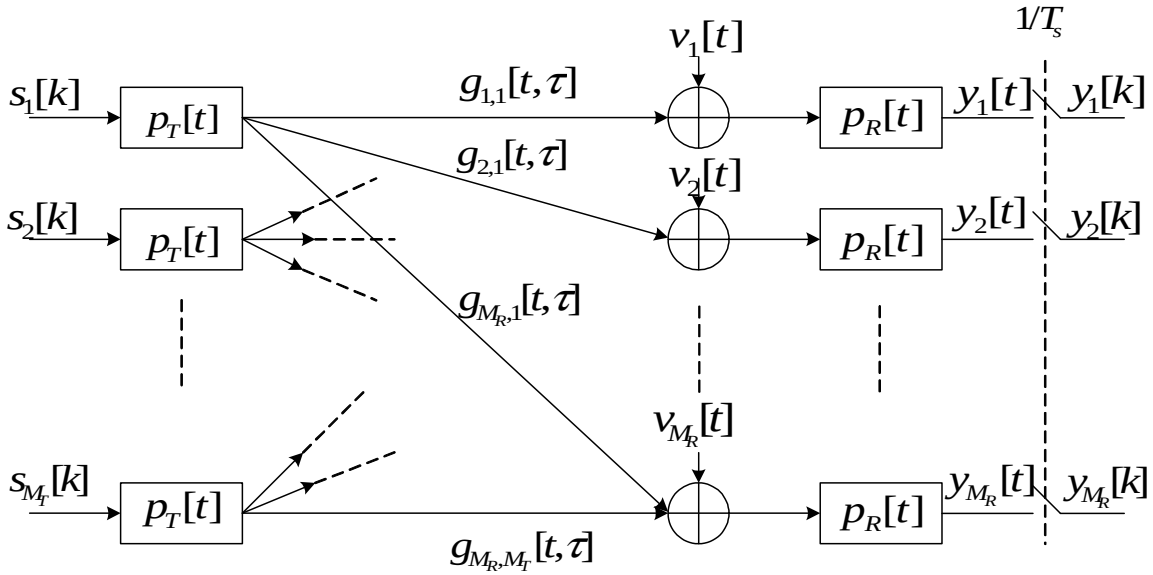

FIGURE 4.1: MIMO wireless channel model.

where $z_m[t] = v_m[t] * p_R[t]$ and $v_m[t]$ is the zero-mean complex-valued white Gaussian noise with a two-sided power spectral density N_0. The sampled version of the signal at each receive antenna m is given by

$$y_m[kT_s] = \sum_{n=1}^{M_T} \sum_{l=-\infty}^{\infty} s_n[l] h_{m,n}[kT_s, kT_s - k\gamma T_s] + z_m[kT_s] \tag{4.3}$$

If one over-samples each transmitted sequence $s_n[k]$ by inserting $\gamma - 1$ zeros between each symbol, then the over-sampled sequence is denoted by

$$x_n[k] = \begin{cases} s_n[\frac{k}{\gamma}], & if\ \frac{k}{\gamma}\ is\ an\ integer \\ 0, & otherwise \end{cases} \tag{4.4}$$

Replacing $s_n[l]$ in (4.3) by $x_n[l]$, one obtains the following equation with a single data rate of $\frac{1}{T_s}$

$$y_m[k] = \sum_{n=1}^{M_T} \sum_{l=-\infty}^{\infty} x_n[k-l] h_{m,n}[k,l] + z_m[k] \tag{4.5}$$

where $h_{m,n}[k,l] = h_{m,n}[kT_s, lT_s]$ is the T_s sampled spaced version of $h_{m,n}(t,\tau)$, and $z_m[k] = z_m[kT_s]$ is the T_s sampled spaced version of $z_m[t]$.

4.2 DISCRETE TIME TAPPED DELAY LINE CHANNEL MODEL

The power delay profile (PDP) for each MIMO sub-channel is assumed to be discrete and is given by

$$G[\tau] = \sum_{i=0}^{L} \sigma_i^2(\tau - \tau_i) \tag{4.6}$$

where $L + 1$ is the total number of resolvable paths and σ_i^2 is the power of the i_{th} path with delay τ_i. However, almost all path delays τ_i are not an integer multiple of the system's symbol period T_{sym}, or chip period T_c (for CDMA systems). It is known that the total number of T_s sample spaced discrete-time channel coefficients $h_{m,n}[k, l]$ is determined by the maximum delay spread of the physical fading channel $g_{m,n}[t, \tau]$ and the time durations of the transmit filter and receive filter, which are usually infinite in theory to maintain limited frequency bandwidth. Therefore, $h_{m,n}[k, l]$ is normally a time-varying noncausal filter with infinite impulse response (IIR). However, in practice, the time-domain tails of the transmit and receive filters are designed to fall off rapidly. Thus, the amplitudes of the channel coefficients will decrease quickly with increasing $|l|$. When the power (or squared amplitude) of a coefficient is smaller than a predefined threshold, for example, 0.01% of the total power of its corresponding sub-channel, it has very little impact on the output signal and can thus be discarded. Therefore, the time-varying noncausal IIR channel can be truncated to a finite impulse response (FIR) channel. It is assumed that the coefficient index l is in the range of $[-L_1, L_2]$, where L_1 and L_2 are non-negative integers and the total number of coefficients for the truncated FIR channel is $L+1$ with $L+1 \leq L_1+L_2+1$. The discrete time tapped delay line for the MIMO channel model is depicted in Fig. 4.2. The

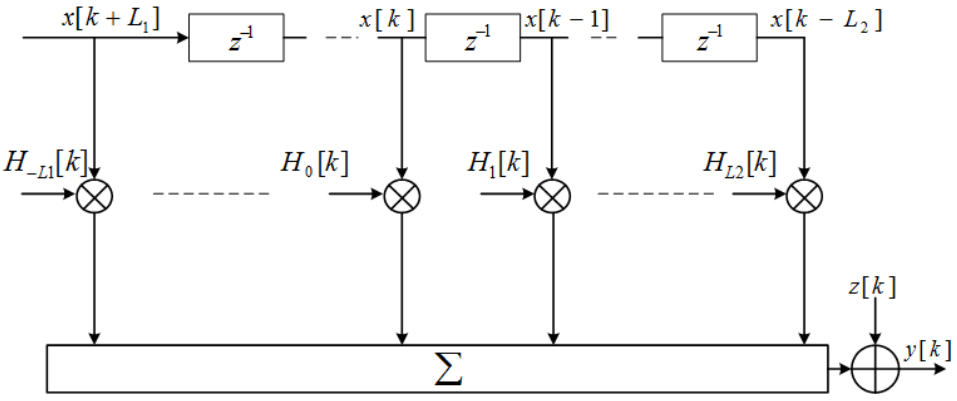

FIGURE 4.2: Tapped delay line model for the MIMO channel.

input-output relationship of the MIMO channel in discrete-time is expressed as

$$\mathbf{y}[k] = \sum_{l=-L_1}^{L_2} \mathbf{H}_l[k].\mathbf{x}[k-l] + \mathbf{z}[k] \tag{4.7}$$

where $\mathbf{x}[k] = [x_1[k]\ x_2[k]\ \cdots\ x_{M_T}[k]]^{\mathcal{T}}$, $\mathbf{z}[k] = [z_1[k]\ z_2[k]\ \cdots\ z_{M_R}[k]]^{\mathcal{T}}$ and $\mathbf{y}[k] = [y_1[k]\ y_2[k]\ \cdots\ y_{M_R}[k]]^{\mathcal{T}}$ are the input vector, noise vector, and output vector, respectively, at time instant k. The matrix $\mathbf{H}_l[k]$ is given by

$$\mathbf{H}_l[k] = \begin{pmatrix} h_{1,1}[k,l] & \cdots & h_{1,M_T}[k,l] \\ \vdots & \ddots & \vdots \\ h_{M_R,1}[k,l] & \cdots & h_{M_R,M_T}[k,l] \end{pmatrix} \tag{4.8}$$

The MIMO channel consists of $M_T M_R(L+1)$ stochastic channel coefficients and a noise vector $\mathbf{z}[k]$ with M_R elements. The discrete time MIMO channel coefficient vector is defined as [40]

$$\mathbf{h}_v(k) = [\mathbf{h}_{1,1}^{\mathcal{T}}(k)\ \cdots\ \mathbf{h}_{1,M_R}^{\mathcal{T}}(k)\ \cdots\ \mathbf{h}_{M_T,1}^{\mathcal{T}}(k)\ \cdots\ \mathbf{h}_{M_T,M_R}^{\mathcal{T}}(k)]^{\mathcal{T}} \tag{4.9}$$

where $\mathbf{h}_{m,n}(k)$ is the $(m,n)_{th}$ sub-channel's $L+1$ FIR filter coefficients at time instant k, given by

$$\mathbf{h}_{m,n}(k) = [h_{m,n}(k,-L_1)\ \cdots\ h_{m,n}(k,L_2)]^{\mathcal{T}} \tag{4.10}$$

and $h_{m,n}(k,l)$ is the l_{th} sub-channel coefficient at time instant k.

4.3 STATISTICAL PROPERTIES OF THE DISCRETE TIME CHANNEL

The noise vector $\mathbf{z}[k]$ is zero-mean Gaussian distributed with auto-covariance matrix $\mathbf{R}_{zz}(k_1-k_2)$ given by

$$\begin{aligned} \mathbf{R}_{zz}(k_1-k_2) &= E[\mathbf{z}[k_1].\mathbf{z}^{\mathcal{H}}[k_2]] \\ &= N_0 R_{p_R,p_R}[(k_1-k_2)T_s].\mathbf{I}_M \end{aligned} \tag{4.11}$$

where $R_{p_R,p_R}[\xi]$ is the auto-correlation function of the receive filter $p_R(t)$ and N_0 is the two-sided power spectral density of the complex-valued AWGN. If the auto-correlation function of the receive filter satisfies the following condition:

$$R_{p_R,p_R}[kT_s] = \begin{cases} 1, & if\ k = 0 \\ 0, & if\ k \neq 0 \end{cases} \tag{4.12}$$

then the discrete-time Gaussian noise $\mathbf{z}[k]$ is still white, from sample to sample and from antenna to antenna. The channel coefficient column vector $\mathbf{h}_v[k]$ is zero-mean Gaussian distributed. Its covariance matrix is given by [40]

$$\mathbf{C}_h[k_1 - k_2] = E[\mathbf{h}_v[k_1].\mathbf{h}_v^{\mathcal{H}}[k_2]]$$

$$= (\mathbf{\Psi}_{Rx} \otimes \mathbf{\Psi}_{Tx} \otimes \mathbf{C}_{ISI}).J_0(2\pi f_d(k_1 - k_2)T_s) \tag{4.13}$$

where $\mathbf{\Psi}_{Rx} \in \mathbb{C}^{M_R \times M_R}$ is the receive antenna correlation matrix, $\mathbf{\Psi}_{Tx} \in \mathbb{C}^{M_T \times M_T}$ is the transmit antenna correlation matrix, $\mathbf{C}_{ISI} \in \mathbb{C}^{(L+1)\times(L+1)}$ is the filter tap ISI covariance matrix and $\mathbf{\Phi}(k) \in \mathbb{C}^{M_T M_R(L+1)\times 1}$ represents a column vector of uncorrelated Rayleigh flat fading coefficients at time instant k. In (4.13), the symbol f_d is the maximum Doppler frequency and J_0 is the Bessel function of the first kind of order zero. The filter tap ISI covariance matrix $\mathbf{C}_{ISI}$ is expressed as

$$\mathbf{C}_{ISI} = \begin{pmatrix} c[-L_1, -L_1] & \cdots & c[-L_1, L_2] \\ \vdots & \ddots & \vdots \\ c[L_2, -L_1] & \cdots & c[L_2, L_2] \end{pmatrix} \tag{4.14}$$

where

$$c[l_1, l_2] = \sum_{i=0}^{L} \sigma_i^2 \bar{R}_{p_T,p_R}[l_1 T_s - \tau_i]\bar{R}^*_{p_T,p_R}[l_2 T_s - \tau_i] \tag{4.15}$$

and $\bar{R}_{p_T,p_R}[\xi]$ is the convolution function of the transmit filter and receive filter. The correlation matrices $\mathbf{\Psi}_{Tx}$ and $\mathbf{\Psi}_{Rx}$ are given by

$$\mathbf{\Psi}_{Tx} = \begin{pmatrix} \rho_{Tx}^{1,1} & \cdots & \rho_{Tx}^{1,M_T} \\ \vdots & \ddots & \vdots \\ \rho_{Tx}^{M_T,1} & \cdots & \rho_{Tx}^{M_T,M_T} \end{pmatrix} \tag{4.16}$$

$$\mathbf{\Psi}_{Rx} = \begin{pmatrix} \rho_{Rx}^{1,1} & \cdots & \rho_{Rx}^{1,M_R} \\ \vdots & \ddots & \vdots \\ \rho_{Rx}^{M_R,1} & \cdots & \rho_{Rx}^{M_R,M_R} \end{pmatrix} \tag{4.17}$$

where $\rho_{Rx}^{m,p}$ is the receiver correlation co-efficient between receive antennas m and p with $0 \leq |\rho_{Rx}^{m,p}| \leq \rho_{Rx}^{m,m} = 1$ and $\rho_{Tx}^{n,q}$ is the transmit antenna correlation coefficient between transmit antenna n and q with $0 \leq |\rho_{Tx}^{n,q}| \leq \rho_{Tx}^{n,n} = 1$. The channel coefficients for the tapped delay line model are derived from the following equation [40]:

$$\mathbf{h}_v(k) = (\mathbf{\Psi}_{Rx}^{1/2} \otimes \mathbf{\Psi}_{Tx}^{1/2} \otimes \mathbf{C}_{ISI}^{1/2}).\mathbf{\Phi}(k) \tag{4.18}$$

The main advantage of this MIMO channel model is that $\mathbf{C}_{ISI}$ translates the effects of the transmit filter, receive filter and channel fading parameters into the receiver sample-spaced, stochastic channel coefficients. The design of $\mathbf{C}_{ISI}$ ensures that no oversampling is needed to deal with multiple fractionally delayed power delay profiles [40].

4.4 Generation of Rayleigh flat fading coefficients

Each flat fading element in $\mathbf{\Phi}(k)$ can be generated using the modified Jakes model proposed in [61]. The fading process for each element in continuous time form is given by

$$Z(t) = Z_c(t) + j.Z_s(t) \tag{4.19}$$

$$Z_c(t) = \sqrt{\frac{2}{M}} \sum_{n=1}^{M} cos(2\pi f_d t cos\alpha_n + \phi_n) \tag{4.20}$$

$$Z_s(t) = \sqrt{\frac{2}{M}} \sum_{n=1}^{M} cos(2\pi f_d t sin\alpha_n + \varphi_n) \tag{4.21}$$

with

$$\alpha_n = \frac{2\pi n - \pi + \theta}{4M} \quad n = 1, 2, \ldots, M \tag{4.22}$$

where φ_n, ϕ_n and θ are statistically independent and uniformly distributed in the interval $[-\pi, \pi)$ for all n.

4.5 Generation of AWGN

When simulating AWGN channel conditions for the received signal at the receive antenna, transformation algorithms, such as the Bray-Marsagalia algorithm [62] and Box-Muller sine-cosine algorithm [63], are frequently used to generate samples that exhibit a Gaussian amplitude probability distribution function (PDF) with a zero mean and a variance of 1, using noise samples with uniformly distributed amplitude values ranging from 0 to 1 as inputs. To simulate AWGN conditions for a specific $\frac{E_b}{N_0}$ value accurately, the noise variance generated by one of the above-mentioned algorithms needs to be scaled by $\sqrt{\kappa}$ [48, p. 29] at each receiver, where

$$\kappa = \frac{\sigma_s^2 f_{samp}}{10^{\frac{Eb/No}{10}} 2 f_{bit}} \tag{4.23}$$

where σ_s^2 is the variance of the transmitted signal, Eb/No is the SNR per bit in dB, f_{samp} is the sampling frequency of the noise and f_{bit} is the input bit frequency of the system.

CHAPTER FIVE

SINGLE-ANTENNA UPLINK MC-DS-CDMA USING ZCZ SEQUENCES WITH JOINT DETECTION

This chapter is mainly concerned with TF-domain spreading MC-DS-CDMA using ZCZ sequences designed specifically for quasi-synchronous uplink transmissions, where the channels are assumed to be frequency-selective and block-fading [38] channels. The system considered in this chapter is an extension of the system in [13] to block-fading channel conditions. The uplink channel assumptions are detailed in the next section, followed by a brief introduction to conventional MC-DS-CDMA. Finally, TF-domain spreading MC-DS-CDMA using ZCZ sequences for frequency-selective block-fading conditions is detailed, where various joint detection algorithms are considered at the receiver.

5.1 UPLINK CHANNEL ASSUMPTIONS

In the uplink of a multicarrier CDMA system there is asynchronism between different users sharing the same bandwidth, which results in MUI. The amount of MUI is directly related to the cross-correlation properties of the CDMA spreading codes employed for each user. A

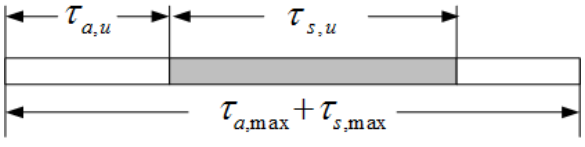

FIGURE 5.1: The asynchronism and delay spread of user u.

quasi-synchronous uplink channel is assumed in this analysis, where the mobile users have a means of aligning their timing to a common reference time (i.e. IS-95) and the asynchronism

between users is kept within a few chips. Let $\tau_{a,u}$ denote the asynchronism of user u (measured relative to some reference user), and let $\tau_{s,u}$ denote the delay spread of user u's channel. The maximum relative user asynchronism $\tau_{a,max}$ arises between the nearest and the farthest mobiles in a cell, and is determined by the radius of the cell. The maximum delay spread of the multipath channel $\tau_{s,max}$ in typical environments is often available by standard sounding techniques. The asynchronism and delay spread of user u is depicted in Fig. 5.1. It is further assumed that the channels of the different users are statistically independent. The relative propagation delay differences between the different users $\tau_{a,u}$ introduce MUI at the receiver, owing to the non-ideal cross-correlation properties of the different users time-domain spreading sequences. However it was shown in [13], that if ZCZ sequences are employed as time-domain spreading sequences and the ZCZ length is greater than the maximum quasi-synchronism between users (i.e. $Z_0 > \tau_{a,max}$), then no interference exists due to propagation delay differences between the different users.

5.2 CONVENTIONAL MC-DS-CDMA

A conventional orthogonal MC-DS-CDMA system has a sub-carrier spacing of $\Delta = \frac{1}{T_c}$ [5] (where T_c is the chip interval on each sub-carrier). The conventional MC-DS-CDMA transmitter structure for a single-user is shown in Fig. 5.2. The input symbol stream before serial to parallel conversion is denoted as $b(t)$, and $b_1, \ldots, b_U$ are the symbols assigned to each of U sub-carriers. The symbols $b_1, \ldots, b_U$ are PSK or QAM symbols. The spreading sequence for each sub-carrier in continuous time form is given as $c(t)$, where T_c is the spreading sequence chip interval on each sub-carrier. The receiver structure is shown in Fig. 5.3, where $r(t)$ is the received signal in continuous time form. In order to obtain frequency diversity in conventional MC-DS-CDMA, it was proposed in [4, 5] that one time spread data sequence needs to modulate multiple sub-carriers (instead of only one sub-carrier) that experience independent flat fading [4, 5]. This type of repetition signalling has the desirable properties of exhibiting a narrow-band interference suppression effect due to the time spreading on each sub-carrier, along with robustness to fading due to repeated transmission on multiple sub-carriers, without requiring the use of a large RAKE receiver [1, p. 843]. In addition to interference suppression and diversity, MC-DS-CDMA requires a lower chip rate per sub-carrier. If it is assumed that there are M sub-carriers, and T_c is the chip duration of an SC-DS-CDMA system, then the chip duration on each sub-carrier of the MC-DS-CDMA system is given by MT_c. In other words, a

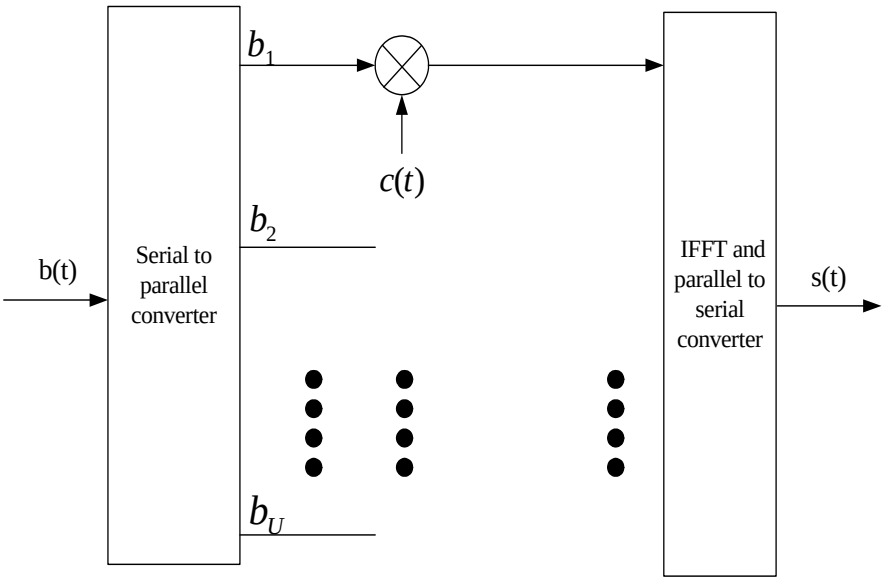

FIGURE 5.2: The block diagram of a conventional MC-DS-CDMA transmitter for a single-user.

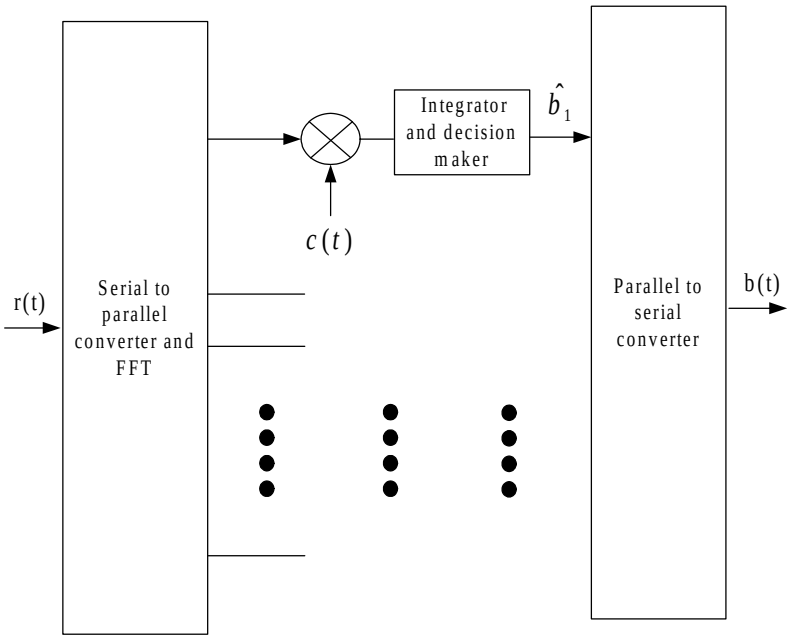

FIGURE 5.3: The block diagram of a conventional MC-DS-CDMA receiver for a single-user.

multicarrier system requires a lower speed, parallel-type of signal processing, in contrast to a fast, serial-type of signal processing in the SC-DS-CDMA receiver case. However, since each user's spread symbol modulates multiple sub-carriers, there is a reduction in data rate in order to obtain frequency diversity [5]. Thus, in conventional MC-DS-CDMA, there is a trade-off between the data rate and the frequency diversity achieved. The trade-off between data rate and frequency diversity is not a desirable result. Ideally, one wishes to achieve maximum data rate

as well as frequency diversity without having to accept any trade-off. Various options have been considered in the literature, to solve the above problem [6, 23].

5.3 TF-DOMAIN SPREADING MC-DS-CDMA USING ZCZ SPREADING SEQUENCES FOR FREQUENCY-SELECTIVE BLOCK-FADING CHANNELS

TF-domain spreading MC-DS-CDMA using ZCZ spreading sequences has been proposed in [13] for the quasi-synchronous uplink channel. However, the system in [13] is only able to achieve frequency diversity in frequency-selective slow fading conditions by frequency-domain spreading over different frequency tones. In this section frequency-selective and block-fading channels are considered, where in addition to frequency diversity, one is also able to achieve temporal diversity [38, 64]. The system in this section is an extension of the system in [13], by frequency-domain spreading over different frequency tones and different fading blocks. At the receiver joint decoding is done over frequency tones and fading blocks. The proposed system is able to achieve frequency and temporal diversity, instead of just the frequency diversity achieved in [13].

5.3.1 System model

In TF-domain spreading MC-DS-CDMA, assume that there are J ZCZ time-domain spreading sequences available of length Q chips, i.e., $a_j(t)$ $(j = 0, \ldots, J-1)$. Each time-domain spreading sequence is associated with P frequency-domain spreading sequences of length $M_B S$, i.e., $\mathbf{c}_{j,p}$ $(j = 0, \ldots, P-1)$, where M_B is the number of fading blocks over which frequency-domain spreading is done. Each user is assigned one time-domain sequence $a_j(t)$ and one frequency-domain sequence $\mathbf{c}_{j,p}$. The maximum number of users supported by TF-domain spreading MC-DS-CDMA is given by $\Gamma = JP$ [13]. Fig. 5.4 shows the transmitter schematic for a single-user in each fading block m. At the transmitter side, a symbol stream $b_{j,p}(t)$ with symbol period T_{sym} is serial to parallel converted into U parallel branches in each fading block m. The symbol associated with time-domain spreading sequence j and frequency-domain spreading sequence p in branch u is given by $b_{j,p,u}$. The information symbols $b_{j,p,u}$ belong to a discrete alphabet $\mathcal{A}$ (i.e. PSK or QAM). Each branch after serial to parallel conversion has a symbol duration of UT_{sym} and is multiplied by the user-specific time-domain ZCZ spreading sequence $a_j(t)$. It is assumed that the block-fading channel stays constant over the symbol

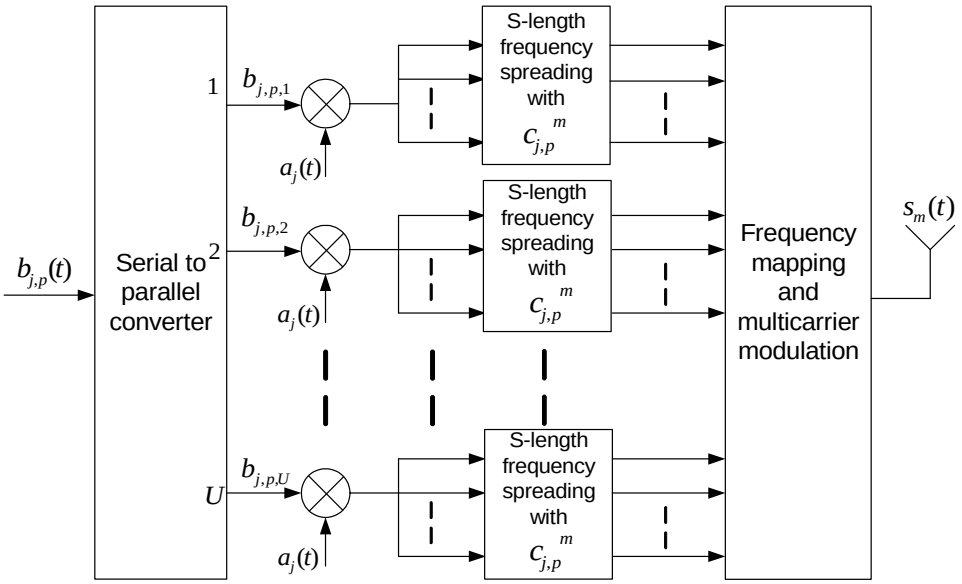

FIGURE 5.4: The TF-domain spreading MC-DS-CDMA transmitter structure for a single-user in each fading block m.

period UT_{sym}; however it may change from symbol to symbol. The above assumption implies that the coherence time $(\Delta t)_c$ [1, p. 807] of the channel is higher than but close to the symbol duration of UT_{sym} (i.e. $(\Delta t)_c \gtrapprox UT_{sym}$). The symbol duration of UT_{sym} is referred to as a fading block. In this analysis the fading blocks are assumed to be statistically independent. Following time-domain spreading, the spread signal in each branch is repeated on S parallel branches, where each branch is multiplied by the corresponding chip value of a user-specific frequency-domain spreading sequence $\mathbf{c}_{j,p} = [c_{j,p}[1]\ c_{j,p}[2]\ \cdots\ c_{j,p}[SM_B]]^{\mathcal{T}}$, where M_B is the number of fading blocks over which frequency-domain spreading is done. It should be noted that frequency-domain spreading is done separately for each branch u. However, in this analysis it is assumed that the same set of frequency-domain spreading codes are used for each branch. The $U.S \times 1$ transmission vector after time-domain and frequency-domain spreading for each user, in fading block m can be expressed as

$$\mathbf{z}_{j,p,m} = \begin{pmatrix} \mathbf{c}_{j,p}^{m} a_j(t) b_{j,p,1} \\ \mathbf{c}_{j,p}^{m} a_j(t) b_{j,p,2} \\ \vdots \\ \mathbf{c}_{j,p}^{m} a_j(t) b_{j,p,U} \end{pmatrix} m = 1, \ldots, M_B \tag{5.1}$$

where $\mathbf{c}_{j,p}^{m} = [c_{j,p}[(m-1)S+1]\ \ c_{j,p}[(m-1)S+2]\ \ \cdots\ \ c_{j,p}[(m-1)S+S]]^{\mathcal{T}}, m = 1, \ldots, M_B$. The cyclic prefix insertion matrix is expressed as $\mathbf{T}_{CP} = [\mathbf{I}_{CP}^{\mathcal{T}}\ \mathbf{I}_{U.S}^{\mathcal{T}}]^{\mathcal{T}}$, where CP is the cyclic prefix length. The matrix $\mathbf{P}$ is defined as a $U.S \times U.S$ permutation matrix that maximally separates

the data of each branch u in the frequency-domain, i.e., the $(x, y)_{th}$ element of $\mathbf{P}$ is equal to 1 if $x = (y-1)mod(U).S + \lfloor \frac{y-1}{U} \rfloor + 1$, and equal to 0 otherwise. The transmitter output for each user in each fading block m, from Fig. 5.4, can be expressed as

$$\mathbf{s}_m(t) = \mathbf{T}_{CP}\mathbf{F}_{U.S}^{\mathcal{H}}\mathbf{P}\mathbf{z}_{j,p,m} \quad m = 1, \ldots, M_B \tag{5.2}$$

The receiver structure for fading block m is depicted in Fig. 5.5. The cyclic prefix removal

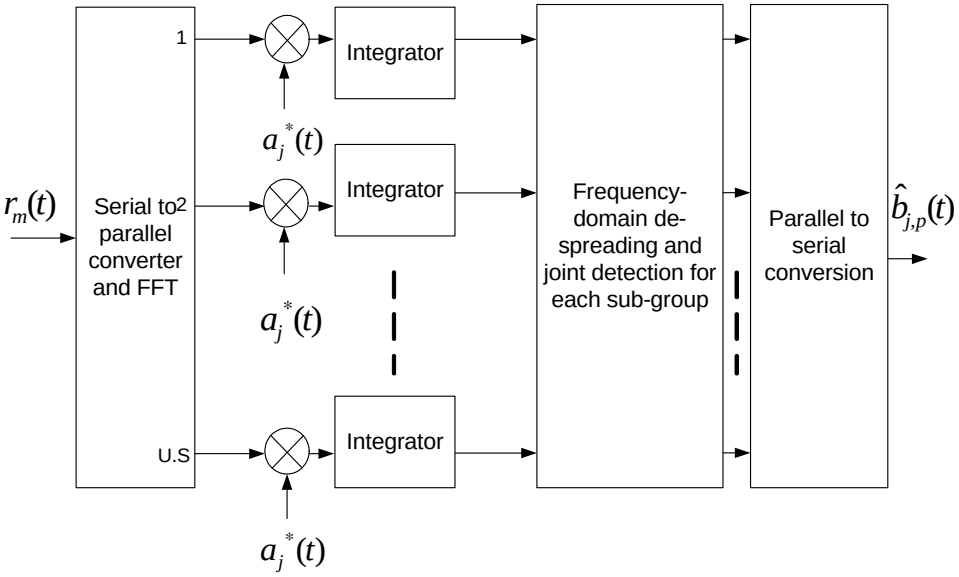

FIGURE 5.5: The TF-domain spreading MC-DS-CDMA receiver structure for a single-user.

matrix at the receiver can be expressed as $\mathbf{R}_{CP} = [\mathbf{0}_{U.S \times CP}\mathbf{I}_{U.S}]$. The received signal after cyclic prefix removal at the receiver can be expressed as

$$\begin{aligned}\mathbf{r}_m(t) &= \sum_{j=0}^{J-1}\sum_{p=0}^{P-1}\mathbf{P}^{\mathcal{T}}\mathbf{F}_{U.S}\mathbf{R}_{CP}\mathbf{H}_{j,p}^{m}\mathbf{T}_{CP}\mathbf{F}_{U.S}^{\mathcal{H}}\mathbf{P}\mathbf{z}_{j,p,m} + \mathbf{n}_m(t) \\ &= \sum_{j=0}^{J-1}\sum_{p=0}^{P-1}\tilde{\mathbf{H}}_{j,p}^{m}\mathbf{z}_{j,p,m} + \mathbf{n}_m(t) \quad m = 1, \ldots, M_B \end{aligned} \tag{5.3}$$

where $\mathbf{n}_m(t)$ is a column vector of white Gaussian noise samples with variance σ_n^2. The linear convolution of each user's frequency-selective channel in fading block m is expressed as a lower triangular Toeplitz matrix given by

$$\mathbf{H}_{j,p}^{m} = \begin{pmatrix} h_{j,p}^{m}[0] & 0 & 0 & \cdots & 0 \\ \vdots & h_{j,p}^{m}[0] & 0 & \cdots & 0 \\ h_{j,p}^{m}[L] & \cdots & \ddots & \cdots & \vdots \\ \vdots & \ddots & \cdots & \ddots & 0 \\ 0 & \cdots & h_{j,p}^{m}[L] & \cdots & h_{j,p}^{m}[0] \end{pmatrix} \tag{5.4}$$

with $L+1$ channel taps. The matrix $\mathbf{R}_{CP}\mathbf{H}^{m}_{j,p}\mathbf{T}_{CP}$ is a circulant matrix. Since circulant matrices can be diagonalized by FFT operations [65], the matrix $\tilde{\mathbf{H}}^{m}_{j,p} = \mathbf{P}^{\mathcal{T}}\mathbf{F}_{U.S}\mathbf{R}_{CP}\mathbf{H}^{m}_{j,p}\mathbf{T}_{CP}\mathbf{F}^{\mathcal{H}}_{U.S}\mathbf{P}$ becomes a diagonal matrix of the channel frequency response in fading block m, expressed as

$$\tilde{\mathbf{H}}^{m}_{j,p} = diag(H^{m}_{j,p}[1], H^{m}_{j,p}[U+1], \ldots, H^{m}_{j,p}[(S-1)U+1], H^{m}_{j,p}[2], H^{m}_{j,p}[U+2], \ldots, H^{m}_{j,p}[(S-1)U+2], \ldots, H^{m}_{j,p}[U], H^{m}_{j,p}[2.U], \ldots, H^{m}_{j,p}[S.U]) \tag{5.5}$$

where

$$H^{m}_{j,p}[n] = \sum_{v=0}^{L} h^{m}_{j,p}[v] \exp(\frac{-j2\pi v(n-1)}{U.S}) \tag{5.6}$$

and $\{h^{m}_{j,p}[v]\}^{L}_{v=0}$ represents the impulse response of the channel for each user in fading block m. The coefficients $\{h^{m}_{j,p}[v]\}^{L}_{v=0}$ are obtained using the methods described in section 4.3. Since the ZCZ sequences $\{a_j(t)\}^{J-1}_{j=0}$ exhibit an interference-free-window (Z_0), where their cross-correlation and autocorrelation functions are zero, no MUI is introduced due to the time-domain spreading codes, on condition that the maximum quasi-synchronism between users $\tau_{a,max}$ is less the than the zero correlation zone length ($\tau_{a,max} \leq Z_0$) [13, 49]. However, the frequency-domain spreading sequences associated with each time-domain spreading sequence $\{\mathbf{c}_{j,p}\}^{P-1}_{p=0}$ lose their orthogonality and introduce MUI when multiple users are supported [6]. Thus, joint detection becomes necessary at the receiver, when TF-domain spreading is employed [6, 8]. At the receiver one has to wait for M_B fading blocks to be received before joint detection is done in order to achieve temporal and frequency diversity, which results in a longer decoding delay and a larger decoding complexity. Joint detection is done separately for each sub-carrier group u at the receiver. Thus, only the decoding of the first sub-carrier group ($u = 1$) associated with the first time-domain spreading sequence $a_1(t)$ is considered at the receiver. After correlating the received signal with $a_1(t)$ at the receiver, the received signal for sub-block $u = 1$ after receiving M_B fading blocks can be expressed as

$$\tilde{\mathbf{r}} = \sum_{p=0}^{P-1} \mathbf{D}_{1,p}\mathbf{c}_{1,p}b_{1,p,1} + \tilde{\mathbf{v}} \tag{5.7}$$

where the $M_BS \times M_BS$ diagonal matrix $\mathbf{D}_{1,p}$ is expressed as

$$\mathbf{D}_{1,p} = diag(H^{1}_{1,p}[1], H^{1}_{1,p}[U+1], \ldots, H^{1}_{1,p}[(S-1)U+1], H^{2}_{1,p}[1], H^{2}_{1,p}[U+1], \ldots, H^{2}_{1,p}[(S-1)U+1], \ldots, H^{M_B}_{1,p}[1], H^{M_B}_{1,p}[U+1], \ldots, H^{M_B}_{1,p}[(S-1)U+1]) \tag{5.8}$$

Equation (5.7) can also be expressed as

$$\tilde{\mathbf{r}} = \Xi\mathbf{b} + \tilde{\mathbf{v}} \tag{5.9}$$

where $\mathbf{b} = [b_{1,0,1}\ b_{1,1,1}\ \cdots\ b_{1,P-1,1}]^{\mathcal{T}}$ and Ξ is the $M_B S \times P$ matrix expressed as

$$\Xi = \begin{pmatrix} c_1[1]H_{1,1}^1[1] & \cdots & c_P[1]H_{1,P}^1[1] \\ c_1[2]H_{1,1}^1[U+1] & \cdots & c_P[2]H_{1,P}^1[U+1] \\ \vdots & \cdots & \vdots \\ c_1[S]H_{1,1}^1[(S-1)U+1] & \cdots & c_P[S]H_{1,P}^1[(S-1)U+1] \\ c_1[S+1]H_{1,1}^2[1] & \cdots & c_P[S+1]H_{1,P}^2[1] \\ c_1[S+2]H_{1,1}^2[U+1] & \cdots & c_P[S+2]H_{1,P}^2[U+1] \\ \vdots & \cdots & \vdots \\ c_1[2S]H_{1,1}^2[(S-1)U+1] & \cdots & c_P[2S]H_{1,P}^2[(S-1)U+1] \\ \vdots & \cdots & \vdots \\ c_1[M_BS-S+1]H_{1,1}^{M_B}[U] & \cdots & c_P[M_BS-S+1]H_{1,P}^{M_B}[1] \\ c_1[M_BS-S+2]H_{1,1}^{M_B}[U+1] & \cdots & c_P[M_BS-S+2]H_{1,P}^{M_B}[U+1] \\ \vdots & \cdots & \vdots \\ c_1[M_BS]H_{1,1}^{M_B}[(S-1)U+1] & \cdots & c_P[M_BS]H_{1,P}^{M_B}[(S-1)U+1] \end{pmatrix} \tag{5.10}$$

The vector $\tilde{\mathbf{v}}$ is a $P \times 1$ column vector of AWGN with variance σ_n^2.

5.3.2 Joint multi-user detection for TF-domain spreading MC-DS-CDMA

Only optimal and basic linear joint detection schemes are considered for TF-domain spreading MC-DS-CDMA using ZCZ sequences. Optimal ML joint detection is considered first, followed by sphere decoding, the ZF (decorrelating) block linear detector and the MMSE block linear detector. The joint detection schemes are analyzed for the received signal vector

$$\tilde{\mathbf{r}} = \Xi\mathbf{b} + \tilde{\mathbf{v}} \tag{5.11}$$

5.3.2.1 Optimal ML joint detection

The optimal MUD is the maximum-likelihood receiver that yields the optimal estimate of the transmitted data, $\mathbf{b}$ from

$$\hat{\mathbf{b}}_{opt} = \arg\{\min_{\mathbf{b}}\{\| \tilde{\mathbf{r}} - \Xi\mathbf{b} \|^2\}\} \tag{5.12}$$

which can also be expressed as

$$\hat{\mathbf{b}}_{opt} = \arg\{\min_{\mathbf{b}}\{\ \mathbf{b}^{\mathcal{H}}\boldsymbol{\Xi}^{\mathcal{H}}\boldsymbol{\Xi}\mathbf{b} - 2real(\mathbf{b}^{\mathcal{H}}\boldsymbol{\Xi}^{\mathcal{H}}\tilde{\mathbf{r}})\ \}\} \tag{5.13}$$

Exhaustive search maximum likelihood detection has a complexity in the order of $O(|\mathcal{A}|^P)$ for TF-domain spreading MC-DS-CDMA using ZCZ codes [13].

5.3.2.2 Sphere decoding

One can write the received signal vector in (5.11) as

$$\begin{aligned}\acute{\tilde{\mathbf{r}}} &= \acute{\mathbf{b}}\begin{pmatrix} real(\boldsymbol{\Xi}^{\mathcal{T}}) & imag(\boldsymbol{\Xi}^{\mathcal{T}}) \\ -imag(\boldsymbol{\Xi}^{\mathcal{T}}) & real(\boldsymbol{\Xi}^{\mathcal{T}}) \end{pmatrix} + \acute{\tilde{\mathbf{v}}} \\ &= \acute{\mathbf{b}}\mathbf{M}_H + \acute{\tilde{\mathbf{v}}}\end{aligned} \tag{5.14}$$

where $\acute{\mathbf{b}} = [real(\mathbf{b}^{\mathcal{T}})\ imag(\mathbf{b}^{\mathcal{T}})] \in \mathbb{Z}^{2P}$ and $\acute{\tilde{\mathbf{v}}} = [real(\tilde{\mathbf{v}}^{\mathcal{T}})\ \ imag(\tilde{\mathbf{v}}^{\mathcal{T}})] \in \mathbb{R}^{2P}$. Thus, one can represent the received signal as a lattice sphere packing [42], and use the sphere decoder (section 3.2.2) for almost optimal detection. Sphere decoding complexity is independent of the underlying constellation size and is on the order of $O((2P)^{\alpha})$ where $3 \leq \alpha \leq 4$ [43, 44].

5.3.2.3 ZF block linear detection

In the decorrelator detector, the receiver multiplies the received vector $\tilde{\mathbf{r}}$ with $(\boldsymbol{\Xi}^{\mathcal{H}}\boldsymbol{\Xi})^{-1}\boldsymbol{\Xi}^{\mathcal{H}}$. Then, the resultant vector is given by $\mathbf{b}+(\boldsymbol{\Xi}^{\mathcal{H}}\boldsymbol{\Xi})^{-1}\boldsymbol{\Xi}^{\mathcal{H}}\tilde{\mathbf{v}}$. The resultant vector is then sent to a hard decision block in order to detect the corrupted symbols. The decorrelator detector eliminates the correlation between different users by restoring their orthogonality. However, while restoring orthogonality, it may amplify noise. Particularly at low SNR, noise amplification degrades BER performance significantly.

5.3.2.4 MMSE block linear detection

The received vector $\tilde{\mathbf{r}}$ is multiplied with

$$\mathbf{M} = \boldsymbol{\Xi}^{\mathcal{H}}(\boldsymbol{\Xi}\boldsymbol{\Xi}^{\mathcal{H}} + \frac{\sigma_n^2}{\sigma_s^2}\mathbf{I}_N)^{-1} \tag{5.15}$$

where σ_n^2 and σ_s^2 are the noise variance and information symbol variance, respectively. The product is then fed to a hard decision block to detect the transmitted symbols. The complexity of the block MMSE equalizer for TF-domain spreading MC-DS-CDMA using ZCZ codes is in the order of $O(P^3)$ [45, P. 102].

5.4 CONCLUDING REMARKS

This chapter focused on the design of an uplink TF-domain spreading MC-DS-CDMA system using ZCZ sequences, which achieves frequency and temporal diversity in frequency-selective block-fading conditions. In contrast to similar systems proposed in [13, 24], which only achieve frequency diversity, the proposed system is able to achieve temporal and frequency diversity. The optimal and sub-optimal joint detection schemes discussed in section 3.2 were considered with respect to the proposed system.

CHAPTER SIX

MULTI-ANTENNA DOWNLINK MC-DS-CDMA WITH JOINT DETECTION

6.1 INTRODUCTION

Several multi-antenna downlink MC-DS-CDMA schemes have been proposed in the literature for the CDMA downlink [8, 9, 66]. These schemes either achieve spatial and frequency diversity in frequency-selective slow fading channels [8, 9], or spatial and temporal diversity in frequency non-selective fast fading channels [66]. However, none of the above-mentioned schemes achieves the full diversity (spatial, frequency and temporal diversity) available in the wireless channel.

In this section, two alternative downlink MC-DS-CDMA schemes are proposed to achieve the full diversity available in the wireless channel, when frequency-selective block-fading [10, 11] channels are considered. The first scheme employs STS [8, 28], which is termed STS-assisted TF-domain spreading MC-DS-CDMA. The second scheme employs STFB codes [12] (originally proposed for MIMO-OFDM) and is termed STFB coded MC-DS-CDMA. Both the systems considered are able to achieve spatial, frequency and temporal diversity instead of just the spatial and frequency diversity achieved in [8, 9], or spatial and temporal diversity achieved in [66]. To the best knowledge of the author, there has hitherto been no proposed multi-antenna downlink MC-DS-CDMA scheme that exploits spatial, frequency and temporal diversity in frequency-selective block-fading channels. Simulations are done for the systems considered using various methods of joint detection at the receiver. In section 6.2, a basic introduction to STS principles is provided for a single carrier DS-CDMA system. Section

6.3 details multi-antenna STS-assisted TF-domain spreading MC-DS-CDMA. STFB coded MC-DS-CDMA is detailed in section 6.4. Comparisons are made between the two proposed systems in section 6.5. Some concluding remarks are given in section 6.6. The assumptions for the proposed MIMO MC-DS-CDMA schemes are given as follows:

- Only synchronous downlink transmission of the different users signals is considered.
- Perfect channel CSI is available at the receiver but not at the transmitter.
- The coherence bandwidth of the channel is given by $\Delta f_c \approx \frac{1}{T_m}$, where T_m is the maximum delay spread of the channel considered. It was shown in [8] that the frequency-domain flat fading condition on each sub-carrier is satisfied if

$$T_c > T_m \tag{6.1}$$

  where T_c is the time-domain spreading sequence chip duration on each sub-carrier. In the rest of this section we assume that (6.1) is satisfied.
- The MC-DS-CDMA schemes have a sub-carrier spacing of $\frac{1}{T_c}$ at each transmit antenna.

6.2 PRINCIPLE OF SPACE-TIME SPREADING

A single carrier transmit diversity scheme using STS was originally investigated in [28]. The STS scheme is an open loop transmit diversity scheme. Each of the symbols are spread using multiple orthogonal sequences, such as Walsh sequences. In this section the STS principle is briefly reviewed for SC-DS-CDMA using $M_T = 2$ transmit antennas and $M_R = 1$ receive antenna, where only one user is considered. For simplicity, the channel is assumed to be a frequency flat fading channel. Let the input data stream of rate $R_{sym} = 1/T_{sym}$ be split into an odd-indexed sub-stream of $\{b_1\}$ and an even-indexed sub-stream of $\{b_2\}$. The data rate of these sub-streams is hence halved to $R_{sym}/2$, and thus the symbol duration of each sub-stream is given by $2.T_{sym}$. Each sub-stream is multiplied in the time-domain with a different orthogonal spreading sequence of length Q chips, where $Q = (2.T_{sym})/T_c$ and T_c is the spreading sequence chip duration. The orthogonal sequences for sub-stream 1 and sub-stream 2 are expressed in continuous time form as $c_1(t)$ and $c_2(t)$, respectively. The signal transmitted from transmit antenna 1 is expressed as

$$s_1(t) = b_1 c_1(t) + b_2 c_2(t) \tag{6.2}$$

The signal transmitted from transmit antenna 2 is expressed as

$$s_2(t) = b_2c_1(t) - b_1c_2(t) \tag{6.3}$$

Let h_1 and h_2 be complex Gaussian flat fading coefficients, with respect to the first and second antennas. Then the received signal at the receive antenna can be expressed as

$$r(t) = h_1(b_1c_1(t) + b_2c_2(t)) + h_2(b_2c_1(t) - b_1c_2(t)) + n(t) \tag{6.4}$$

where $n(t)$ represents the AWGN. Upon correlating the received signal with $c_1(t)$ and $c_2(t)$ at the receiver, one obtains

$$d_1 = h_1b_1 + h_2b_2 + n_1 \tag{6.5}$$

$$d_2 = -h_2b_1 + h_1b_2 + n_2 \tag{6.6}$$

where

$$n_i = \int_0^{2.T_{sym}} n(t)c_i(t)dt \quad i = 1, 2 \tag{6.7}$$

Equations (6.5) and (6.6) can be expressed in matrix form as

$$\mathbf{d} = \mathbf{Hb} + \mathbf{n} \tag{6.8}$$

where $\mathbf{d} = [d_1 \;\; d_2]^{\mathcal{T}}$, $\mathbf{n} = [n_1 \;\; n_2]^{\mathcal{T}}$, $\mathbf{b} = [b_1 \;\; b_2]^{\mathcal{T}}$ and $\mathbf{H}$ is expressed as

$$\mathbf{H} = \begin{pmatrix} h_1 & h_2 \\ -h_2 & h_1 \end{pmatrix} \tag{6.9}$$

It is assumed that the receiver has perfect CSI. Multiplying, (6.8) with $\mathbf{H}^{\mathcal{H}}$, the decision variables are given by

$$\begin{aligned} \mathbf{Z} &= real(\mathbf{H}^{\mathcal{H}}\mathbf{d}) \\ &= real(\mathbf{H}^{\mathcal{H}}\mathbf{Hb}) + real(\mathbf{H}^{\mathcal{H}}\mathbf{n}) \end{aligned} \tag{6.10}$$

where $real(\mathbf{H}^{\mathcal{H}}\mathbf{H})$ is expressed as

$$real(\mathbf{H}^{\mathcal{H}}\mathbf{H}) = \begin{pmatrix} |h_1|^2 + |h_2|^2 & 0 \\ 0 & |h_1|^2 + |h_2|^2 \end{pmatrix} \tag{6.11}$$

which shows that the optimal two-fold spatial diversity can be achieved compared to the case of using a single transmit antenna. The general case for M_T transmit antennas is detailed in [28]. However, the study conducted in [28] showed that STS schemes designed for $M_T = 2, 4$ and 8 transmit antennas (for real symbols) constitute the most attractive ones, since they are

capable of providing maximal transmit diversity without requiring extra STS sequences. If this constraint is not met, then more than M_T spreading sequences are required per user in order to exploit the spatial diversity of the channel. The next section employs STS in conjunction with TF-domain spreading MC-DS-CDMA for frequency-selective block-fading channels.

6.3 STS-ASSISTED TF-DOMAIN SPREADING MC-DS-CDMA WITH JOINT DETECTION FOR FREQUENCY-SELECTIVE BLOCK-FADING CHANNELS

The system model proposed in this section is an extension of the system design in [8], to block-fading channel conditions. The system in [8] is designed only to exploit frequency and spatial diversity in frequency-selective slow fading channel conditions. However, the system model proposed in this section is able to achieve spatial, frequency and temporal diversity in frequency-selective and block-fading [38, 64] conditions.

6.3.1 System model

Consider a multi-user, multicarrier frequency-selective and block-fading MIMO communication system with M_T transmit antennas, one receive antenna and $U.S$ sub-carriers per transmit antenna. Without loss of generality, only one receive antenna is considered in this analysis. In addition, only real-valued data symbols using BPSK modulation are considered. The study conducted in [28], showed that STS-schemes designed for $M_T = 2, 4$ and 8 transmit antennas constitute the most attractive schemes, since they are capable of providing maximal transmit diversity without requiring extra STS sequences. This problem relates to a problem in orthogonal designs [27]. Thus, only these attractive schemes are considered in this analysis. The transmitter schematic for the k_{th} user is shown in Fig. 6.1. At the transmitter side, a block of $U.M_T$ data symbols for user k, each having a symbol duration of T_{sym}, is serial to parallel converted to U parallel sub-blocks with M_T symbols in each sub-block. The symbols in each block after serial to parallel conversion have a symbol duration of UM_TT_{sym}. It is assumed that the channel stays constant over this symbol interval (i.e. UM_TT_{sym}); however it may change from symbol to symbol. The above assumption implies that the coherence time $(\Delta t)_c$ [1, p. 807] of the channel is higher than but close to the symbol duration of UM_TT_{sym}

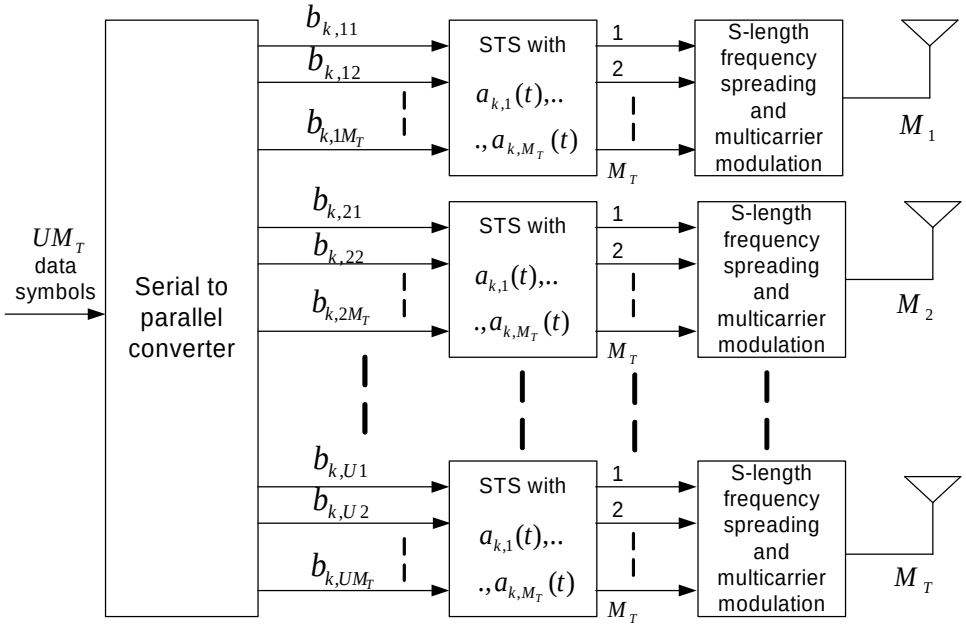

FIGURE 6.1: Transmitter structure for a single-user.

(i.e. $(\Delta t)_c \gtrapprox UM_T T_{sym}$). In this section the symbol duration of $UM_T T_{sym}$ is referred to as a fading block. It is assumed that the fading coefficients change from one fading block to the next.

The M_T symbols in each sub-block u are space-time spread using the schemes of [28]. The matrix $\mathbf{B}_{k,u}$ for sub-block u is defined as a $M_T \times M_T$ matrix, which can be expressed as [8]

$$\mathbf{B}_{k,u} = \begin{pmatrix} v_{1,1}\hat{b}^u_{k,11} & v_{1,2}\hat{b}^u_{k,12} & \cdots & v_{1,M_T}\hat{b}^u_{k,1M_T} \\ v_{2,1}\hat{b}^u_{k,21} & v_{2,2}\hat{b}^u_{k,22} & \cdots & v_{2,M_T}\hat{b}^u_{k,2M_T} \\ \vdots & \vdots & \ddots & \vdots \\ v_{M_T,1}\hat{b}^u_{k,M_T1} & v_{M_T,2}\hat{b}^u_{k,M_T2} & \cdots & v_{M_T,M_T}\hat{b}^u_{k,M_TM_T} \end{pmatrix} \tag{6.12}$$

where $v_{i,j}$ represents the sign of the element in the i_{th} row and j_{th} column and $\hat{b}^u_{k,ij}$ is the data symbol assigned to the i_{th} row and j_{th} column of sub-block u, which is determined by the STS design rule given in [8, 28]. Each $\hat{b}^u_{k,ij}$ is one of the M_T input data symbols $\{b_{k,u1}, \ldots, b_{k,uM_T}\}$ of user k. The matrix $\mathbf{B}_k$ is defined as

$$\mathbf{B}_k = [\mathbf{B}^{\mathcal{T}}_{k,1}\ \mathbf{B}^{\mathcal{T}}_{k,2}\ \cdots\ \mathbf{B}^{\mathcal{T}}_{k,U}]^{\mathcal{T}} \tag{6.13}$$

For example, in the case where $k = 1$, $M_T = 2$ and $U = 1$, the matrix $\mathbf{B}_1$, using the STS design rule given in [8, 28], is expressed as

$$\mathbf{B}_1 = \mathbf{B}_{1,1} = \begin{pmatrix} b_{1,11} & b_{1,12} \\ b_{1,12} & -b_{1,11} \end{pmatrix} \tag{6.14}$$

The STS operation is done with the $U \times UM_T$ matrix $\mathbf{C}_k$, defined as

$$\mathbf{C}_k^{\mathcal{T}} = \begin{pmatrix} a_{k,1}(t) & 0 & \cdots & 0 \\ a_{k,2}(t) & 0 & \cdots & 0 \\ \vdots & \vdots & \ddots & \vdots \\ a_{k,M_T}(t) & 0 & \cdots & 0 \\ 0 & a_{k,1}(t) & \cdots & 0 \\ 0 & a_{k,2}(t) & \cdots & 0 \\ \vdots & \vdots & \ddots & \vdots \\ 0 & a_{k,M_T}(t) & \cdots & 0 \\ \vdots & \vdots & \ddots & \vdots \\ 0 & 0 & \vdots & a_{k,1}(t) \\ 0 & 0 & \vdots & a_{k,2}(t) \\ \vdots & \vdots & \ddots & \vdots \\ 0 & 0 & \vdots & a_{k,M_T}(t) \end{pmatrix} \tag{6.15}$$

where $a_{k,i}(t)$, $i = 1, 2, \ldots, M_T$, are the k_{th} user's M_T STS time-domain orthogonal codes in continuous form. Each spreading sequence $a_{k,i}(t)$ has Q chips. Each user is assigned M_T STS time-domain orthogonal codes. The signal matrix after space-time spreading for user k is expressed as $\mathbf{D}_k = \mathbf{C}_k\mathbf{B}_k$. For the case where $k = 1$, $U = 1$ and $M_T = 2$, the matrices $\mathbf{C}_1$ and $\mathbf{D}_1 = \mathbf{C}_1\mathbf{B}_1$ are expressed as

$$\mathbf{C}_1 = [a_{1,1}(t) \;\; a_{1,2}(t)] \tag{6.16}$$

$$\mathbf{D}_1 = [d_{1,1} \quad d_{1,2}]$$

$$= [(b_{1,11}a_{1,1}(t) + b_{1,12}a_{1,2}(t)) \quad (b_{1,12}a_{1,1}(t) - b_{1,11}a_{1,2}(t))] \tag{6.17}$$

Each space-time spread signal is then spread in the frequency-domain over S frequency tones and M_B fading blocks, using S sub-carriers in each of M_B fading blocks, with a spreading code of length M_BS. Let $\mathbf{g}_k = [g_k[1] \;\cdots\; g_k[M_BS]]^{\mathcal{T}}$ be the k_{th} user's frequency-domain orthogonal code in discrete form, which will be used for frequency-domain spreading over M_B fading blocks. Each user k is assigned only one frequency domain spreading code. Let Γ_f be the number of users separated by different frequency-domain spreading codes, where $1 \leq \Gamma_f \leq M_BS$. Each user is assigned M_T STS time-domain sequences and one frequency-domain sequence. The frequency spreading matrix for fading block m and user k is expressed as

$$\mathbf{P}_{k,m} = [\mathbf{W}_k[(m-1)S + 1] \;\cdots\; \mathbf{W}_k[(m-1)S + S]]^{\mathcal{T}}, \;\; m = 1, \ldots, M_B \tag{6.18}$$

where the matrix $\mathbf{W}_k[s]$ is the $U \times U$ diagonal matrix expressed as

$$\mathbf{W}_k[s] = \mathbf{I}_U.g_k[s] \tag{6.19}$$

After frequency spreading in fading block m, user k's signal is expressed as $\mathbf{P}_{k,m}\mathbf{D}_k$. For the case where $k = 1$, $U = 1$, $S = 4$, $M_T = 2$ and $M_B = 2$, the matrix $\mathbf{P}_1\mathbf{D}_1$ in fading block $m = 1$ is expressed as

$$\mathbf{P}_{1,1}\mathbf{D}_1 = \begin{pmatrix} d_{1,1}c_1[1] & d_{1,2}c_1[1] \\ d_{1,1}c_1[2] & d_{1,2}c_1[2] \\ d_{1,1}c_1[3] & d_{1,2}c_1[3] \\ d_{1,1}c_1[4] & d_{1,2}c_1[4] \end{pmatrix} \tag{6.20}$$

where column 1 is the vector transmitted from transmit antenna 1 in fading block 1 and column 2 is the vector transmitted from transmit antenna 2 in fading block 1. The rows in (6.20) represent $S = 4$ different frequency tones. The matrix $\mathbf{P}_2\mathbf{D}_1$ in fading block $m = 2$ is expressed as

$$\mathbf{P}_{1,2}\mathbf{D}_1 = \begin{pmatrix} d_{1,1}c_1[5] & d_{1,2}c_1[5] \\ d_{1,1}c_1[6] & d_{1,2}c_1[6] \\ d_{1,1}c_1[7] & d_{1,2}c_1[7] \\ d_{1,1}c_1[8] & d_{1,2}c_1[8] \end{pmatrix} \tag{6.21}$$

where column 1 is the vector transmitted from transmit antenna 1 in fading block 2 and column 2 is the vector transmitted from transmit antenna 2 in fading block 2, where the rows in (6.21) again represent $S = 4$ different frequency tones. It is assumed that the sub-carriers in each sub-group u are maximally separated in the frequency domain. The transmitted signal matrix, after cyclic prefix insertion for user k and fading block m, can be expressed as

$$\mathbf{S}_{k,m}(t) = \mathbf{T}_{CP}\mathbf{F}_{U.S}^{\mathcal{H}}\mathbf{P}_{k,m}\mathbf{D}_k \quad m = 1, \ldots, M_B \tag{6.22}$$

The cyclic prefix insertion matrix at each transmitter is expressed as $\mathbf{T}_{CP} = [\mathbf{I}_{CP}^{\mathcal{T}}\ \mathbf{I}_{U.S}^{\mathcal{T}}]^{\mathcal{T}}$, where $\mathbf{I}_{CP}$ represents the last CP rows of $\mathbf{I}_{U.S}$ and CP is the cyclic prefix length. Define the matrix $\mathbf{H}_{m,g}$ as a $(U.S + CP) \times (U.S + CP)$ lower triangular Toeplitz matrix, which represents the linear convolution of the frequency-selective channel from transmit antenna g to receive antenna one in fading block m, expressed as

$$\mathbf{H}_{m,g} = \begin{pmatrix} h_{m,g}[0] & 0 & 0 & \cdots & 0 \\ \vdots & h_{m,g}[0] & 0 & \cdots & 0 \\ h_{m,g}[L] & \cdots & \ddots & \cdots & \vdots \\ \vdots & \ddots & \cdots & \ddots & 0 \\ 0 & \cdots & h_{m,g}[L] & \cdots & h_{m,g}[0] \end{pmatrix} \tag{6.23}$$

where the coefficients $\{h_{m,g}[v]\}_{v=0}^{L}$ represent the impulse response of the channel from transmit antenna g to receive antenna one in fading block m. The coefficients $\{h_{m,g}[v]\}_{v=0}^{L}$ are obtained using the method described in section 4.3. The received signal for fading block m, after cyclic prefix removal at the receiver, can be expressed as

$$\mathbf{r}_m(t) = \sum_{k=1}^{(\Gamma_f Q)/M_T} \sum_{g=1}^{M_T} \mathbf{F}_{US}\mathbf{R}_{CP}\mathbf{H}_{m,g}\mathbf{T}_{CP}\mathbf{F}_{US}^{\mathcal{H}}(\mathbf{P}_{k,m}\mathbf{D}_k)_g + \mathbf{n}_m(t)$$

$$= \sum_{k=1}^{(\Gamma_f Q)/M_T} \sum_{g=1}^{M_T} \tilde{\mathbf{H}}_{m,g}(\mathbf{P}_{k,m}\mathbf{D}_k)_g + \mathbf{n}_m(t) \quad m = 1, \ldots, M_B \tag{6.24}$$

where $\mathbf{X}_g$ represents the g_{th} column of the matrix $\mathbf{X}$ and $\mathbf{n}_m(t)$ is $U.S \times 1$ vector of complex valued Gaussian noise with variance σ_n^2. The channel matrix $\tilde{\mathbf{H}}_{m,g} = \mathbf{F}_{US}\mathbf{R}_{CP}\mathbf{H}_{m,g}\mathbf{T}_{CP}\mathbf{F}_{US}^{\mathcal{H}}$ represents a diagonal matrix of the frequency response of the channel from transmit antenna g to receive antenna one in fading block m, and is expressed as $\tilde{\mathbf{H}}_{m,g} = diag(H_{m,g}[1], H_{m,g}[2], \ldots, H_{m,g}[U.S])$, where

$$H_{m,g}[p] = \sum_{v=0}^{L} h_{m,g}[v] \exp(\frac{-j2\pi v(p-1)}{U.S}) \tag{6.25}$$

The receiver schematic at the receive antenna is depicted in Fig. 6.2. At the receive

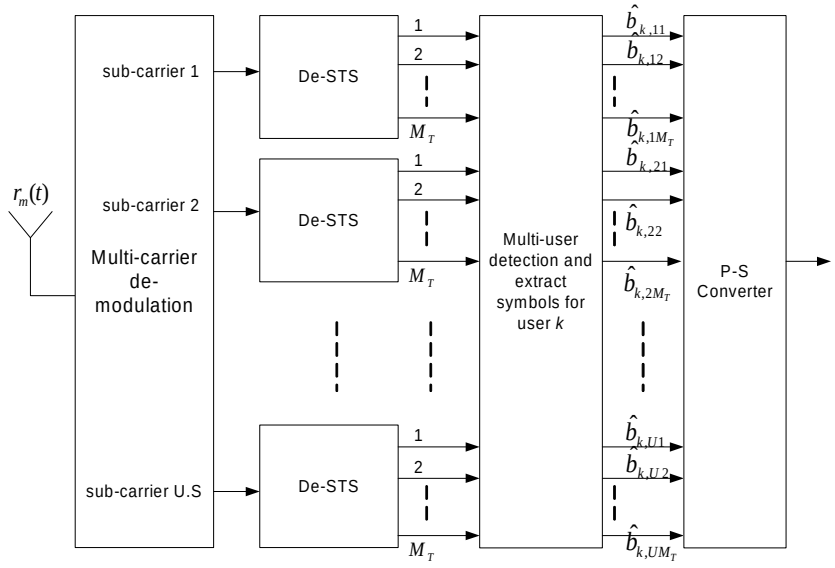

FIGURE 6.2: Receiver schematic at the receive antenna.

antenna, the received signal is first demodulated using fast fourier transform (FFT)-based multicarrier demodulation, obtaining $U.S$ number of parallel streams corresponding to the signals transmitted on $U.S$ sub-carriers. Each stream is space-time de-spread using the approach

of [28]. In the downlink, the time-domain orthogonal STS-spreading sequences (i.e. $a_{k,i}(t)$) are orthogonal, and thus no interference arises between STS time-domain spreading sequences after de-spreading. However, the users separated by different frequency-domain spreading codes (i.e. Γ_f) experience MUI [8]. It should be noted that one has to wait for M_B fading blocks to arrive at the receiver before joint detection can take place. The system in [8] is a special case of the system proposed here when $M_B = 1$.

6.3.2 Signal detection

After space-time de-spreading at the receiver [8, 28], the decision variables in terms of the first data symbol in sub-block u, sub-carrier $(s-1)U+u$ and fading block m are expressed as $Z_{(s-1)U+u,m,1}$, $u = 1,\ldots,U$, $s = 1,\ldots,S$ and $m = 1,\ldots,M_B$. The vector $\mathbf{z}_{u,1}$ is given by

$$\mathbf{z}_{u,1} = [Z_{u,1,1}\ Z_{U+u,1,1}\ \cdots\ Z_{(S-1)U+u,1,1}\ Z_{u,2,1}\ Z_{U+u,2,1}$$
$$\cdots\ Z_{(S-1)U+u,2,1}\ \cdots\ Z_{u,M_B,1}\ Z_{U+u,M_B,1}\cdots\ Z_{(S-1)U+u,M_B,1}]^{\mathcal{T}} \tag{6.26}$$

which can be expressed in matrix form as

$$\mathbf{z}_{u,1} = \mathbf{ARb} + \mathbf{n} \tag{6.27}$$

The columns of the $M_BS \times \Gamma_f$ matrix $\mathbf{R}$ are the frequency domain spreading codes for the Γ_f users, expressed as

$$\mathbf{R} = \begin{pmatrix} g_1[1] & g_2[1] & \cdots & g_{\Gamma_f}[1] \\ g_1[2] & g_2[2] & \cdots & g_{\Gamma_f}[2] \\ \vdots & \vdots & \ddots & \vdots \\ g_1[M_BS] & g_2[M_BS] & \cdots & g_{\Gamma_f}[M_BS] \end{pmatrix} \tag{6.28}$$

The column vector $\mathbf{b}$ contains the BPSK symbols for each of the Γ_f users in sub-block u

$$\mathbf{b} = [b_{1,u1}, b_{2,u1},\ldots,b_{\Gamma_f,u1}]^{\mathcal{T}} \tag{6.29}$$

and $\mathbf{n}$ is the $\Gamma_f \times 1$ vector of AWGN. The matrix $\mathbf{A}$ in (6.27) is the $M_BS \times M_BS$ diagonal channel matrix after space-time de-spreading at the receiver for sub-block u, given by

$$\mathbf{A} = diag(\sum_{g=1}^{M_T}|H_{1,g}[u]|^2, \sum_{g=1}^{M_T}|H_{1,g}[U+u]|^2,\ldots,\sum_{g=1}^{M_T}|H_{1,g}[(S-1)U+u]|^2, \sum_{g=1}^{M_T}|H_{2,g}[u]|^2, \sum_{g=1}^{M_T}|H_{2,g}[U+u]|^2,$$
$$\ldots,\sum_{g=1}^{M_T}|H_{2,g}[(S-1)U+u]|^2,\ldots,\sum_{g=1}^{M_T}|H_{M_B,g}[u]|^2, \sum_{g=1}^{M_T}|H_{M_B,g}[U+u]|^2,\ldots,\sum_{g=1}^{M_T}|H_{M_B,g}[(S-1)U+u]|^2) \tag{6.30}$$

Detection of the MC-DS-CDMA signals of (6.27) is similar to the detection of the conventional MC-CDMA signals using solely frequency-domain spreading, where single-user detectors or multi-user detectors [60] can be employed. The performance using the maximum-likelihood sphere decoder [41–44] , MF detector, ZF block linear detector and the MMSE block linear detector [45, p. 99-104] is investigated. Only the sub-optimal linear detectors are discussed in this section.

6.3.2.1 MF detector

In the context of the MF block linear detector, the decision variables associated with $\{b_{k,u1}\}_{k=1}^{\Gamma_f}$ are obtained by multiplying (6.27) with $\mathbf{R}^{\mathcal{H}}$, which can be expressed as

$$\begin{aligned}\mathbf{z} = \mathbf{R}^{\mathcal{H}}\mathbf{z}_{u,1} &= \mathbf{R}^{\mathcal{H}}\mathbf{A}\mathbf{R}\mathbf{b} + \mathbf{R}^{\mathcal{H}}\mathbf{n} \\ &= \mathbf{\Xi}\mathbf{b} + \mathbf{R}^{\mathcal{H}}\mathbf{n} \end{aligned} \tag{6.32}$$

where $\mathbf{\Xi} = \mathbf{R}^{\mathcal{H}}\mathbf{A}\mathbf{R}$. The resultant vector is then sent to a hard decision block in order to detect the corrupted symbols.

6.3.2.2 ZF block linear detector

In the context of the ZF block linear detector, the decision variables associated with $\{b_{k,u1}\}_{k=1}^{\Gamma_f}$ are obtained by multiplying (6.32) with the inverse of $\mathbf{\Xi}$, i.e., with $\mathbf{\Xi}^{-1}$, which can be expressed as $\mathbf{\Xi}^{-1}\mathbf{z}$. The resultant vector is then sent to a hard decision block in order to detect the corrupted symbols.

6.3.2.3 MMSE block linear detector

In the context of the MMSE block linear detector, the decision variables associated with $\{b_{k,u1}\}_{k=1}^{\Gamma_f}$ are obtained by multiplying both sides of (6.32) with

$$(\mathbf{\Xi} + \sigma_n^2\mathbf{I}_{\Gamma_f})^{-1} \tag{6.33}$$

where σ_n^2 is the noise variance. The resultant vector is then sent to a hard decision block in order to detect the corrupted symbols.

6.4 STFB CODED MC-DS-CDMA WITH JOINT DETECTION FOR FREQUENCY-SELECTIVE BLOCK-FADING CHANNELS

Up to this point, STFB codes have only been considered for MIMO-OFDM [67], and have not yet been considered for MIMO multicarrier CDMA schemes. The system model that follows combines STFB codes with MC-DS-CDMA.

6.4.1 System model

Consider a multi-user, multicarrier frequency-selective block-fading MIMO communication system with M_T transmit antennas, M_R receive antennas, $U.S$ sub-carriers per transmit antenna and Γ users. The channel between each transmit and receive antenna is composed of $L+1$ Rayleigh fading paths. The transmitter structure for the k_{th} user is depicted in Fig. 6.3. A

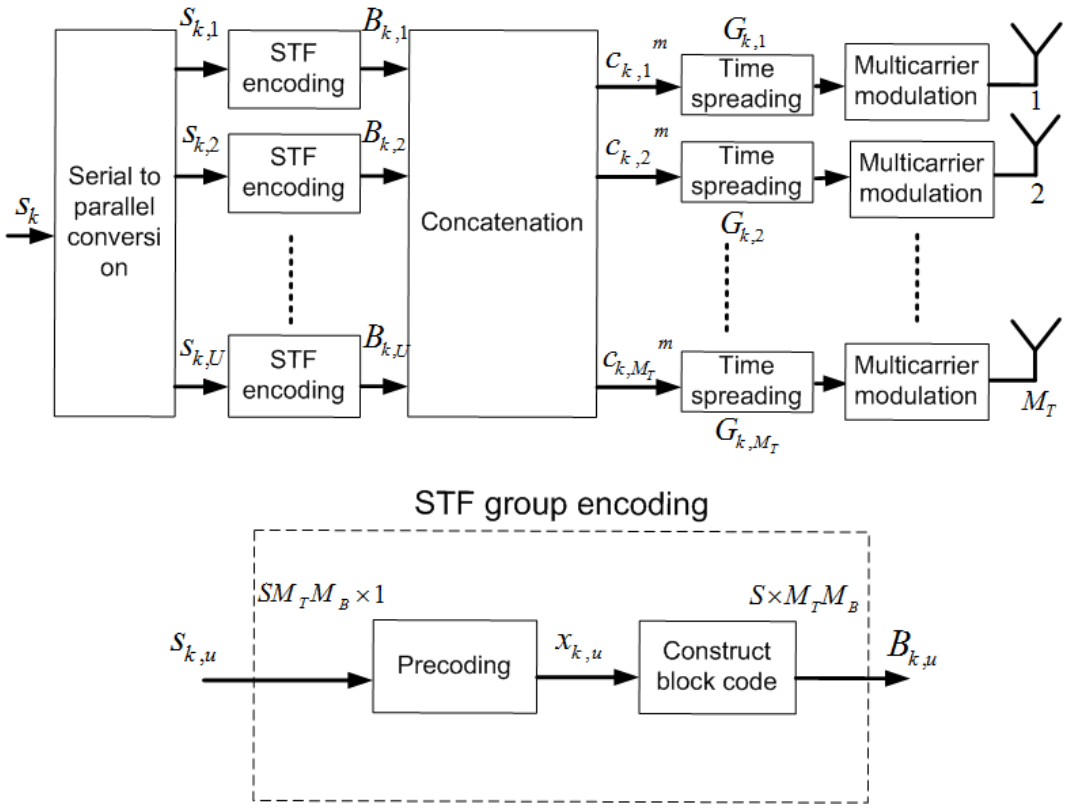

FIGURE 6.3: STFB coded MC-DS-CDMA transmitter structure for a single-user.

block of $M_T.M_B.U.S$ information symbols $\mathbf{s}_k$, from a discrete alphabet $\mathcal{A}$ (i.e. PSK or QAM), is serial to parallel converted into U parallel sub-blocks, with $M_B.M_T.S$ data symbols in each sub-block. It is assumed that $S = (L+1).M_T$ in this analysis. The symbol duration before

serial to parallel conversion is denoted by T_{sym} and the symbol duration after serial to parallel conversion is given by $M_T.U.S.T_{sym}$. It is assumed that the channel stays constant over the symbol interval $M_T.U.S.T_{sym}$; however, it may change from symbol to symbol. The above assumption implies that the coherence time $(\Delta t)_c$ [1, p. 807] of the channel is higher than but close to the symbol duration of $M_T.U.S.T_{sym}$ (i.e. $(\Delta t)_c \gtrapprox M_T.U.S.T_{sym}$). The symbol duration of $M_T.U.S.T_{sym}$ is referred to as a fading block in this analysis. Space, time and frequency coding is done over M_B fading blocks at the transmitter. In this section, it is assumed that the fading coefficients change from one fading block to the next.

Each sub-block after serial to parallel conversion $\mathbf{s}_{k,u} \in \mathcal{A}^{S.M_T.M_B}$ $(u = 1, \ldots, U)$, is further divided into M_T equal sub-blocks $\mathbf{s}^t_{k,u} \in \mathcal{A}^{SM_B}$ $(t = 1, \ldots, M_T)$, where $\mathbf{s}_{k,u} = [(\mathbf{s}^1_{k,u})^{\mathcal{T}} \cdots (\mathbf{s}^{M_T}_{k,u})^{\mathcal{T}}]^{\mathcal{T}}$. Each $\mathbf{s}^t_{k,u}$ is precoded with the same non-redundant, LCP matrix Θ (discussed in section 3.1.3). The precoded symbols are given by

$$\mathbf{x}^t_{k,u} = \Theta \mathbf{s}^t_{k,u}, \ \forall\ t = 1, \ldots, M_T \tag{6.34}$$

where $\mathbf{x}^t_{k,u} = [x^t_{k,u}(1) \cdots x^t_{k,u}(S.M_B)]^{\mathcal{T}}$. The design of the unitary precoder Θ is given by

$$\Theta = \mathbf{F}^{\mathcal{H}}_{M_B.S} diag(1\ \varphi \cdots \varphi^{M_B.S-1}) \tag{6.35}$$

where $\varphi = \exp(\frac{j2\pi}{4M_B.S})$. The vector $\mathbf{x}_{k,u}$ is given by $\mathbf{x}_{k,u} = [(\mathbf{x}^1_{k,u})^{\mathcal{T}} \cdots (\mathbf{x}^{M_T}_{k,u})^{\mathcal{T}}]^{\mathcal{T}}$. The $M_T.M_B.S$ precoded symbols in each sub-group u (i.e. $\mathbf{x}_{k,u}$) are then layered over space, time and frequency in the space-time-frequency sub-matrix $\mathbf{B}_{k,u}$, using some permutation strategy. The same permutation strategy is applied to each sub-matrix $\mathbf{B}_{k,u}$, for each user k. Thus, only the construction of one $\mathbf{B}_{k,u}$ is discussed, which is given in (6.36) and (6.37). The $S \times M_T.M_B$ matrix $\mathbf{B}_{k,u}$ is given by

$$\mathbf{B}_{k,u} = \begin{pmatrix} \mathbf{X}^1_1 & \mathbf{X}^2_1 & \cdots & \mathbf{X}^{M_B}_1 \\ \mathbf{X}^1_2 & \mathbf{X}^2_2 & \cdots & \mathbf{X}^{M_B}_2 \\ \vdots & \vdots & \ddots & \vdots \\ \mathbf{X}^1_{L+1} & \mathbf{X}^2_{L+1} & \cdots & \mathbf{X}^{M_B}_{L+1} \end{pmatrix} \tag{6.36}$$

where each $M_T \times M_T$ matrix $\mathbf{X}^m_s$ is given by

$$\mathbf{X}^m_s = \begin{pmatrix} x^1_{k,u}(k^m_s + 1) & x^2_{k,u}(k^m_s + 1) & \cdots & x^{M_T}_{k,u}(k^m_s + 1) \\ x^{M_T}_{k,u}(k^m_s + 2) & x^1_{k,u}(k^m_s + 2) & \cdots & x^{M_T-1}_{k,u}(k^m_s + 2) \\ \vdots & \vdots & \ddots & \vdots \\ x^2_{k,u}(k^m_s + M_T) & x^3_{k,u}(k^m_s + M_T) & \cdots & x^1_{k,u}(k^m_s + M_T) \end{pmatrix} \tag{6.37}$$

The index k_s^m in (6.37) is given by $k_s^m = (m-1)(L+1)M_T + (s-1)M_T$. The $U.S \times M_T.M_B$ matrix $\mathbf{C}_k$ can be represented as

$$\mathbf{C}_k = [\mathbf{B}_{k,1}^{\mathcal{T}} \mathbf{B}_{k,2}^{\mathcal{T}} \cdots \mathbf{B}_{k,U}^{\mathcal{T}}]^{\mathcal{T}} = [\mathbf{C}_k^1 \, \mathbf{C}_k^2 \cdots \mathbf{C}_k^{M_B}] \tag{6.38}$$

where each $U.S \times M_T$ matrix $\mathbf{C}_k^m$, is transmitted during fading block m, and can be represented as

$$\mathbf{C}_k^m = [\mathbf{c}_{k,1}^m \, \mathbf{c}_{k,2}^m \cdots \mathbf{c}_{k,M_T}^m] \tag{6.39}$$

Each column of symbols in (6.39) is transmitted from a different transmit antenna in fading block m. User k uses orthogonal time domain spreading sequences $\mathbf{g}_{k,t}$, $k = 1, \ldots, \Gamma$, $t = 1, \ldots, M_T$, where each user is assigned M_T time-domain spreading sequences. User separation is only done with the time-domain spreading sequences. Each of the time domain spreading sequences has the form

$$\mathbf{g}_{k,t} = \frac{1}{\sqrt{Q}}[g_{k,t}(0) \cdots g_{k,t}(Q-1)]^{\mathcal{T}} \tag{6.40}$$

where $g_{k,t}(q)$, $q = 0, \ldots, Q-1$ denotes the spreading chip at time q. If orthogonal Walsh-Hadamard codes are employed, the maximum number of users supported by the system is given by

$$\Gamma = \lfloor \frac{Q}{M_T} \rfloor \tag{6.41}$$

Each $(Q.U.S) \times (U.S)$ spreading matrix is given by

$$\mathbf{G}_{k,t} = \mathbf{g}_{k,t} \otimes \mathbf{I}_{U.S} \tag{6.42}$$

Each $\mathbf{c}_{k,t}^m$ in (6.39) is multiplied with a different spreading matrix $\mathbf{G}_{k,t}$ before transmission. The STFB code $\mathbf{C}_k^m$ in (6.39) after spreading is given by

$$C_k^m = [\mathbf{G}_{k,1}\mathbf{c}_{k,1}^m \quad \cdots \quad \mathbf{G}_{k,M_T}\mathbf{c}_{k,M_T}^m] \tag{6.43}$$

where C_k^m is a $Q.U.S \times M_T$ matrix. Fig 6.4 depicts the flow chart for the transmission procedure described above. The spreading codes, assigned to each transmit antenna (for user k), are orthogonal and provide spatial separation at the receiver. Let $\mathcal{F}$ be the $(Q.U.S) \times (Q.U.S)$ block diagonal matrix of the $U.S \times U.S$ FFT matrix given by $\mathcal{F} = \mathbf{I}_Q \otimes \mathbf{F}_{U.S}$ (represents the FFT operation at the chip-rate). Similarly, the block diagonal inverse FFT matrix can be expressed as $\mathcal{F}^{\mathcal{H}}$ (represents the IFFT operation at the chip-rate). The cyclic prefix insertion matrix at each transmit antenna is expressed as

$$\mathbf{T} = \mathbf{I}_Q \otimes \mathbf{T}_{CP} \tag{6.44}$$

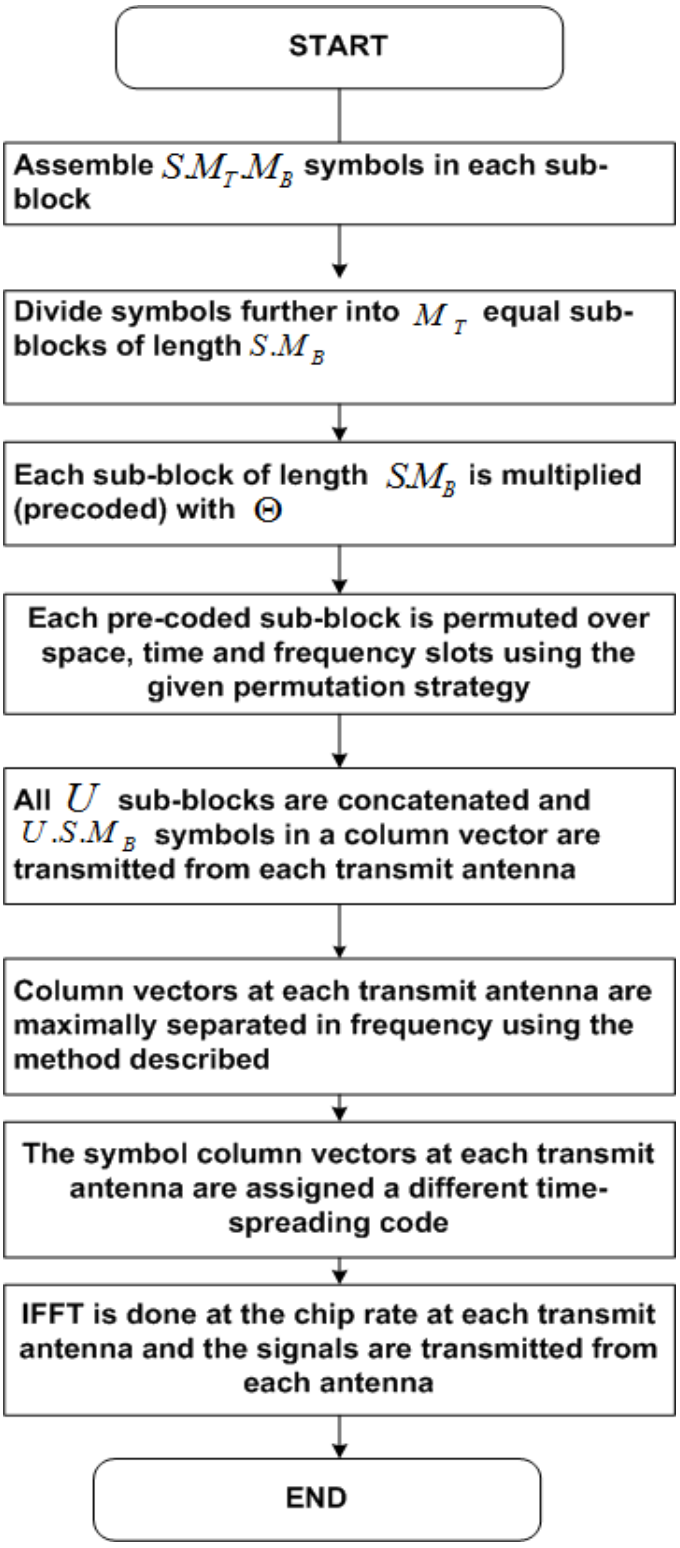

FIGURE 6.4: Flow chart of the transmission procedure at the transmitter.

where $\mathbf{T}_{CP} = [\mathbf{I}_{CP}^{\mathcal{T}} \mathbf{I}_{U.S}^{\mathcal{T}}]^{\mathcal{T}}$ and CP is the cyclic prefix length. The total number of sub-carriers at each transmit antenna is divided into U groups, with S sub-carriers in each group. Sub-carriers

belonging to the same group are maximally separated in the frequency domain using the matrix Υ. The matrix Υ is defined as a $U.S \times U.S$ permutation matrix that maximally separates the data of each sub-group u in the frequency domain, i.e., the $(x, y)_{th}$ element of Υ is equal to 1 if $x = (y-1)mod(U).S + \lfloor \frac{y-1}{U} \rfloor + 1$, and equal to 0 otherwise. The transmitted signal matrix for user k is expressed as

$$\mathcal{S}_k^m = \mathcal{F}^{\mathcal{H}} \mathbf{T} (\mathbf{I}_Q \otimes \Upsilon) C_k^m \tag{6.45}$$

The cyclic prefix removal matrix at each receive antenna can be expressed as

$$\mathbf{R} = \mathbf{I}_Q \otimes \mathbf{R}_{CP} \tag{6.46}$$

where $\mathbf{R}_{CP} = [\mathbf{0}_{U.S \times CP} \mathbf{I}_{U.S}]$. The CIR of each MIMO channel path, for fading block m is given by $\mathbf{h}_{i,t}^m = [h_{i,t}^m(0) \dots h_{i,t}^m(L)]$, $i = 1, \dots, M_R$, $t = 1, \dots, M_T$ and $m = 1, \dots, M_B$. $\mathbf{H}_{i,t}^m$ is a $(U.S + CP) \times (U.S + CP)$ lower triangular Toeplitz matrix which represents the linear convolution of the frequency-selective channel in fading block m, expressed as

$$\mathbf{H}_{i,t}^m = \begin{pmatrix} h_{i,t}^m(0) & 0 & 0 & \cdots & 0 \\ \vdots & h_{i,t}^m(0) & 0 & \cdots & 0 \\ h_{i,t}^m(L) & \cdots & \ddots & \cdots & \vdots \\ \vdots & \ddots & \cdots & \ddots & 0 \\ 0 & \cdots & h_{i,t}^m(L) & \cdots & h_{i,t}^m(0) \end{pmatrix} \tag{6.47}$$

The $(U.S + CP).Q \times (U.S + CP).Q$ block-diagonal channel matrix of the linear convolutive frequency-selective block-fading channel for each MIMO path, and each fading block m, can be represented as $\mathbb{H}_{i,t}^m = \mathbf{I}_Q \otimes \mathbf{H}_{i,t}^m$. The receiver structure at each receive antenna for user k in fading block m, is shown in Fig. 6.5. After cyclic prefix removal, FFT and de-spreading at the receiver, the received symbols during fading block m at the i_{th} receive antenna can be expressed as

$$\mathbf{y}_i^m = \sum_{k=1}^{\Gamma} \sum_{t=1}^{M_T} \Upsilon^{\mathcal{T}} \mathbf{G}_{k,t}^{\mathcal{H}} \mathcal{F} \mathbf{R} \mathbb{H}_{i,t}^m \mathbf{T} \mathcal{F}^{\mathcal{H}} \mathbf{G}_{k,t} \Upsilon \mathbf{c}_{k,t}^m + \nu_i^m \tag{6.48}$$

where ν_i^m is the $U.S \times 1$ vector of AWGN with variance σ_n^2. The matrix $\Upsilon^{\mathcal{T}} \mathbf{G}_{k,t}^{\mathcal{H}} \mathcal{F} \mathbf{R} \mathbb{H}_{i,t}^m \mathbf{T} \mathcal{F}^{\mathcal{H}} \mathbf{G}_{k,t} \Upsilon$ forms a diagonal matrix of the frequency response of the channel. Owing to cyclic prefix insertion at the transmitter and removal at the receiver, the linear convolution of the channel becomes a circular convolution. $\mathbf{y}_i^m$ can be simplified to

$$\mathbf{y}_i^m = \sum_{k=1}^{\Gamma} \sum_{t=1}^{M_T} \widetilde{\mathbf{H}}_{i,t}^m \mathbf{c}_{k,t}^m + \nu_i^m \tag{6.49}$$

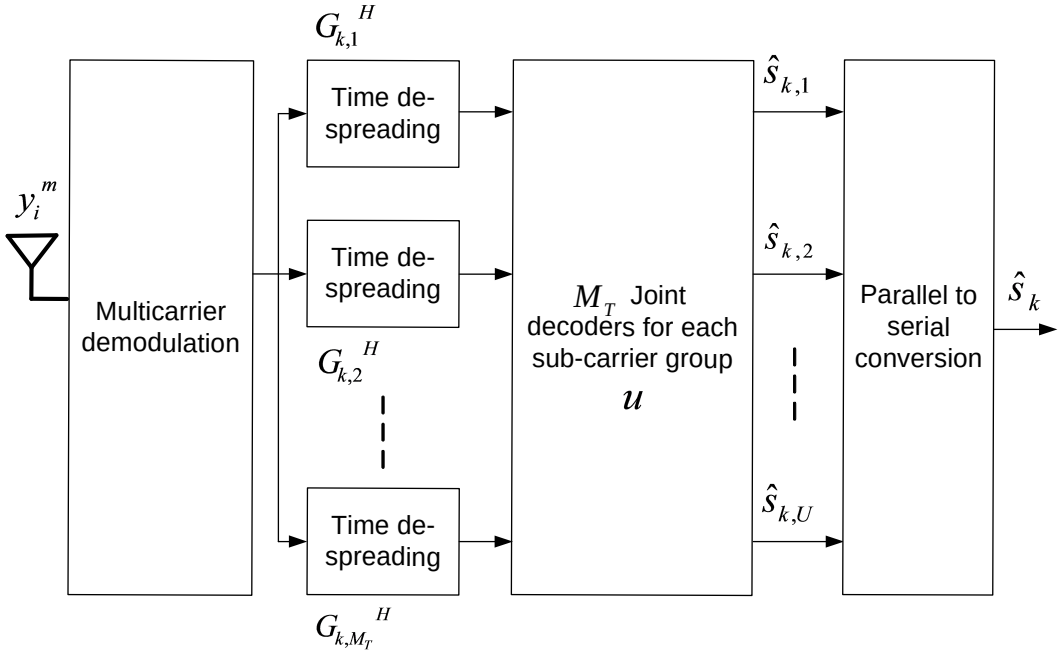

FIGURE 6.5: STFB coded MC-DS-CDMA receiver structure for a single-user at each receive antenna.

where

$$\widetilde{\mathbf{H}}_{i,t}^{m} = diag(H_{i,t}^{m}(1), H_{i,t}^{m}(U+1), \ldots, H_{i,t}^{m}((S-1).U+1), H_{i,t}^{m}(2), H_{i,t}^{m}(U+2),$$

$$\ldots, H_{i,t}^{m}((S-1).U+2), \ldots, H_{i,t}^{m}(U), H_{i,t}^{m}(2.U), \ldots, H_{i,t}^{m}(S.U)) \tag{6.50}$$

$\widetilde{\mathbf{H}}_{i,t}^{m}$ is the $U.S \times U.S$ matrix of the frequency response of the channel in fading block m and

$$H_{i,t}^{m}(p) = \sum_{l=0}^{L} h_{i,t}^{m}(l) \exp(\frac{-j2\pi l(p-1)}{U.S}) \tag{6.51}$$

where the channel coefficients $\{h_{i,t}^{m}(l)\}_{l=0}^{L}$ are generated using the method described in section 4.3. Since the different users time domain spreading sequences are orthogonal, each user can be separated from the other users perfectly at the receiver. Thus, the proposed system is MUI free. However, M_T single-user joint detectors are used for joint detection at the receiver, for each $\mathbf{B}_{k,u}$. Thus, the multi-user detection problem for STS-assisted MC-DS-CDMA in the previous section is replaced with a single-user joint detection problem. The flow chart for the receiver is given in Fig. 6.6.

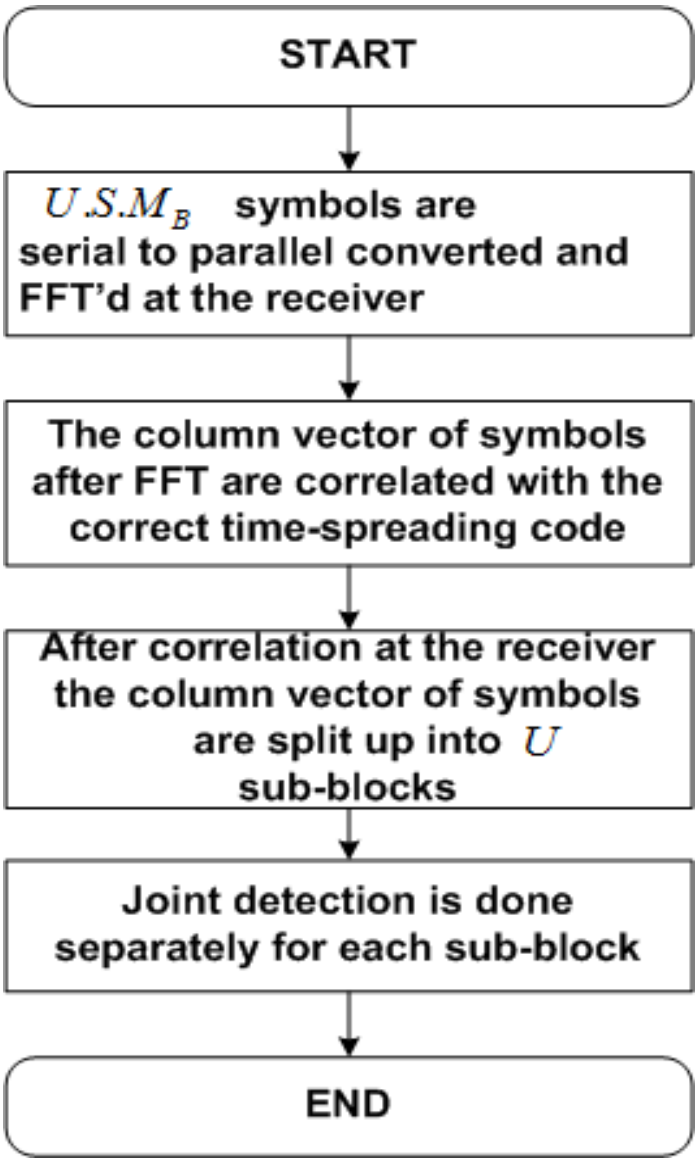

FIGURE 6.6: Flow chart of the reception procedure at the receiver.

6.4.2 Signal detection

The symbols in each sub-group u for user k are decoded in exactly the same way. Thus, only the symbols in sub-group $u = 1$ are considered. The received $M_BS \times 1$ vector $\mathbf{z}$, of the first $M_B.S$ received symbols in sub-group $u = 1$, is given by

$$\mathbf{z} = \hat{\mathbf{H}}\Theta\mathbf{s}_{k,1}^{1} + \mathbf{n} \tag{6.52}$$

$$= \Xi\mathbf{s}_{k,1}^{1} + \mathbf{n} \tag{6.53}$$

where $\Xi = \hat{\mathbf{H}}\Theta$ and $\mathbf{n}$ is the $M_B.S \times 1$ vector of complex white Gaussian noise samples. The $M_R.M_B.S \times M_B.S$ matrix $\hat{\mathbf{H}}$ is defined as

$$\hat{\mathbf{H}} = \begin{pmatrix} diag(\hat{\mathbf{h}}_1) \\ diag(\hat{\mathbf{h}}_2) \\ \vdots \\ diag(\hat{\mathbf{h}}_{M_R}) \end{pmatrix} \tag{6.54}$$

where $\hat{\mathbf{h}}_i = [\hat{\mathbf{h}}_{i,1}^{\mathcal{T}}\ \hat{\mathbf{h}}_{i,2}^{\mathcal{T}}\ \cdots\ \hat{\mathbf{h}}_{i,M_B}^{\mathcal{T}}]^{\mathcal{T}}$ and $\hat{\mathbf{h}}_{i,m}$ is expressed as

$$\hat{\mathbf{h}}_{i,m} = [H_{i,1}(1)^m\ H_{i,2}(U+1)^m\ \cdots\ H_{i,M_T}((M_T-1).U+1)^m\ H_{i,1}((M_T).U+1)^m$$
$$H_{i,2}((M_T+1).U+1)^m\ \cdots\ H_{i,M_T}((S-1).U+1)^m]^{\mathcal{T}} \tag{6.55}$$

Detection of the MC-DS-CDMA signals of (6.53) can be done using joint detection at the receiver. The performance using the MF detector, ZF block linear detector and the MMSE block linear detector (discussed in section 3.2.1.) is investigated.

6.4.2.1 MF detector

In the context of the MF detector, the decision variables associated with $\mathbf{z}$ are obtained by multiplying (6.53) with $\Xi^{\mathcal{H}}$, which can be expressed as

$$\Xi^{\mathcal{H}}\mathbf{z} = \Xi^{\mathcal{H}}\Xi\mathbf{s}_{k,1}^1 + \Xi^{\mathcal{H}}\mathbf{n} \tag{6.56}$$

The resultant vector is then sent to a hard decision block in order to detect the corrupted symbols.

6.4.2.2 ZF block linear detection

In the ZF detector, the receiver multiplies the received vector $\mathbf{z}$ with $(\Xi^{\mathcal{H}}\Xi)^{-1}\Xi^{\mathcal{H}}$. Then, the resultant vector is given by $\mathbf{s}_{k,1}^1 + (\Xi^{\mathcal{H}}\Xi)^{-1}\Xi^{\mathcal{H}}\mathbf{n}$. The resultant vector is then sent to a hard decision block in order to detect the corrupted symbols.

6.4.2.3 MMSE block linear detection

The received vector $\mathbf{z}$ is multiplied with

$$\mathbf{M} = \Xi^{\mathcal{H}}(\Xi\Xi^{\mathcal{H}} + \frac{\sigma_n^2}{\sigma_s^2}\mathbf{I}_{M_B.S})^{-1} \tag{6.57}$$

where σ_n^2 and σ_s^2 are the noise variance and information symbol variance, respectively. The product is then fed to a hard decision block to detect the transmitted symbols.

6.4.3 Examples

Let the first user be the user of interest ($k = 1$), and assume that $U = 1$, $M_T = L + 1 = 2$ and $S = 4$ frequency tones. The sub-script k is omitted for convenience. Only the $M_B = 1$ and $M_B = 2$ cases are considered in this section.

$M_B = 1$:

In this case no temporal diversity is exploited. The super-script m is dropped for convenience, since only $M_B = 1$ fading block is considered. The proposed MC-DS-CDMA STFB code matrix can be represented as

$$C = [\mathbf{G}_1\mathbf{c}_1 \ \mathbf{G}_2\mathbf{c}_2] \tag{6.58}$$

where

$$[\mathbf{c}_1 \ \mathbf{c}_2] = \begin{pmatrix} x_1(1)^1 & x_1(1)^2 \\ x_1(2)^2 & x_1(2)^1 \\ x_1(3)^1 & x_1(3)^2 \\ x_1(4)^2 & x_1(4)^1 \end{pmatrix} \tag{6.59}$$

and $[x_1(1)^t \dots x_1(4)^t]^T = \Theta[s_1(1)^t \dots s_1(4)^t]^T$, $t = 1, 2$. $\mathbf{s}_1^t$ represents the symbol block before constellation rotation, Θ is the 4×4 algebraic precoder (rotation matrix given in Table 3.1) and the sub-script t represents the algebraic layer number. Each column in (6.58) is modulated at the chip-rate on $U.S = 4$ sub-carriers. Because of the orthogonality of the spreading codes, the symbols transmitted from each transmit antenna can be spatially separated at the receiver. After de-spreading and correlation at the receiver, the t algebraic layers in (6.59) are decoded independently. Each layer is decoded with a joint decoder.

$M_B = 2$:

The proposed MC-DS-CDMA STFB code matrix is given by

$$C = [\mathbf{G}_1\mathbf{c}_1^1 \ \mathbf{G}_2\mathbf{c}_2^1 \ \mathbf{G}_1\mathbf{c}_1^2 \ \mathbf{G}_2\mathbf{c}_2^2] \tag{6.60}$$

where

$$[\mathbf{c}_1^1 \ \mathbf{c}_2^1 \ \mathbf{c}_1^2 \ \mathbf{c}_2^2] = \begin{pmatrix} x_1(1)^1 & x_1(1)^2 & x_1(5)^1 & x_1(5)^2 \\ x_1(2)^2 & x_1(2)^1 & x_1(6)^2 & x_1(6)^1 \\ x_1(3)^1 & x_1(3)^2 & x_1(7)^1 & x_1(7)^2 \\ x_1(4)^2 & x_1(4)^1 & x_1(8)^2 & x_1(8)^1 \end{pmatrix} \tag{6.61}$$

where $[x_1(1)^t \dots x_1(8)^t]^T = \Theta[s_1(1)^t \dots s_1(8)^t]^T$, $t = 1, 2$. Θ is the 8×8 algebraic rotation matrix (rotation matrix given in Table 3.1) and the sub-script t represents the algebraic layer number. During the first fading block, columns 1 and 2 in (6.60) are modulated using $U.S = 4$

sub-carriers (at the chip-rate), from transmit antennas 1 and 2, respectively. During the second fading block, columns 3 and 4 in (6.60) are modulated using $U.S = 4$ sub-carriers, from transmit antennas 1 and 2, respectively. After de-spreading and correlation at the receiver, each layer t in (6.61) is decoded independently, with a joint decoder.

6.5 COMPARISONS

In this section, STS-assisted MC-DS-CDMA (discussed in section 6.3) is compared with STFB coded MC-DS-CDMA (discussed in section 6.4) with regard to certain parameters as given in Table 6.1. From Table 6.1, STFB coded MC-DS-CDMA assigns more data symbols per

TABLE 6.1: Comparisons

Parameter	**STS-assisted MC-DS-CDMA**	**STFB coded MC-DS-CDMA**
No. of symbols per user	$M_T.U$	$M_T.U.S.M_B$
No. of users	$\lfloor \frac{Q.M_B.S}{M_T} \rfloor$	$\lfloor \frac{Q}{M_T} \rfloor$
No. of time-domain sequences	M_T, for $M_T = 2, 4$ and 8 (real symbols)	M_T
to achieve full diversity	or $M_T = 2$ (complex symbols)	
Sub-carrier group size	$S \geq L + 1$	$S \geq (L + 1)M_T$
Diversity order achievable	$M_T.M_R.(L + 1).M_B$	$M_T.M_R.(L + 1).M_B$

user. However, STS-assisted MC-DS-CDMA is able to accommodate more users in the same bandwidth. The two systems have different user allocations; however, both systems are able to achieve the same bandwidth efficiency and diversity order. Both systems rely on joint detection at the receiver. For the same diversity order, the minimum sub-carrier group size S, for STS-assisted MC-DS-CDMA is smaller than that for STFB coded MC-DS-CDMA. This is due to the fact that STS-assisted MC-DS-CDMA achieves spatial diversity using STS, whereas the frequency and temporal diversity are achieved by spreading (or coding) over time (i.e. fading blocks) and frequency (i.e. sub-carriers). STFB coded MC-DS-CDMA achieves spatial, frequency and temporal diversity by spreading (or coding) over space (i.e. antennas), time (i.e. fading blocks) and frequency (sub-carriers) where no STS is employed. Thus, in general, STS-assisted MC-DS-CDMA has a smaller joint decoding complexity at the receiver due the

smaller group size S, for the same diversity order. However, in STS-assisted MC-DS-CDMA, there is a constraint on the number of transmit antennas employed. If one considers the transmission of real symbols from a real constellation (e.g. BPSK) at the transmitter, then STS-assisted MC-DS-CDMA only achieves full diversity if $M_T = 2, 4$ or 8. If one considers the transmission of complex symbols from a complex constellation (e.g.QPSK or QAM) at the transmitter, then STS-assisted MC-DS-CDMA only achieves full diversity if $M_T = 2$. The above-mentioned constraints relate to a problem in orthogonal designs [27, 28]. No such constraint exists for STFB coded MC-DS-CDMA and full diversity is always achieved using M_T time-domain spreading sequences per user.

6.6 CONCLUDING REMARKS

In this chapter two alternative MIMO downlink MC-DS-CDMA schemes were proposed that achieve full diversity (spatial, frequency and temporal diversity) in frequency-selective block-fading channel conditions. The first scheme in section 6.3 achieves spatial diversity using STS, whereas frequency and temporal diversity are achieved by coding over frequency and time. The second scheme in section 6.4 achieves spatial, frequency and temporal diversity by coding over space, frequency and time, where no STS is employed. Comparisons are made between the two systems in section 6.5, highlighting the advantages and drawbacks associated with each system. Both systems are able to achieve the same bandwidth efficiency and diversity order.

CHAPTER SEVEN
RESULTS

The simulation results for all systems considered in this dissertation are presented in this section. Section 7.1 presents simulation results for TF-domain spreading MC-DS-CDMA discussed in section 5.3. Simulation results for STS-assisted MC-DS-CDMA (discussed in section 6.3) are presented in section 7.2. Finally, simulation results for STFB coded MC-DS-CDMA (discussed in section 6.4) are given in section 7.3.

7.1 TF-DOMAIN SPREADING UPLINK MC-DS-CDMA FOR FREQUENCY-SELECTIVE BLOCK-FADING CONDITIONS

Simulations are carried out to investigate the performance of TF-domain spreading MC-DS-CDMA using ZCZ sequences for frequency-selective block-fading channel conditions discussed in section 5.3, by choosing BER as a figure of merit. BPSK modulation is employed in all simulations. The performance is investigated using the optimal ML decoder, the sphere decoder [42–44] and the MMSE block linear detector discussed in [45, p.104] at the receiver. In the simulations, the channel coefficients are constant during one symbol block duration (i.e. UT_{sym}), but change from one block to another one. In this section the (64,4,14)-ZCZ sequences discussed in section 2.3.1 are used as time-domain spreading sequences. A quasi-synchronous uplink channel is considered in these simulations where the following assumptions are made.

- No MUI is introduced due to the different user's ZCZ time-domain spreading sequences, on condition that the maximum quasi-synchronism between users $\tau_{a,max}$ is less than the zero correlation zone length ($\tau_{a,max} \leq Z_0$) [13].

- If T_c is the ZCZ time domain spreading sequence chip duration on each sub-carrier, then the maximum quasi-synchronism between users $\tau_{a,max}$ is assumed to be $\tau_{a,max} = 5T_c$.
- The delay spread of each user's channel is assumed to be the same (i.e. τ_s=$\tau_{s,u}$ $\forall$ μ), where each user's channel has $L + 1$ channel taps.
- The channels of the different users are statistically independent.
- Perfect CSI is available at the receiver.

The columns of a Walsh-Hadamard matrix are used as frequency domain spreading codes unless otherwise specified.

7.1.1 Comparative performance

In this section, TF-domain spreading MC-DS-CDMA for frequency-selective block-fading conditions is compared with TF-domain spreading MC-DS-CDMA for frequency-selective slow fading conditions [13]. The simulation parameters are given in Table 7.1 for both systems. In [13], joint decoding is only carried out over one fading block at the receiver (i.e $M_B = 1$).

TABLE 7.1: Simulation parameters

Symbol	Value	Description
$U.S$	32	Total number of sub-carriers
U	8	Number of parallel sub-blocks
Q	64	ZCC spreading sequence length
S	4	Sub-carriers in each group
T_{sym}	1μs	Input symbol duration before
T_c	0.5μs	ZCC sequence chip duration on each sub-carrier
CP	0.25×$U.S$	Cyclic prefix length
$L + 1$	4	Number of Rayleigh fading paths
τ_s	0.375μs	Total delay spread

However, to illustrate the performance gain achieved in block-fading conditions, the system in [13] is compared to the system proposed in section 5.3, where joint decoding is carried

out over two fading blocks (i.e. $M_B = 2$) at the receiver. For the system in [13] ($M_B = 1$), the performance is investigated at full load with $\Gamma_f = SM_B = 4$ users, where the frequency spreading codes were taken as the columns of a 4×4 Walsh-Hadamard matrix. For the system proposed here ($M_B = 2$), the performance is investigated at full load with $\Gamma_f = SM_B = 8$ users and the frequency spreading codes are taken as the columns of an 8×8 Walsh-Hadamard matrix. This was done in order to achieve the same data transmission rate for both systems. Fig. 7.1 shows the performance results using the optimal ML detector and the MMSE block linear detector at the receiver. One observes from Fig. 7.1, that there is an approximate 2.7 dB performance improvement for the optimal ML detector at a BER of 10^{-4}. One observes only a slight performance improvement when the MMSE detector is employed at the receiver. Thus, the proposed system out-performs the system proposed in [13] owing to the additional temporal diversity exploited in block-fading conditions.

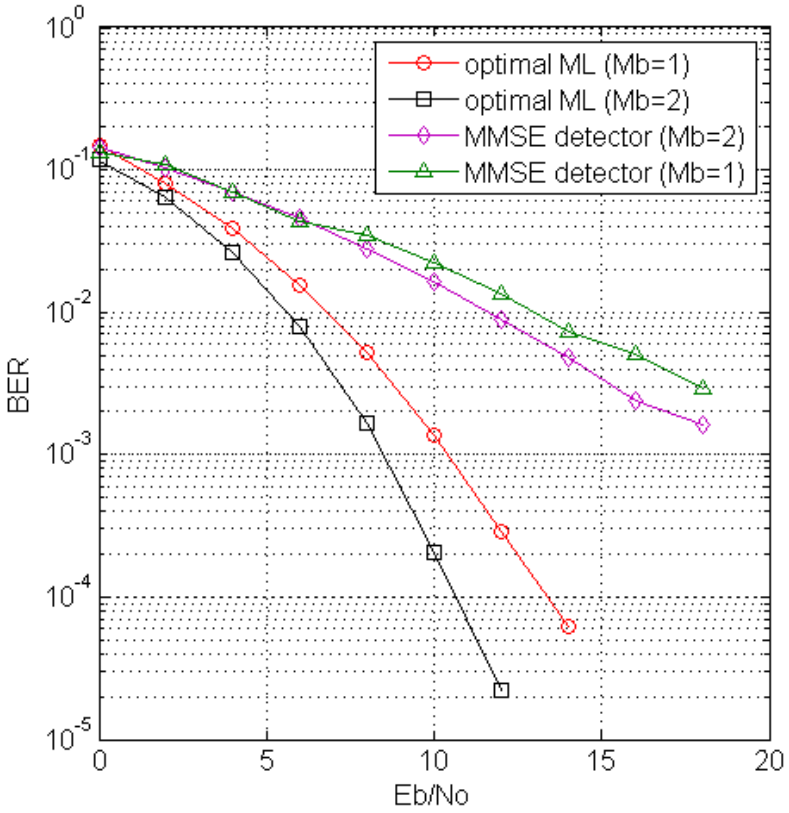

FIGURE 7.1: Performance comparison with the system in [13], using the optimal ML detector and the MMSE block linear detector at the receiver.

7.1.2 Performance using a sphere decoder

In this section, the performance of the system is investigated using a sphere decoder at the receiver using the parameters in Table 7.1. Figure 7.2 investigates the performance using a sphere decoder for $\Gamma_f = 4$, 6 and 8 users. In Fig. 7.2, the frequency spreading codes are taken as the columns of an 8×8 linear constellation precoding (LCP) matrix ([55] and section 3.1.3). The optimal 8×8 LCP matrix can be expressed as

$$\Theta = \mathbf{F}_8^{\mathcal{H}} diag(1, \theta, \ldots, \theta^7) \tag{7.1}$$

where $\theta = \exp(j2\pi/32)$. One can see the gradual performance degradation using a sphere

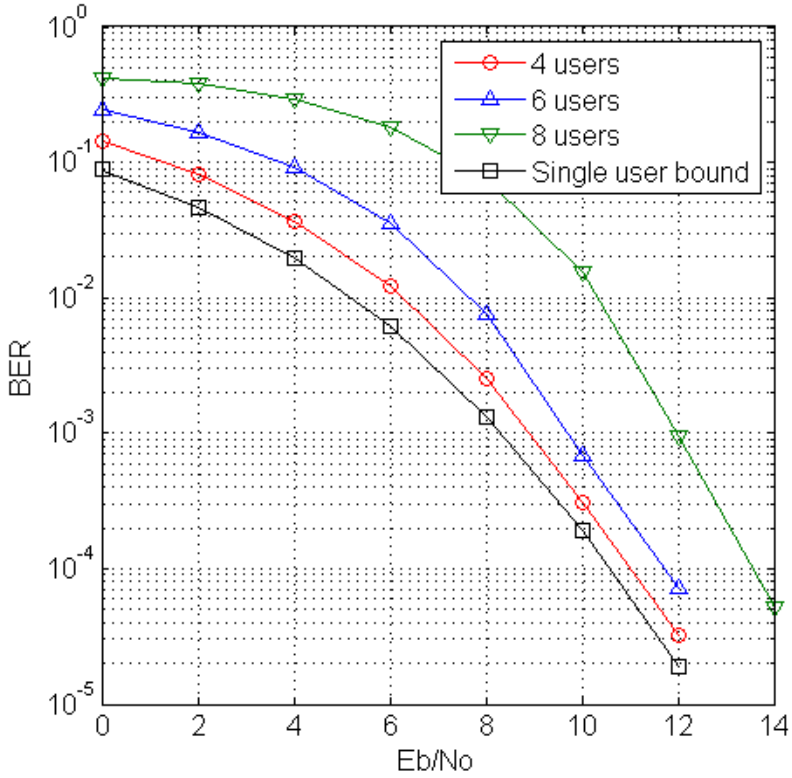

FIGURE 7.2: Performance using a sphere decoder for $\Gamma_f = 4$, 6 and 8 users.

decoder when increasing the number of users in Fig. 7.2. At medium to large SNR, the performance approaches the single-user bound.

7.1.3 Concluding remarks

In this section it was verified that TF-domain spreading MC-DS-CDMA using ZCZ sequences for frequency-selective block-fading channels achieves the full diversity available in the

wireless channel (time and frequency diversity), in the uplink. In addition, the proposed system outperforms the system proposed in [13] owing to the additional temporal diversity exploited in block-fading channels. The system was simulated with a sphere decoder, optimal ML decoder and MMSE detector at the receiver.

7.2 STS-ASSISTED DOWNLINK MC-DS-CDMA FOR FREQUENCY-SELECTIVE BLOCK-FADING CONDITIONS

Simulations are carried out to investigate the performance of STS-assisted TF-domain spreading MC-DS-CDMA for frequency-selective and block-fading channel conditions discussed in section 6.3, by choosing BER as a figure of merit. BPSK modulation is employed in all simulations. The performance is investigated using optimal maximum likelihood decoding, sphere decoding as well as the MF, ZF and MMSE block linear detectors discussed in [45] at the receiver. Simulations are carried out with and without antenna correlation using the MIMO channel model discussed in Chapter 4. In the simulations, the channel coefficients are constant during one symbol block duration (i.e. UM_TT_{sym}), but change from one block to another block.

TABLE 7.2: Simulation parameters

Symbol	Value	Description
M_T	2	Transmit antennas
M_R	1	Receive antennas
$U.S$	16	Total number of sub-carriers
U	4	Number of parallel sub-blocks
Q	8	STS Walsh-Hadamard spreading sequence length
S	4	Sub-carriers in each group
T_{sym}	1μs	Input symbol duration
T_c	2μs	STS sequence chip duration on each sub-carrier
CP	$0.25\times U.S$	Cyclic prefix length
$L+1$	4	Number of Rayleigh fading paths
T_m	0.5μs	Total delay spread

7.2.1 Comparative performance

Comparisons are made with the system proposed in [8], at the same data transmission rate. The parameters in Table 7.2 are used for both systems. In [8], joint decoding is only carried out

over one fading block at the receiver (i.e $M_B = 1$). However, to illustrate the performance gain achieved in block-fading conditions, the system in [8] is compared to the system proposed here, where joint decoding is carried out over two fading blocks (i.e. $M_B = 2$) at the receiver. For the system in [8] ($M_B = 1$), the performance is investigated at full load with $\Gamma_f = S M_B = 4$ users, where the frequency spreading codes were taken as the columns of a 4×4 Walsh-Hadamard matrix. For the system proposed here ($M_B = 2$), the performance is investigated at full load with $\Gamma_f = S M_B = 8$ users and the frequency spreading codes are taken as the columns of an 8×8 Walsh-Hadamard matrix. This was done in order to achieve the same data transmission rate for both systems. One observes from Fig. 7.3, that there is an approximate 1 dB performance improvement when employing the ZF detector at the receiver at a BER of 10^{-4}. However, the MF detector actually shows a performance loss when joint decoding is done over $M_B = 2$ fading blocks at the receiver. Fig. 7.4 investigates the performance improvement when sphere decoding and MMSE decoding are carried out at the receiver. For sphere decoding there is an approximate 2.7 dB performance improvement at a BER of 10^{-4}. For MMSE decoding there

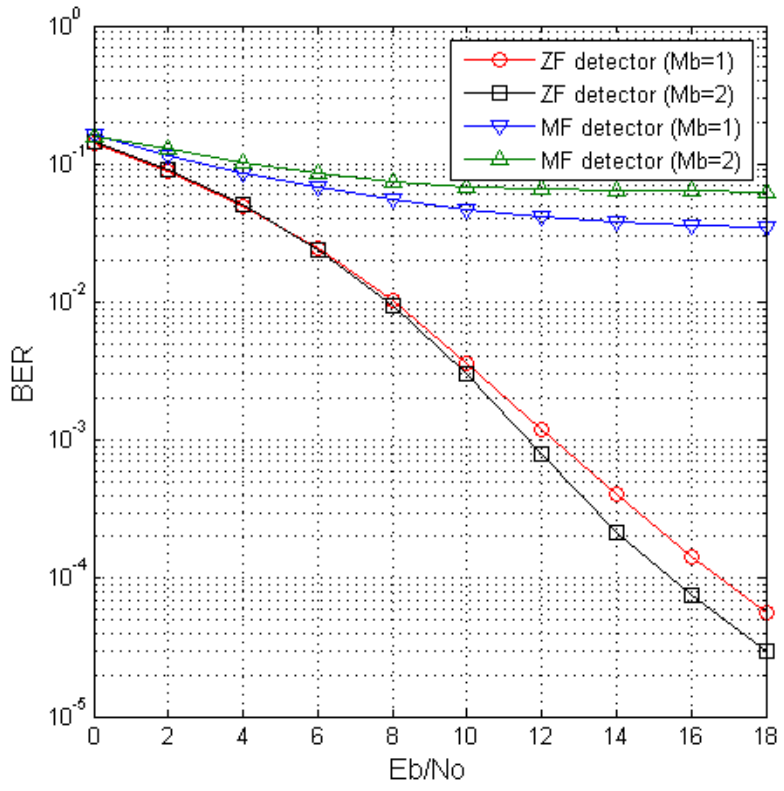

FIGURE 7.3: Performance comparison with the system in [8], using the MF detector and the ZF detector at the receiver.

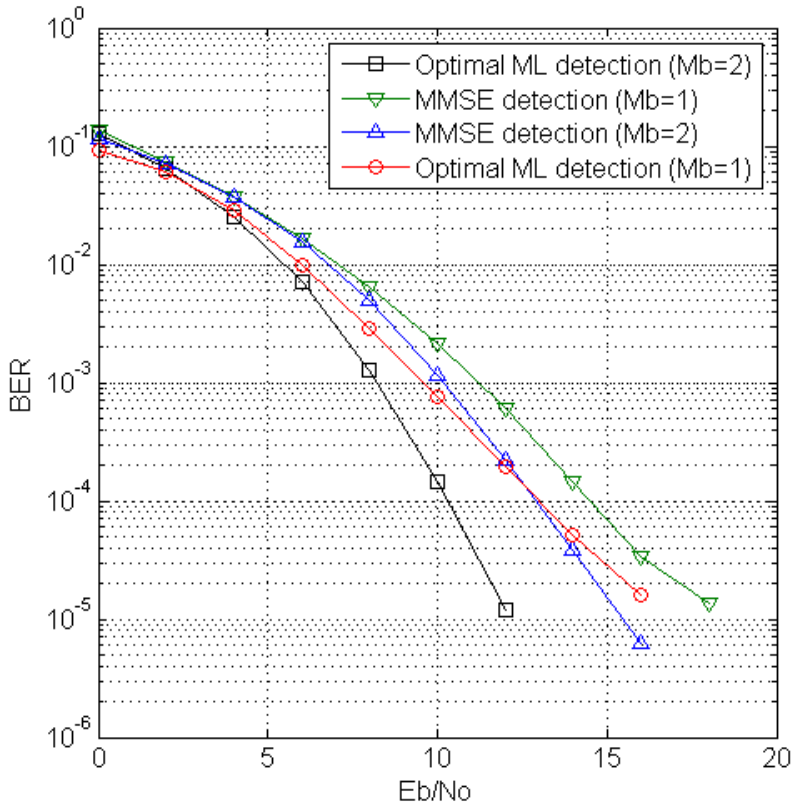

FIGURE 7.4: Performance comparison with the system in [8], using a sphere decoder and the MMSE detector at the receiver.

is an approximate 1.5 dB performance improvement at a BER of 10^{-4}. The improvement in performance can be attributed to the fact that the system in [8] is only able to achieve spatial and frequency diversity (i.e. diversity order of $M_T M_R(L+1)M_B = 8$). However, in the proposed system joint decoding is carried out over two fading blocks, achieving a diversity order of $M_T M_R(L+1)M_B = 16$.

7.2.2 Performance using different frequency spreading codes

In this section, instead of just using the columns of a Walsh-Hadamard matrix as frequency spreading codes as in [8], the columns of an algebraic LCP matrix (in section 3.1.3) are employed as frequency spreading codes and comparisons are made between the two. The parameters in Table I are again used in this section. Joint decoding is done over two fading blocks ($M_B = 2$) at the receiver. Both Walsh-Hadamard and LCP matrices are of size 8×8. The optimal 8×8 LCP matrix is given in equation (7.1). Fig. 7.5 investigates the performance using

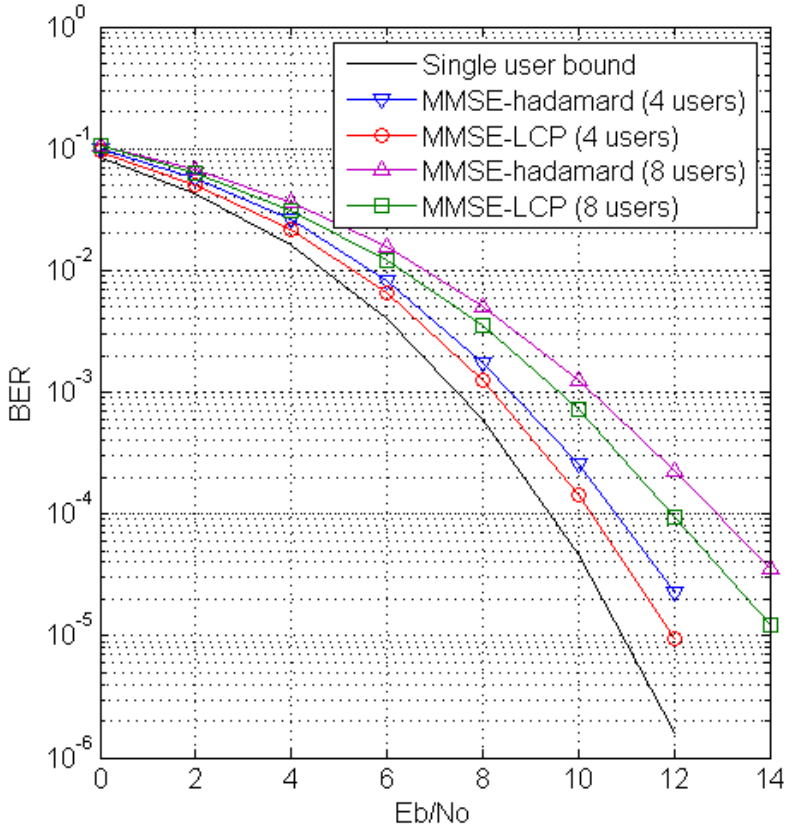

FIGURE 7.5: Performance using different frequency-domain spreading codes for $\Gamma_f = 4$ users and $\Gamma_f = 8$ users.

an MMSE detector at the receiver for $\Gamma_f = 4$ users and $\Gamma_f = 8$ users. For $\Gamma_f = 4$ users there is an approximate 0.6 dB performance improvement at a BER of 10^{-4} and for $\Gamma_f = 8$ users there is an approximate 1 dB performance improvement at a BER of 10^{-4}. Thus, one can conclude that the columns of an LCP matrix perform slightly better than the columns of a Walsh-Hadamard matrix when used as frequency-domain spreading codes due to the optimum coding gain that they provide [54, 55]. Fig. 7.6 illustrates the gradual performance degradation when employing the columns of an 8×8 LCP matrix as frequency spreading codes for $\Gamma_f = 1, 4, 6$ and 8 users. Fig. 7.6 also employs an MMSE detector at the receiver.

7.2.3 Performance in a realistic channel

In this section, the performance in an $L + 1 = 20$ tap suburban alternative channel [68] is investigated using the parameters in Table II. The suburban alternative PDP [68] is given in Table 7.3. Joint decoding is done over $M_B = 2$ fading blocks using a sphere decoder at the

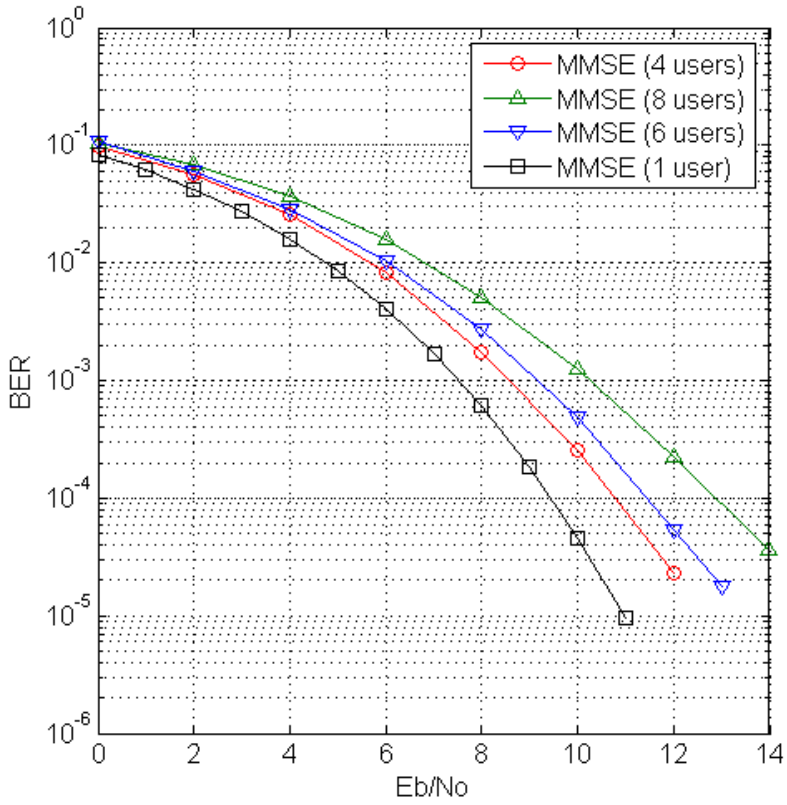

FIGURE 7.6: Performance using the columns of an LCP matrix as frequency-domain spreading codes for $\Gamma_f = 1, 4, 6$, and 8 users.

receiver, with $\Gamma_f = 8$ users. The columns of a 16×16 LCP matrix are used as frequency-domain spreading codes. The 16×16 LCP matrix (section 3.1.3) is expressed as

$$\Theta = \mathbf{F}_{16}^{\mathcal{H}} diag(1, \theta, \ldots, \theta^{15}) \tag{7.2}$$

where $\theta = \exp(j2\pi/64)$. Only antenna correlation is considered in this section. In the first case $\rho_{RX} = \rho_{TX} = 0.4$ (40 % correlation) is considered, where ρ_{RX} and ρ_{TX} are the transmit and receive antenna correlation coefficients, respectively. In the second case $\rho_{RX} = \rho_{TX} = 0.7$ (70 % antenna correlation) is considered. Finally, $\rho_{RX} = \rho_{TX} = 0.9$ (90 % antenna correlation) is considered. From Fig. 7.7, there is a negligible performance difference with 40 % antenna correlation. The performance is slightly worse with 70 % antenna correlation. The performance with 90 % antenna correlation shows an approximate 2 dB performance loss at a BER of 10^{-5}.

TABLE 7.3: Suburban alternative power delay profile

Delay (ns)	Magnitude (dB)	Delay (ns)	Magnitude (dB)
0	0	1910	-6.4
110	-1.8	2100	-11.8
290	-4.2	2310	-12.8
490	-4.6	2510	-12.1
700	-7.5	2700	-16.3
870	-7.6	2850	-15.3
1100	-8.4	3120	-18.4
1320	-10	3280	-19.6
1470	-8.6	4880	-20.2
1690	-8.3	7170	-21.6

TABLE 7.4: Simulation parameters for the suburban alternative channel

Symbol	Value	Description
M_T	2	Transmit antennas
M_R	2	Receive antennas
$U.S$	64	Total number of sub-carriers
U	8	Number of parallel sub-blocks
Q	8	STS Walsh-Hadamard spreading sequence length
S	8	Sub-carriers in each group
T_{sym}	1μs	Input symbol duration
T_c	8μs	STS sequence chip duration on each sub-carrier
CP	0.3125$\times U.S$	Cyclic prefix length
$L+1$	20	Number of Rayleigh fading paths
T_m	7.12μs	Total delay spread

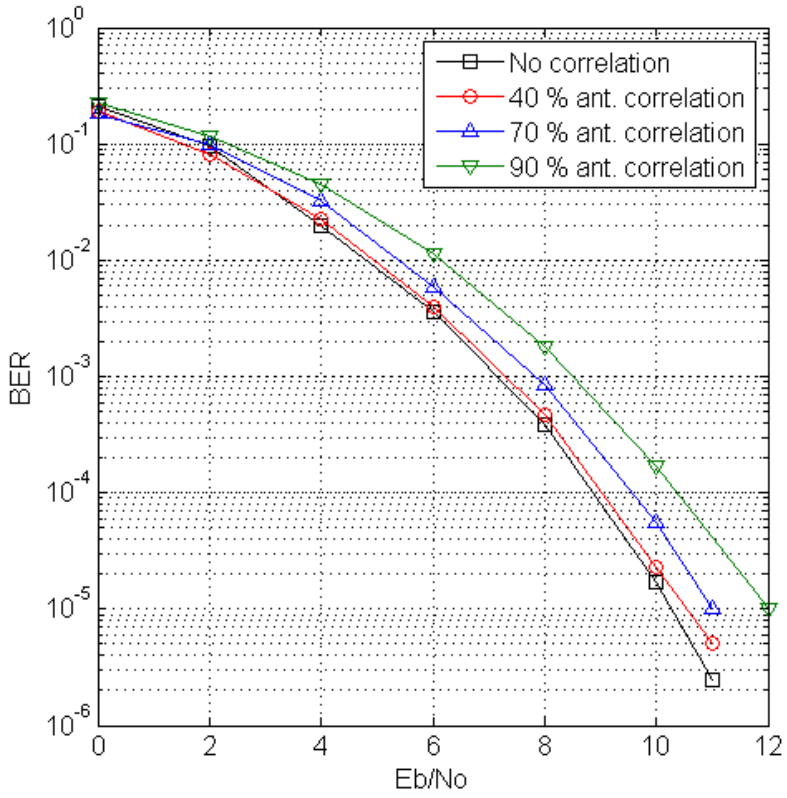

FIGURE 7.7: Performance in the suburban alternative channel with $\Gamma_f = 8$ users for 0 %, 40 %, 70 % and 90 % antenna correlation.

7.2.4 Concluding remarks

In this section it was verified that STS-assisted TF-domain spreading MC-DS-CDMA achieves the full diversity available in the wireless channel (space, time and frequency diversity). It is shown that when using a sphere decoder at the receiver, the proposed system provided a performance improvement of approximately 2.7 dB at a BER of 10^{-4} over the scheme in [8], due to the additional temporal diversity exploited in block-fading conditions. The performance of the system was investigated when the columns of an LCP matrix (section 3.1.3) were used as frequency-domain spreading codes. The LCP matrix outperformed the Walsh-Hadamard matrix (used in [8]), in all cases considered. In addition, it was shown that when introducing antenna correlation in the suburban alternative channel [68], there was only a slight degradation in BER performance for 40 % and 70 % correlation.

7.3 STFB CODED DOWNLINK MC-DS-CDMA FOR FREQUENCY-SELECTIVE BLOCK-FADING CONDITIONS

Simulations are carried out to investigate the performance of STFB coded MC-DS-CDMA for frequency-selective block-fading conditions discussed in section 6.4, by choosing BER as a figure of merit. BPSK modulation is employed in all simulations. Simulations are carried out with and without antenna correlation using the MIMO channel model discussed in Chapter 4. In the simulations, the channel coefficients are constant during one symbol block duration (i.e. $M_T.U.S.T_{sym}$), but change from one block to another one.

TABLE 7.5: Simulation parameters

Symbol	Value	Description
M_T	2	Transmit antennas
M_R	1 and 2	Receive antennas
$U.S$	16	Total number of sub-carriers
S	4	Number of sub-carriers in each group
U	4	Number of sub-carrier groups
Q	8	Walsh-Hadamard spreading sequence length
T_{sym}	1μs	Input symbol duration
T_c	2μs	Chip duration on each sub-carrier
CP	$0.25\times N$	Cyclic prefix length
$L+1$	2	Number of Rayleigh fading paths
T_m	0.5μs	Delay spread

7.3.1 Performance in uncorrelated conditions

Simulations are done for a broadband data rate of 1 Mbps. In this section the sphere decoder is used for joint detection at the receiver. The system was simulated using the parameters given in Table 7.5. Fig. 7.8 presents simulation results for $M_B = 1, 2$ and $M_R = 1, 2$. Simulation

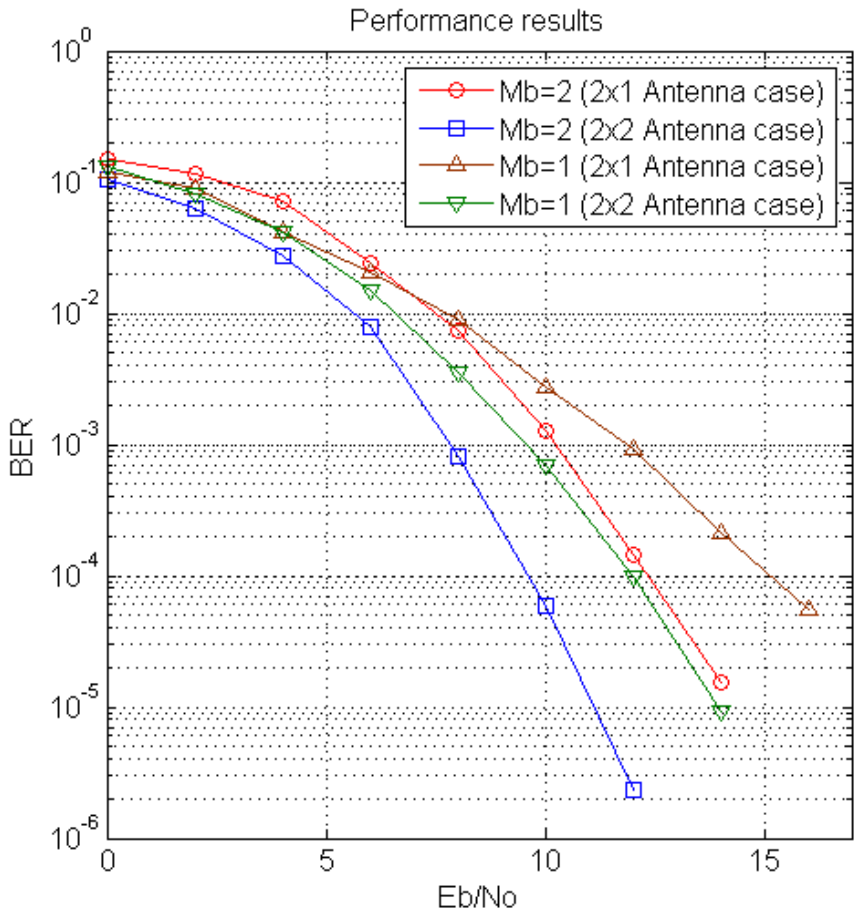

FIGURE 7.8: Performance results without antenna correlation.

results reveal that for the $M_B = 1$ case, the proposed system achieves a diversity order of $M_T M_R(L+1)M_B = 4$ when $M_R = 1$, and $M_T M_R(L+1)M_B = 8$ when $M_R = 2$. For the $M_B = 2$ case, the proposed system achieves a diversity order of $M_T M_R(L+1)M_B = 8$ when $M_R = 1$, and $M_T M_R(L+1)M_B = 16$ when $M_R = 2$. Thus, the proposed downlink scheme achieves diversity in space, time and frequency (full diversity).

7.3.2 Performance in correlated conditions

A broadband data rate of 1 Mbps is again considered. The proposed system was simulated with antenna correlation using the parameters given in Table 7.5, with $M_R = 2$ receive antennas. Only antenna correlation is considered. Joint decoding is done over $M_B = 1$ and $M_B = 2$ fading blocks. In the first case $\rho_{RX} = \rho_{TX} = 0.4$ (40 % correlation) is considered, where ρ_{RX} and ρ_{TX} are the transmit and receive antenna correlation coefficients, respectively. In the second

case $\rho_{RX} = \rho_{TX} = 0.7$ (70 % antenna correlation) is considered. Finally, $\rho_{RX} = \rho_{TX} = 0.9$ (90 % antenna correlation) is considered. Fig. 7.9 shows the performance results with antenna correlation, when $M_B = 1$. With 40 % antenna correlation, there is only a small degradation

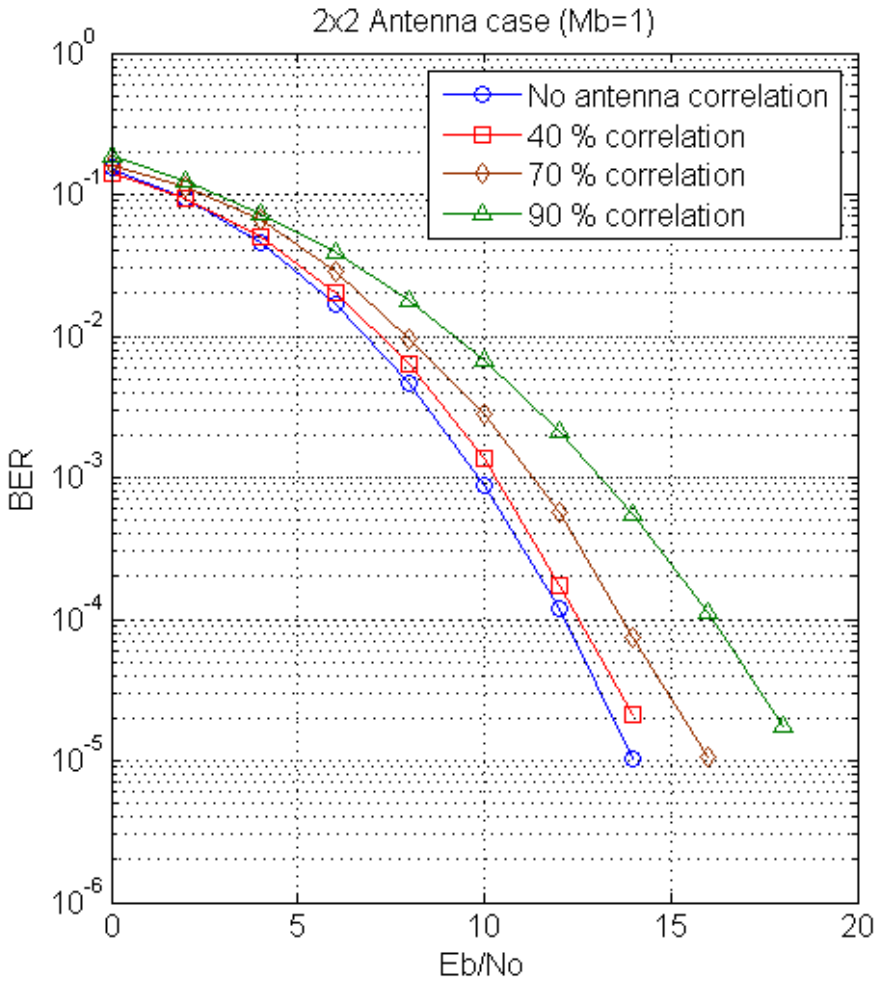

FIGURE 7.9: Performance results when antenna correlation is introduced, when $M_B = 1$.

in performance. For 70 and 90 % antenna correlation, the performance degradation is more severe. There is an approximate 4 dB performance loss for 90 % antenna correlation, compared to the uncorrelated case. Fig. 7.10 shows the performance results with antenna correlation, when $M_B = 2$. It is observed from Fig. 7.10 that the performance degradation is similar to that of Fig. 7.9. For the $M_B = 2$ case in Fig. 7.10, the performance degradation with 90 % antenna correlation is less severe than that of Fig. 7.9.

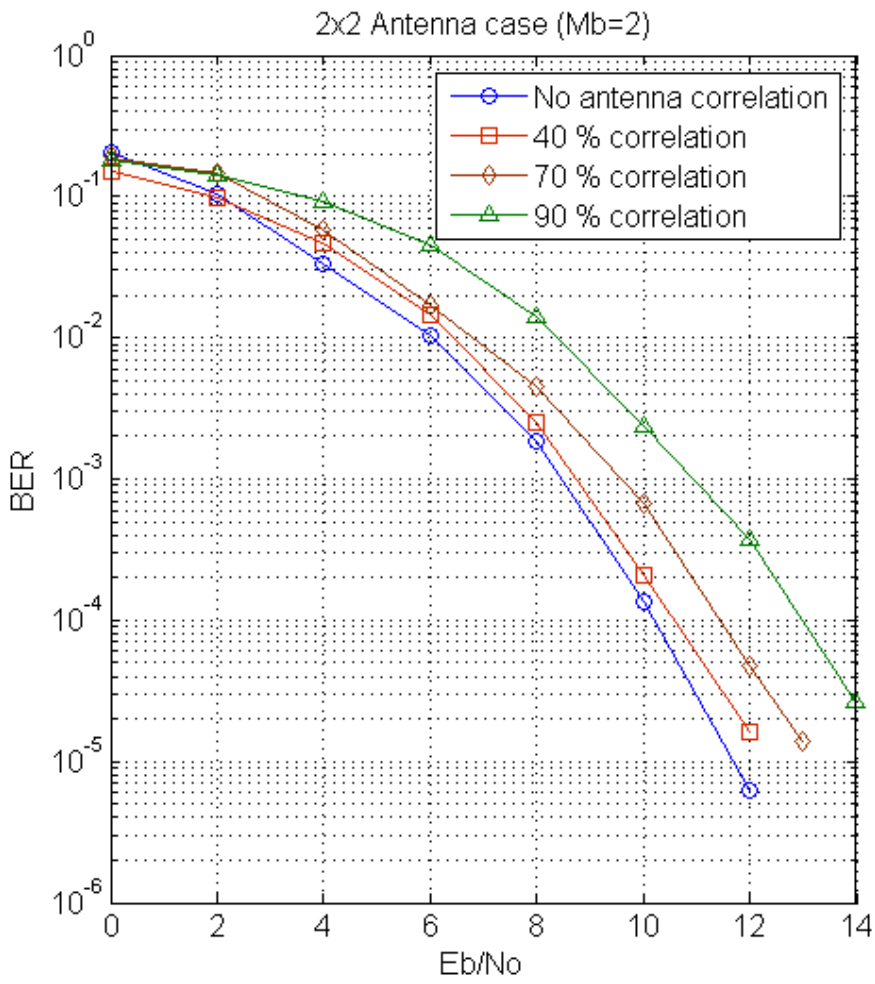

FIGURE 7.10: Performance results when antenna correlation is introduced, when $M_B = 2$.

7.3.3 Performance using linear joint detection

In this section the performance of STFB coded MC-DS-CDMA using the linear joint detection algorithms (discussed in section 3.2) is investigated. The simulation parameters are given in Table 7.5, with the only differences being that $M_R = 2$ and $L + 1 = 4$. Joint decoding is done over $M_B = 2$ fading blocks. The performance using optimal ML detection, the ZF detector, the MMSE detector and the MF detector is shown in Fig. 7.11. It is shown in Fig. 7.11 that optimal ML detection performs better than the other joint detection schemes. The MMSE detector has a considerable performance improvement over the ZF and MF detectors.

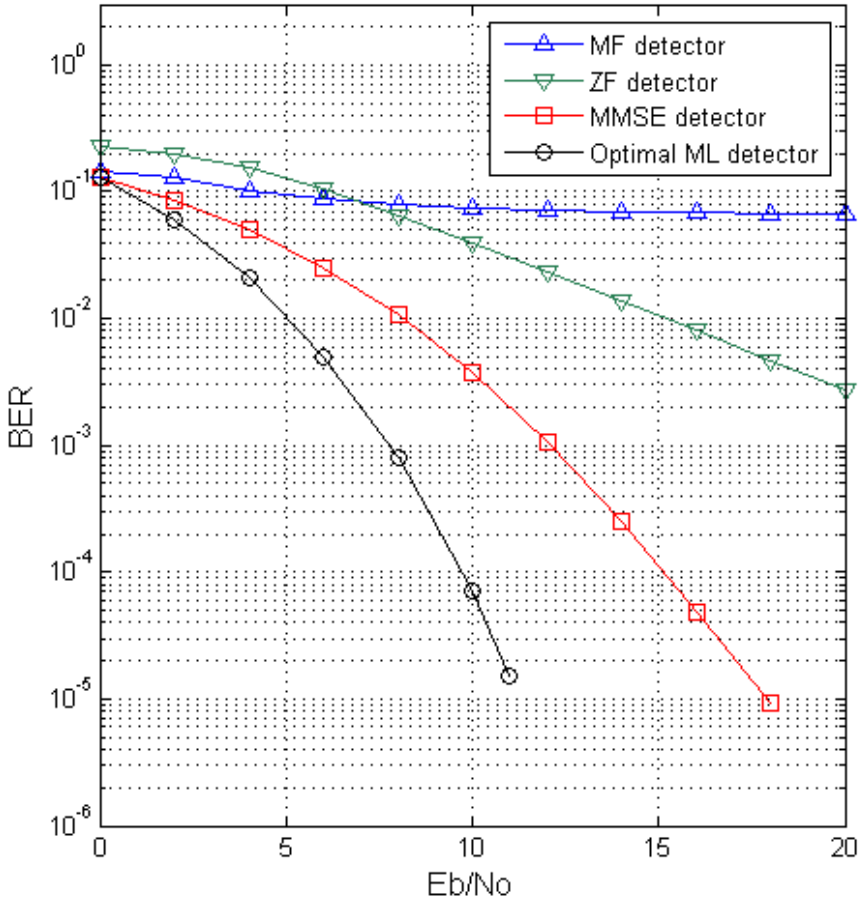

FIGURE 7.11: Performance results using optimal ML detection, the ZF detector, the MMSE detector and the MF detector, for $M_B = 2$.

7.3.4 Performance comparison with STS-assisted MC-DS-CDMA

STFB coded MC-DS-CDMA (section 6.4) is compared with the STS-assisted TF-domain spreading MC-DS-CDMA proposed in section 6.3, using the parameters given in Table 7.5. For STFB coded MC-DS-CDMA, joint decoding is done over $M_B = 2$ fading blocks at the receiver. For STS-assisted TF-domain spreading MC-DS-CDMA joint decoding is done over $M_B = 1$ and $M_B = 2$ fading blocks at the receiver. For STS-assisted TF-domain spreading MC-DS-CDMA, the columns of a 4×4 and 8×8 LCP matrix [55] are used as frequency-domain spreading codes over $M_B = 1$ and $M_B = 2$ fading blocks, respectively. A sphere decoder is used for joint detection at the receiver for all systems considered. In STS-assisted MC-DS-CDMA, $\Gamma_f = 4$ users are employed for $M_B = 1$ and $\Gamma_f = 8$ users are employed for $M_B = 2$, so that all systems considered have the same data transmission rate.

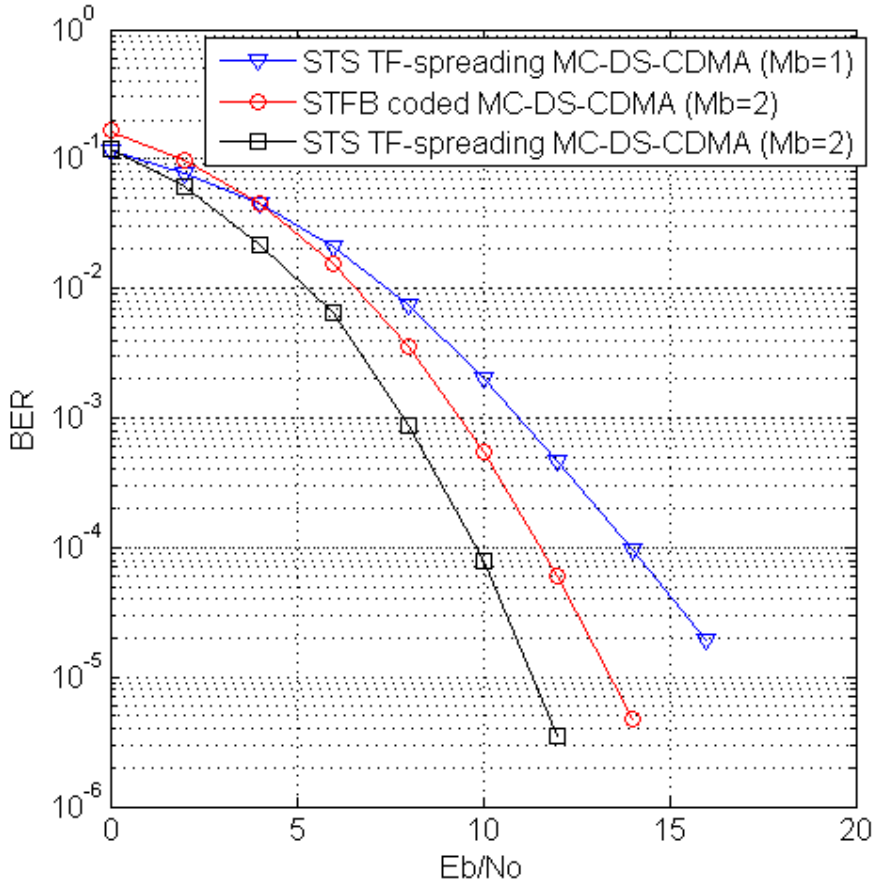

FIGURE 7.12: Performance results comparing STS-assisted TF-domain spreading MC-DS-CDMA and STFB coded MC-DS-CDMA.

Fig. 7.12 shows the simulation results. Fig. 7.12 shows that STFB coded MC-DS-CDMA designed for $M_B = 2$ outperforms STS-assisted MC-DS-CDMA (section 6.3) designed for $M_B = 1$ by 3 dB at 2×10^{-5} in block-fading conditions. However, STS-assisted MC-DS-CDMA designed for $M_B = 2$ outperforms STFB coded MC-DS-CDMA designed for $M_B = 2$ by approximately 2 dB at 2×10^{-5}. Thus one can conclude that STS-assisted MC-DS-CDMA designed for $M_B = 2$ is the most optimal system of the three.

7.3.5 Concluding remarks

In this section it was verified that STFB coded MC-DS-CDMA achieves the full diversity available in the wireless channel (space, time and frequency diversity). It was also verified that when antenna correlation is present there is a degradation in BER performance. However, the performance is still acceptable at correlation values below 70 %. It was also verified that at the

same data transmission rate, STS-assisted TF-domain spreading MC-DS-CDMA (section 6.3) is able to achieve a better BER performance than STFB coded MC-DS-CDMA, even though both schemes achieve the same diversity order. This can be attributed to the fact that STS-assisted TF-domain spreading MC-DS-CDMA achieves spatial diversity by using space-time spreading, which provides more coding gain.

CHAPTER EIGHT

CONCLUSIONS AND FUTURE RESEARCH

8.1 CONCLUSIONS

In this dissertation, uplink and downlink TF-domain spreading MC-DS-CDMA systems designed for frequency-selective block-fading conditions were investigated.

In Chapter 2, conventional Walsh-Hadamard and orthogonal Gold sequences were discussed with respect to sequence length L_{seq}, family size M_{seq} and autocorrelation/cross-correlation properties. The advantages of ZCZ sequences over conventional orthogonal sequences were then highlighted, and the construction procedure for a set of almost optimal quadriphase ZCZ sequences was detailed.
Chapter 3 summarized the ideas behind constellation rotation, and detailed the optimal construction of algebraic LCP (rotation) matrices that maximize diversity and coding gains. Optimal and sub-optimal joint detection schemes were then discussed for CDMA systems in the second part of Chapter 3.
Chapter 4 detailed the triply selective MIMO channel model, used as a platform for BER simulations in Chapter 7.
In Chapter 5, a unique system model for TF-domain spreading MC-DS-CDMA using ZCZ codes was presented to exploit frequency and temporal diversity in frequency-selective block-fading conditions, for quasi-synchronous uplink transmissions.
In Chapter 6, two unique MIMO MC-DS-CDMA schemes were proposed to exploit spatial, frequency and temporal diversity (full-diversity) in frequency-selective block-fading conditions, for synchronous downlink transmissions.

Finally, simulation results were provided in Chapter 7, for all systems considered in this dissertation using the MIMO channel model discussed in Chapter 4. It was shown that MC-DS-CDMA systems designed for frequency-selective block-fading conditions are able to achieve a higher diversity order (and thus better BER performance) than MC-DS-CDMA systems designed for frequency-selective slow fading conditions due to the additional temporal diversity available in the channel. The introduction of antenna or spatial correlation on both multi-antenna MC-DS-CDMA schemes considered, degraded the BER performance. However, for both systems, the performance loss was not too severe and still acceptable for values below 70 % correlation.

8.2 FUTURE RESEARCH

The work in this thesis can serve as a launch pad for a number of future research topics. The future work presented below is subdivided into two categories, namely channel estimation and synchronization.

8.2.1 Channel estimation

In this work, it is assumed that the receiver has perfect knowledge about the channel (i.e. fading parameters, delay and noise power). In practice this assumption is not valid, and instead the receiver has to estimate the channel characteristics. There are several ways for the receiver to estimate the CSI (e.g. pilot-assisted channel estimation and decision directed channel estimation). However, regardless of the method used in estimating the channel conditions, there is an error associated with this estimate. The error between the actual channel and the estimated channel can degrade the joint detection performance significantly. Therefore, it is important to study the effect of imperfect channel estimates on the performance of the MC-DS-CDMA schemes discussed in this dissertation. Alternatively, one could consider employing blind joint detection methods for the MC-DS-CDMA schemes considered, where CSI is not required. The design of blind joint detection algorithms for MC-DS-CDMA is a topic that requires further investigation.

8.2.2 Synchronization

In this dissertation it was assumed that perfect synchronization was achieved at the receiver for each user, for all of the MC-DS-CDMA systems considered. However, this is not a valid assumption in practice, where timing and carrier phase offsets dramatically degrade the BER performance of multicarrier systems. Thus, an interesting research avenue would be an analysis of different synchronization schemes, for the uplink and downlink MC-DS-CDMA schemes considered in this dissertation as well as the effects of timing and carrier phase offsets on the system performance with multiple users.

REFERENCES

[1] J. G. Proakis, *Digital Communications*. Fourth edition, New York: McGraw-Hill, 2001.

[2] N. Yee, J. P. Linnartz, and G. Fettweis, "Multi-carrier CDMA in indoor wireless radio network," *IEICE Transactions on Communications*, vol. E77-B, no. 7, pp. 900–904, July 1994.

[3] V. M. DaSilva and E. S. Sousa, "Multicarrier orthogonal CDMA signals for quasi-synchronous communication systems," *IEEE Journal on Selected Areas in Communications*, vol. 12, no. 5, pp. 842–852, June 1994.

[4] S. Kondo and L. B. Milstein, "Performance of multicarrier DS CDMA systems," *IEEE Transactions on Communications*, vol. 44, no. 2, pp. 238–246, Feb 1996.

[5] E. A. Sourour and M. Nakagawa, "Performance of orthogonal multicarrier CDMA in a multipath fading channel," *IEEE Transactions on Communications*, vol. 44, no. 3, pp. 356–367, March 1996.

[6] L. L. Yang and L. Hanzo, "Multicarrier DS-CDMA: a multiple access scheme for ubiquitous broadband wireless communications," *IEEE Communications Magazine*, vol. 41, no. 10, pp. 116–124, Oct 2003.

[7] L. L. Yang, W. Hua, and L. Hanzo, "Multiuser detection assisted time- and frequency-domain spread multicarrier code-division multiple-access," *IEEE Transactions on Vehicular Technology*, vol. 55, no. 1, pp. 397–405, Jan 2006.

[8] L. L. Yang and L. Hanzo, "Performance of broadband multi-carrier DS-CDMA using space-time spreading-assisted transmit diversity," *IEEE Transactions on Wireless Communications*, vol. 4, no. 3, pp. 885–894, May 2005.

[9] H. Dahman, Y. Shayan, and X. Wang, "Space-time-frequency spreading and coding for multi-user MIMO-OFDM systems," *in Proceedings of ICC*, pp. 4537–4542, May 2008.

[10] E. Biglieri, G. Caire, and G. Taricco, "Limiting performance for block fading channels with multiple antennas," *IEEE Transactions on Information Theory*, vol. 47, no. 5, pp. 1273–1289, May 2001.

[11] H. E. Gamal and A. R. Hammons, "On the design of algebraic space-time codes for MIMO block fading channels," *IEEE Transactions on Information Theory*, vol. 49, no. 1, pp. 151–163, Jan 2003.

[12] W. Zhang, X. G. Xia, and P. C. Ching, "High-rate full-diversity space-time-frequency codes for broadband MIMO block-fading channels," *IEEE Transactions on Communications*, vol. 55, no. 1, pp. 25–34, Jan 2007.

[13] H. Wei, L. L. Yang, and L. Hanzo, "Time- and frequency-domain spreading assisted MC DS-CDMA using interference rejection spreading codes for quasi-synchronous communications," *in Proceedings of IEEE VTC*, vol. 1, no. 26-29, pp. 389–393, Sep 2004.

[14] R. W. Chang, "Synthesis of band-limited orthogonal signals for multichannel data transmission," *Bell Systems Technical Journal*, vol. 45, pp. 1775–1796, Dec 1966.

[15] S. B. Weinstein and P. Ebert, "Data transmission by frequency-division multiplexing using the discrete Fourier transform," *IEEE Transactions on Communication Technology*, vol. 19, no. 5, pp. 628–634, Oct 1971.

[16] A. Peled and A. Ruiz, "Frequency domain data transmission using reduced computational complexity algorithms," *in Proceedings of ICASSP*, vol. 5, pp. 964–967, April 1980.

[17] H. Sari and G. Karam, "Orthogonal frequency-division multiple access and its application to CATV network," *European Transactions on Telecommunications*, vol. 9, no. 6, pp. 507–516, Nov 1998.

[18] W. Y. Zou and Y. Wu, "COFDM: an overview," *IEEE Transactions on Broadcasting*, vol. 41, no. 1, pp. 1–8, March 1995.

[19] N. Yee, J. P. Linnartz, and G. Fettweis, "Multicarrier CDMA in indoor wireless radio network," *in Proceedings of PIMRC*, pp. 109–113, Sep 1993.

[20] S. Hara and R. Prasad, "Overview of multicarrier CDMA," *IEEE Communications Magazine*, vol. 35, no. 12, pp. 126 –133, Dec 1997.

[21] B. M. Popovic, "Spreading sequences for multicarrier CDMA systems," *IEEE Transactions on Communications*, vol. 47, no. 6, pp. 918–926, June 1999.

[22] Q. Chen, E. S. Souza, and S. Pasupathy, "Performance of a coded multi-carrier DS-CDMA system in multipath fading channels," *Wireless Personal Communications*, vol. 2, no. 1-2, pp. 167–183, March 1995.

[23] L. Rugini, P. Banelli, and G. B. Giannakis, "Local ML detection for multi-carrier DS-CDMA downlink systems with grouped linear precoding," *IEEE Transactions on Wireless Communications*, vol. 5, no. 2, pp. 306–311, Feb 2006.

[24] H. Wei and L. Hanzo, "On the uplink performance of LAS-CDMA," *IEEE Transactions on Wireless Communications*, vol. 5, no. 5, pp. 1187–1196, May 2006.

[25] G. G. Raleigh and J. M. Cioffi, "Spatio-temporal coding for wireless communication," *IEEE Transactions on Communications*, vol. 46, no. 3, pp. 357–366, March 1998.

[26] S. M. Alamouti, "A simple transmit diversity technique for wireless communication," *IEEE Journal on Selected Areas in Communications*, vol. 16, no. 8, pp. 1451–1458, Oct 1998.

[27] V. Tarokh, H. Jafarkhani, and A. R. Calderbank, "Space-time block codes from orthogonal designs," *IEEE Transactions on Information Theory*, vol. 45, no. 5, pp. 1456–1467, July 1999.

[28] B. Hochwald, T. L. Marzetta, and C. B. Papadias, "A transmitter diversity scheme for wideband CDMA systems based on space-time spreading," *IEEE Journal on Selected Areas in Communications*, vol. 19, no. 1, pp. 48–60, Jan 2001.

[29] D. S. Shiu, G. J. Foschini, M. J. Gans, and J. M. Kahn, "Fading correlation and its effect on the capacity of multielement antenna systems," *IEEE Transactions on Communications*, vol. 48, no. 3, pp. 502–513, March 2000.

[30] A. F. Molisch, *Wireless Communications*. John Wiley and Sons, Ltd., Oct 2005.

[31] H. Donelan and T. O'Farrell, "Method for generating sets of orthogonal sequences," *Electronics Letters*, vol. 35, no. 18, pp. 1537–1538, Sep 1999.

[32] P. Z. Fan, N. Suehiro, and X. Deng, "Class of binary sequences with zero correlation zone," *Electronics Letters*, vol. 35, no. 10, pp. 777–778, May 1999.

[33] X. M. Deng and P. Z. Fan, "Spreading sequences sets with zero correlation zone," *Electronics Letters*, vol. 36, no. 11, pp. 993–994, May 2000.

[34] J. S. Cha, S. Kameda, M. Yokoyama, H. Nakase, K. Masu, and K. Tsubouchi, "New binary sequences with zero correlation duration for approximately synchronized CDMA," *Electronics Letters*, vol. 36, no. 11, pp. 991–993, May 2000.

[35] J. S. Cha, "Class of ternary spreading sequences with zero correlation duration," *Electronics Letters*, vol. 2, no. 10, pp. 636–637, May 2001.

[36] S. J. Xu and D. B. Li, "Ternary complementary orthogonal sequences with zero correlation window," *in Proceedings of IEEE PIMRC*, vol. 2, pp. 1669–1672, Sep 2003.

[37] H. Torii, M. Nakamura, and N. Suehiro, "A new class of zero-correlation zone sequences," *IEEE Transactions on Information Theory*, vol. 50, no. 3, pp. 559–565, March 2004.

[38] X. Ma and G. B. Giannakis, "Maximum-diversity transmissions over doubly selective wireless channels," *IEEE Transactions on Information Theory*, vol. 49, no. 7, pp. 1832–1840, July 2003.

[39] H. Wei, L. L. Yang, and L. Hanzo, "Downlink space-time spreading using interference rejection codes," *IEEE Transactions on Vehicular Technology*, vol. 55, no. 6, pp. 1838–1847, Nov 2006.

[40] C. Xiao, J. Wu, S. Y. Leong, Y. R. Zheng, and K. B. Letaief, "A discrete time model for triply selective MIMO Rayleigh fading channels," *IEEE Transactions on Wireless Communications*, vol. 3, no. 5, pp. 1678–1688, Sep 2004.

[41] L. Brunel, "Multiuser detection techniques using maximum likelihood sphere decoding in multicarrier CDMA systems," *IEEE Transactions on Wireless Communications*, vol. 3, no. 3, pp. 949–957, May 2004.

[42] M. O. Damen, A. Chkeif, and J. C. Belfiore, "Lattice code decoder for space-time codes," *IEEE Communication Letters*, vol. 4, no. 5, pp. 161–163, May 2000.

[43] H. Vikalo and B. Hassibi, "On the sphere decoding algorithm I. Expected complexity," *IEEE Transactions on Signal Processing*, vol. 53, no. 8, pp. 2806–2818, Aug 2005.

[44] ——, "On the sphere decoding algorithm II. Generalizations, second order statistics and applications to communications," *IEEE Transactions on Signal Processing*, vol. 53, no. 8, pp. 2819–2834, Aug 2005.

[45] L. Hanzo, L. L. Yang, E. L. Kuan, and K. Yen, *Single- and Multi-Carrier DS-CDMA: Multi-User Detection, Space-Time Spreading, Synchronization, Standards and Networking*. New York: IEEE Press/Wiley, Aug 2003.

[46] W. Zhang, X.-G. Xia, P. Ching, and H. Wang, "Rate two full-diversity space-frequency code design for MIMO-OFDM," *IEEE 6th Workshop on Signal Processing Advances*, pp. 303–307, June 2005.

[47] L. R. Welch, "Lower bounds on maximum cross-correlation of signals," *IEEE Transactions on Information Theory*, vol. IT-20, no. 3, pp. 397–399, May 1974.

[48] L. Staphorst, "Viterbi decoded linear block codes for narrowband and wideband wireless communication over mobile fading channels," *Masters dissertation, University of Pretoria*, July 2005.

[49] P. Fan and L. Hao, "Generalized orthogonal sequences and the applications in synchronous CDMA systems," *IEICE Transactions on Fundamentals of Electronics, Communications and Computer Sciences*, no. 11, pp. 2054–2066, Nov 2000.

[50] X. H. Tang, P. Z. Fan, and S. Matsufuji, "Lower bounds on the maximum correlation of sequence set with low or zero correlation zone," *Electronics Letters*, vol. 36, no. 13, pp. 551–552, March 2000.

[51] K. Takatsukasa, S. Matsufuji, Y. Watanabe, N. Kuroyanagi, and N. Suehiro, "Ternary ZCZ sequence sets for cellular CDMA systems," *IEICE Transactions on Fundamentals of Electronics, Communications and Computer Sciences*, vol. E85-A, no. 9, pp. 2135 –2140, Sep 2002.

[52] J. Boutros, E. Viterbo, C. Rastello, and J. C. Belfiore, "Good lattice constellations for both Rayleigh fading and Gaussian channel," *IEEE Transactions on Information Theory*, vol. 42, no. 2, pp. 502–518, March 1996.

[53] X. Giraud, E. Boutillon, and J. C. Belfiore, "Algebraic tools to build modulation schemes for fading channels," *IEEE Transactions on Information Theory*, vol. 43, no. 3, pp. 938–952, May 1997.

[54] Y. Xin, Z. Wang, and G. B. Giannakis, "Space-time diversity systems based on linear constellation precoding," *IEEE Transactions on Wireless Communications*, vol. 2, no. 2, pp. 294–309, March 2003.

[55] Z. Lui, Y. Xin, and G. B. Giannakis, "Linear constellation pre-coding for OFDM with maximum multi-path diversity and coding gains," *IEEE Transactions on Communications*, vol. 51, no. 3, pp. 416–427, March 2003.

[56] V. M. DaSilva and E. S. Sousa, "Fading-resistant modulation using several transmitter antennas," *IEEE Transactions on Communications*, vol. 10, no. 10, pp. 1236–1244, Oct 1997.

[57] E. Viterbo and F. Oggier, *Algebraic Number Theory and Code Design for Rayleigh Fading Channels*. Now publishers inc., 2004.

[58] D. Rainish, "Diversity transform for fading channels," *IEEE Transactions on Communications*, vol. 44, no. 12, pp. 1653–1661, Dec 1996.

[59] R. A. Mollin, *Algebraic Number Theory*. London, U. K. : Chapman and Hall, 1999.

[60] S. Verdu, *Multiuser detection*. Cambridge, U.K.: Cambridge Univ. Press, 1998.

[61] Y. R. Zheng and C. Xiao, "Improved models for the generation of multiple uncorrelated Rayleigh fading waveforms," *IEEE Communication Letters*, vol. 6, no. 6, pp. 256–258, June 2002.

[62] G. Marsagalia and T. A. Bray, "A convenient method for generating normal variables," *SIAM Rev.*, vol. 6, no. 3, pp. 260–264, July 1964.

[63] R. F. W. Coates, G. J. Janacek, and K. V. Lever, "Monte Carlo simulation and random number generation," *IEEE Journal on Selected Areas in Communications*, vol. 6, no. 1, pp. 58–66, Jan 1988.

[64] A. M. Sayeed and B. Aazhang, "Joint multipath-doppler diversity in mobile wireless communications," *IEEE Transactions on Communications*, vol. 47, no. 1, pp. 123–132, Jan 1999.

[65] Z. Wang and G. B. Giannakis, "Wireless multicarrier communications: where Fourier meets Shannon," *IEEE Signal Processing Magazine*, vol. 17, no. 3, pp. 29–48, May 2000.

[66] L. L. Yang, "Performance of multiantenna multicarrier DS-CDMA using OVSF codes assisted space-time spreading in time-selective fading channels," *IET Proceedings on Communication*, vol. 2, no. 5, pp. 708–719, May 2008.

[67] W. Su, Z. Safar, and K. J. R. Liu, "Towards maximum achievable diversity in space, time, and frequency: performance analysis and code design," *IEEE Transactions on Wireless Communications*, vol. 4, no. 4, pp. 1847–1857, July 2005.

[68] K. Jeong, S. H. Kim, K. M. Chung, J. C. Kim, J. H. Yu, J. S. Lee, and S. H. Seo, "Multipath channel models for wireless local and metropolitan area networks," *in Proceedings of ICITA*, vol. 2, no. 4-7, pp. 295–298, July 2005.